The Role of Microglia and Astrocyte in Spinocerebellar Ataxia Type 1

A Dissertation Submitted to The Faculty of The University of Minnesota By:

Austin Ferro

In Partial Fulfillment of The Requirements For The Degree of Doctor of Philosophy

Advisors: Marija Cvetanovic and Alfonso Araque

November 2020

Acknowledgments:

I would like to thank my esteemed committee for their continual support and dedication to my education. Their continual pursuit of excellence was inspiring and provided me with much motivation. I would like to thank Drs. Harry Orr and Michael Koob for the generous gift of mice, and the Orr lab for providing technical support. I would also like to thank the GPN's staff, including past and present Directors of Graduate Studies. Lastly, I would like to thank both Drs. Marija Cvetanovic and Alfonso Araque for their mentorship which provided me the technical and theoretical skills used in this dissertation.

This dissertation is dedicated to Beverly J. Brown (1943-2020). Without your loving support I would have never been able to purse my dreams.

Abstract:

Spinocerebellar ataxia type 1 (SCA1) is a fatal dominantly inherited neurodegenerative disease. Even though there has been illuminating work on the effect of the disease-causing protein, a polyQ expanded ATAXIN-1 (ATXN1) on neurons, the relative contribution to disease of glia has been unknown. Here I present my work on glial-neuron interactions in the context of SCA1; focusing on the neuroinflammatory and activation of microglia as well as the previously undiscovered cell-autonomous effect of polyQ expanded ATXN1 on astrocytes. Using the Lysm-Cre *Ikkβ*$^{flx/tlx}$ line to assess the role of microglial activation in the transgenic *ATXN1[82Q]* mouse model of SCA1, I show that inhibition of microglial reactivity does not have a large effect on SCA1 disease pathology. Instead, we found that the Lysm-Cre *Ikkβ*$^{flx/tlx}$ line itself had motor performance deficits in the absence of Purkinje cell degeneration. Correlating with this motor performance deficiency, Lysm-Cre *Ikkβ*$^{flx/tlx}$ mice had a prominent deficiency in climbing fiber removal onto Purkinje cells. Due to the low impact of microglia on SCA1 pathology, I then focus on astrocytes and in particular, astrocytic Kir4.1/*Kcnj10*. Astrocytic *Kcnj10* was downregulated throughout the brain of the knock-in *Atxn1*$^{154Q/2Q}$ mouse line. To investigate the potential role of cell-autonomous effects of *Atxn1* on astrocytic transcription, I used the novel conditional humanized *ATXN1*$^{floxed\ 146Q/2Q}$ line to delete polyQ expanded ATXN1 from astrocytes. Conditional astrocytic deletion of polyQ ATXN1 did not influence failure to gain weight nor a prominent effect on rotarod pathology. Yet, there was a trending rescue of *Kcnj10* expression in the medulla, suggesting a cell-autonomous effect of ATXN1 on astrocytic transcription. In conclusion, my thesis work concerning the role of both microglia and astrocyte in the pathogenesis of SCA1 has revealed the importance of NFκB signaling in cerebellar development as well as the potential cell-autonomous effect of polyQ ATXN1 on astrocytes.

Table of Contents

List of Tables

List of Figures

Chapter 1: Introduction

1.1 The Ataxias

The ataxias are a family of neurological disorders characterized by loss of balance and coordinated motor function[2]. Ataxias are classified as hereditary, sporadic, or acquired to denote what is known of their etiology. Hereditary ataxias are caused by a wide range of known genetic mutations with varying patterns of inheritance[3]. Sporadic ataxias have an unknown cause with potential environmental and genetic components[3]. Acquired ataxias, on the other hand, include disorders with endogenous or exogenous causes that are not genetic in nature, such as those arising from focal cerebellar damage caused by toxic agents, vitamin deficiencies, immune reactions, infection, and injury[4–6].

Autosomal dominant cerebellar ataxias caused by the expansion of CAG trinucleotide repeats, including SCA types 1, 2, 3, 6, 7, and 17, are among the best understood ataxias[2,7]. As CAG encodes for glutamine, these ataxias belong to the group of polyglutamine (polyQ) diseases that includes Huntington's disease, spinal bulbar muscular atrophy, and dentatorubral and pallidoluysian atrophy[3,8]. The clinical manifestations of polyQ ataxias are very similar and often include progressive cerebellar ataxia, oculomotor abnormalities, dysarthria (difficulties in speech), pigmentary retinopathy, peripheral neuropathy, and cognitive dysfunction[9].

SCA1 is a debilitating SCA which is characterized by the classical ataxia motor phenotypes and the early onset death of patients. As stated, SCA1 is caused by a polyQ expansion mutation in the ATXN1 protein which causes large scale cerebellar, pontine, and medullar degeneration. A non-pathogenic allele of *ATXN1* may have anywhere of 20-39 CAGs, coding for the polyQ region, in tandem repeat whereas a pathogenic allele may have 40< CAGs in repeat. Alleles tend towards anticipation, an increase in CAG length over generations causing an earlier onset of disease, due to the instability of the CAG repeat sequence[10,11]. Purkinje cells are some of the earliest and most prominently affected brain cell types, and thus the most well characterized in SCA1. Purkinje cell dysfunction

is largely thought to be due to altered ATXN1 nuclear function, causing a downstream neurodegenerative transcriptional and splicing program, alongside non-nuclear alterations such as mitochondrial dysfunction[12].

The degeneration caused by pathological ATXN1 leads to extensive dendritic remodeling and eventual cell death which is the major cause of the classical motor and cognitive phenotypes in both patients and models of disease. Classically, degeneration beings in the cerebellar cortex, and spreads to neighboring hindbrain regions such as the pons and medulla. Unlike the degeneration of the cerebellar cortex, the degeneration of the pons and medulla is largely thought to contribute to the early onset mortality of patients and animal models[13]. However, the contribution of non-neuronal cells, including microglia and astrocytes to the pathology of ataxia has been much less explored.

Microglia and astrocytes have emerged as key players in age- and disease-associated neurodegeneration, contributing to both protective tissue support and disease progression[14]. Indeed, both microglia and astrocytes have been shown to contribute to various forms of neurodegeneration through cell autonomous and cell nonautonomous mechanisms[15–17]. These studies provide evidence that microglia and astrocyte may play active roles in diseases traditionally thought to be predominantly neuronal. Yet, little is known about how these non-neuronal cells may contribute to the ataxias and, in particular, SCA1. Here, I will review the importance of microglia and astrocyte, their specific functions in the cerebellum and the evidence for and against their contribution to the pathogenesis of the ataxias and discuss potential underlying mechanisms.

1.2 Uniqueness of Cerebellar Microglia

Microglia are the resident macrophages of the central nervous system and have a wide variety of functions during development as well as in adulthood that are dependent on inflammatory state, and location and age. Unlike other brain cells, microglia originate

from the erythromyeloid progenitors that in mice develop around embryonic day 8.5 (E8.5) in the yolk sack. Erythromyeloid progenitors migrate to the brain starting around E9.5 and continue to do so until the blood–brain barrier is formed around E14[18,19]. During this early developmental stage, microglia have lasting effects on the developing neural architecture, including their well-understood role in superfluous cellular and synaptic pruning[20,21]. Supporting this developmental effect on microglia, recent studies using genome-wide chromatin and gene expression profiling demonstrated that microglia undergo three distinct developmental stages: early microglia (until E14), pre-microglia (from E14 to a few weeks after birth), and adult microglia (from a few weeks after birth)[22].

These developmental steps are regulated by distinct transcriptional factors that allow for different roles of microglia at each of these stages of life[22,23]. The chromatin remodeler *Mcm5* was found to be a major transcription factor for early microglia, whereas pre-microglia began to express canonical microglial transcription factors such as *Egr1* and *Sall1*, and the expression of these factors continued into the adult microglia when they upregulate the adult factors such as *Jun*, *Fos*, and *Mef2A*, which are believed to set up homeostatic functional transcription[22]. Furthermore, the temporally and transcriptionally distinct microglial states were confirmed and expanded upon in a single cell microgilal RNAseq published by Beth Steven's group (2018)[24]. Clustering analysis showed the increased proportion of microglia taking on a more reactive state over time. Between P100 and P540, there were 2-4 times the number of reactive microglia expressing a number of chemokines and cytokines (e.g. macrophage inflammatory protein-1β [*Ccl4*], *Ccl3,* and *Il1β*), and these cells were nearly absent in the healthy developing brain [24].

Even though there is this age dependent shift towards reactivity, sensome genes, through which microglia sense the environment[25], are expressed even in the early stages of development. This indicates that microglia are environmentally alert at all stages of development and may respond to brain insults even during neurodevelopment. Moreover,

evidence suggests that exposure to insults during early development can sensitize microglia in in ways that may contribute to brain pathology in adulthood[22,23].

Human cerebellar development extends from the early embryonic period until the first postnatal years and this protracted postnatal development leaves the cerebellum vulnerable to extrinsic and intrinsic injury[26–28]. During normal early cerebellar postnatal cerebellar development [P3] in mice, normal apoptosis of Purkinje neurons was strongly reduced by selective elimination of microglia, indicating that microglia contribute to the elimination of superfluous Purkinje neurons[20]. At P6–7, mouse microglia promote gamma-aminobutyric acid (GABA)-ergic inhibition on Purkinje cells and prune superfluous synapses[29]. The elimination of immature, functionally redundant synapses during postnatal development is essential for the formation of the functional cerebellar network and disruption of these developmental processes can lead to cerebellar dysfunction[30–32]. Importantly, studies on mouse models of SCA1 have demonstrated that disruption of these processes may also predispose the cerebellum to age-induced neurodegeneration[33,34].

To maintain adult brain homeostasis, microglia constantly extend and retract their processes to survey the local environment for synaptic activity[35], pathogen presence, and injury[36,37]. Madry et al. (2018)[38] recently established that constant microglial surveillance depends on the expression of the two-pore domain potassium (K^+) channel (THIK1). They demonstrated that tonic THIK1 activity maintains microglia l membrane potential and that blocking THIK1 reduces microglial ramification and surveillance. These results implicate a potential role of extracellular K+ concentration, arising from local neuronal activity, as a control mechanism for microglial surveillance. While it is unclear whether physiological changes in extracellular K+ concentration are sufficiently large to alter microglial surveillance, pathological changes in neuronal or astrocytic function are likely to do so. For example, it is possible that enhanced neuronal activity[39] and/or reduced clearance by

astrocytes[40] may increase extracellular K+, thereby altering microglial surveillance and morphology through THIK1.

Furthermore, microglia are attracted to areas of high physiological neuronal activity, whether drawn by THIK1 signaling to areas of increased extracellular K+[38] or by adenosine signaling through the purinergic receptor P2Y12 [38,43]. Li et al. demonstrated that microglia briefly (~5 min) contact highly active neurons, subsequently reducing their activity[35]. Intriguingly, during ischemic injury, the duration of these microglia–neuron contacts is prolonged (~1 h) and can lead to synapse removal[39]. Furthermore, Davalos et al. (2005) demonstrated that increase in ATP causes rapid recruitment of microglia[36]. Regional heterogeneity of neurons[41] coupled with the intimate phenotype driving crosstalk between microglia and neurons suggests microglial heterogeneity which can further alter normal and pathological functions. Indeed, several studies to date have provided evidence of spatial and temporal microglial heterogeneity under steady-state conditions[42–44]. Understanding the regional characteristics of microglia is important to determine their function in healthy brains and their possible contribution to regional susceptibility in neurological diseases.

Heterogeneity may be particularly important for cerebellar diseases, including ataxias, as cerebellar microglia seem to be unique among brain microglia in terms of morphology, tiling density, gene expression, mobility, phagocytosis, bioenergetics, and aging characteristics. A study by Lawson et al. (1990) was one of the first reports indicating that cerebellar microglia may have unique characteristics compared to microglia in other brain regions[44]. Different regions of adult mouse brain, including cerebral cortex, hippocampus, hypothalamus, thalamus, and cerebellum, were analyzed using F4/80 (membrane glycoprotein specific for mononuclear phagocytes) immunohistochemistry to assess microglial density and morphology. Lawson et al. found that the cerebellum exhibits the lowest microglial density of any part of the brain (~30 cells/mm^2 compared to

a total brain mean of 70 cells/mm^2). Also notable was the pattern of microglial density in the cerebellum. While most brain regions contained fewer microglia in white matter than in gray matter, the opposite pattern was found in the cerebellum (e.g., fewer microglia in gray matter of cerebellum than in the white matter)[44].

Further studies demonstrated that microglia in the cerebellum have a unique transcriptome. Grabert et al. analyzed gene expression of adult mouse microglia isolated from different brain regions[43]. They found enhanced expression of genes regulating immune alertness and energy metabolism in cerebellar microglia compared to microglia in other brain regions, such as the cortex and striatum. It is important to note that the hyper-alert immune state of cerebellar microglia is distinct from the conventional microglial activation associated with injury. It is unclear whether these results indicate that cerebellar microglia may be better equipped to remove foreign and infectious threats. Alternatively, they may need less stimulation to become reactive. In addition, this study reported that cerebellar microglia exhibited an accelerated age-dependent increase in immune-related genes compared to the microglia from other brain regions[43]. These results indicate that cerebellar microglia exhibit a more alert immune phenotype throughout life that amplifies with aging. This age dependent enhancement of microglial hyper-vigilance may contribute to the age-dependent onset of cerebellar ataxias. This is likely to be even more critical in types of cerebellar ataxias where microglia are altered from the early stages of disease, prior to onset of symptoms of ataxia[45]. As such, it is of utmost importance to understand the molecular mechanisms underlying the unique characteristics of cerebellar microglia so we can better understand their contribution to cerebellar disease.

Several recent studies have uncovered some mechanisms underlying microglial heterogeneity. For example, the epigenetic regulator polycomb repressive complex 2 (PRC2) was identified as a factor determining the heterogeneous phagocytic potential of microglia, including the enhanced phagocytic phenotype of cerebellar microglia[42]. Using

translating ribosome affinity purification and chromatin immunoprecipitation followed by sequencing, the authors have found that PRC2 leads to a repression of phagocytic genes in many brain regions, while also promoting the expression of phagocytic genes in the cerebellar microglia. Woodruff-Pak et al., (2010)therefore suggested that the increased phagocytosis of cerebellar microglia may be associated with the more pronounced age-dependent neuronal loss that occurs in the healthy cerebellum compared to other brain regions[46,47]. While the exacerbated loss of Purkinje neurons in the cerebellum starts in adolescence[46], it is unclear whether it is the cause or the consequence of hyper-alert microglia. Gene expression profile comparisons of cerebellar microglia before and after adolescence may be useful in indicating whether enhanced neuronal loss in the cerebellum results from the unique phenotype of cerebellar microglia.

With evidence for the direct microglial control of Purkinje cell number in normal aging, the critical developmental roles of cerebellar microglia, as well as their unique immune-alert phenotype in the adult cerebellum, microglia are therefore poised to have profound effects on insults to the cerebellum. Furthermore, the characteristics of cerebellar microglia may contribute to the increased vulnerability of cerebellum in diseases such as the ataxias.

1.3 Microglia in Neurodegenerative Diseases and the Ataxias

While fundamental knowledge about microglia in the healthy brain is increasing, the role of microglia is best understood in the context of brain disease. Due to their sensory abilities and innate immune function, microglia alter their transcriptomics, proteomics, morphology, and function when confronted with a wide variety of disease states and/or insults to the brain[48,49]. This profound change in microglia is commonly considered an “activated state” and seems to be ubiquitously present in many brain diseases and injury

conditions. However, the functional outcomes of the activated state of microglia are less clear[50,51].

One of the critical signaling pathways that contributes to microglial activation is the canonical nuclear factor kappa-light-chain-enhancer of activated B cells (NF-κB) pathway[52,53]. The NF-κB pathway is classically initiated when inhibitors of κB are marked for degradation by inhibitors of κB kinases, releasing the NF-κB subunits to translocate to the nucleus where they activate transcription of proinflammatory genes[54]. The NF-κB signaling cascade can be activated in microglia by tumor necrosis factor receptor stimulation or Toll-like receptor stimulation. When initiated, it induces the release of proinflammatory cytokines such as tumor necrosis factor alpha (TNF-α), extensive morphological changes (ramification), increases in overall microglial density, and increases in the expression of ionized calcium-binding adapter molecule 1 (IBA1) protein[55].

Microglial activation via the NF-κB, or other proinflammatory pathways (e.g. p38-mitogen-activated protein kinase, JAK/STAT or JNK), can impact the overall neural architecture in several ways: by affecting the neuronal function through direct signaling and released proinflammatory cytokines[56], by regulating the inflammatory state of non-neuronal cells that will in turn cause a variety of secondary effects in neurons[57], through modulation of extracellular proteins and protein aggregates[58–60], and through the direct inappropriate phagocytosis of neural and glial tissues via the classical complement pathway[61–63].

While each of these facets have been characterized in neurodegeneration, divergent theories remain regarding their functional outcomes, namely, whether they are beneficial or harmful[64]. For example, in Alzheimer's disease (AD), evidence shows that microglia could serve to actively reduce pathology[60] as well as to exacerbate intrinsic neural dysfunction[61,62]. Likely, microglia occupy a spectrum between these two extremes,

which complicates interpretations when singular functions of microglia are modulated to study their role in disease. While much less studied, similar uncertainty surrounds the role of microglia in the ataxias.

Microglial activation in the cerebellum was observed during post-mortem analysis in several types of ataxias and in several rodent models of ataxia, including SCA6[65], SCA21[66], Friedreich's ataxia[67], ataxia-telangiectasia (A-T)[68], and multiple system atrophy[69]. Moreover, several animal models have demonstrated microglial activation preceding behavioral symptoms and cerebellar pathology. In the 118Q knock-in mouse model (MPI118Q/118Q) of SCA6, in which a polyQ expansion in the calcium channel Cav2.1 causes cerebellar pathology and ataxic behavior, microglial activation precedes apparent Purkinje cell degeneration[65]. This early microglial activation pattern can also be seen in the transmembrane protein 240 (TMEM240) viral expression model of SCA21, with microglial activation preceding the onset of motor deficits[66]. Early activation of cerebellar microglia can also be found in the rat ATM knockout model of A-T, where ATM−/− rats had pre-symptomatic and progressive NF-κB-dependent microglial activation. Activation of microglia in the A-T rat model correlated with disease severity and preceded Purkinje cell pathology[68]. The prevalence of early microglial activation in these models indicates a mechanism by which microglia actively contribute to pathogenesis and makes them a promising therapeutic target for preventative treatment in the ataxias.

The role of early microglial activation in ataxia is perhaps best characterized in SCA1. Early microglial activation can be found in several models of SCA1. Both the Purkinje cell specific transgenic model (*ATXN1[82Q]*)[70] and the knock-in mouse model (*Atxn1* $^{154Q/2Q}$)[71] show increases in microglial number and TNF-α expression, a possible mechanism for microglia-driven neuroinflammation in disease[45]. Correlative evidence to support this theory was found using the TET-off conditional transgenic mouse model of SCA1, *cATXN1[30Q]-D776* [73]. In a 6-week on 6-week off paradigm, stopping the

expression of mutant ATXN1 after the first 6 weeks of life ameliorated ataxia in these mice. This behavioral recovery was found to coincide with a significant decrease in density of cerebellar microglia and in cerebellar TNF-α expression[45,72].

However, pharmacological approaches to test the role of early microglial activation in SCA1 suggest a limited effect on disease state. Pharmacological depletion of microglia in *ATXN1[82Q]* mice showed only a limited rescue of rotarod performance. Microglia proliferation and survival is dependent on continual activation of colony stimulating factor 1 (CSF1R)[73]. Qu et al. used PLX3397, a novel inhibitor of CSF1R, to deplete microglia by 69% in the cerebella of *ATXN1[82Q]* mice[74]. The depletion of microglia in the *ATXN1[82Q]* mice reduced TNF-α expression, when compared to vehicle treated *ATXN1[82Q]* mice, yet the effects did not correlate with reduced Purkinje cell neuropathology or astrogliosis, where both progressed equally to that of vehicle treated *ATXN1[82Q]* mice[74].

The hypervigilance and the non-cell autonomous activation of microglia seen in the transgenic *ATXN1[82Q]* model is applicable to other ataxias where the pathogenic protein(s) are not expressed in microglia. However, this is not the case for many ataxias, such as in A-T. A-T is a pleiotropic disease characterized by cerebellar Purkinje neuron degeneration, cancer, and immune dysfunction. A-T is caused by loss of function mutations in the ATM gene. The encoded ATM protein is a PI3K family kinase that is essential for the double-strand (ds)DNA break repair machinery and for cellular redox balance.

Cell autonomous effects of ATM dysfunction have been well studied in neurons. However, recent studies indicate that the predominant Purkinje cell degeneration evidenced in A-T may not be solely explained by neuronal ATM loss. Initial evidence [75] demonstrated that ATM inhibition solely in glial cells was sufficient to activate innate immune response and induce neurodegeneration. Interestingly, a later study showed that cortical and cerebellar neurons in ATM null mice respond differently to immune

challenge[76], in a manner that seemed to correlate with microglial phenotype. Together with previously mentioned reports of microglial activation, these results suggested that microglia might contribute to A-T pathogenesis and area-specific susceptibility[77].

A recent study from Dr. Karl Herrup's laboratory provides new insight into the mechanism of microglial reactivity in A-T[78]. Song et al. show that ATM deficient microglia undergo cell autonomous activation triggered by presence of single and double stranded DNA in the cytoplasm. In particular, they demonstrate that deficient DNA repair caused by genetic and pharmacological inhibition of ATM results in the leaching of single and double stranded DNA into the cytoplasmic compartment of the microglia. In microglia, the presence of this cytoplasmic self-DNA induces signaling via stimulator of interferon genes (STING) protein, a critical regulator of the innate immune response to cytosolic nucleic acids (Figure 1A). STING activation results in nuclear factor kappa B (NF-κB)-dependent transcriptional upregulation of interleukin 1 (*IL-1β*) and production of pro-IL-1β. While loss of ATM function caused accumulation of single and double stranded self-DNA in the cytoplasm of neurons, this alone did not seem to cause inflammation. This may be due to the absence of STING in neurons, as single cell RNA sequencing indicates that in the brain STING seems to be predominantly expressed in microglia (Figure 1B)[79]. This was further evidenced by the requirement of neurons to be cultured with microglia in order to observe pathology, and loss of ATM in neurons was insufficient to cause pathology.

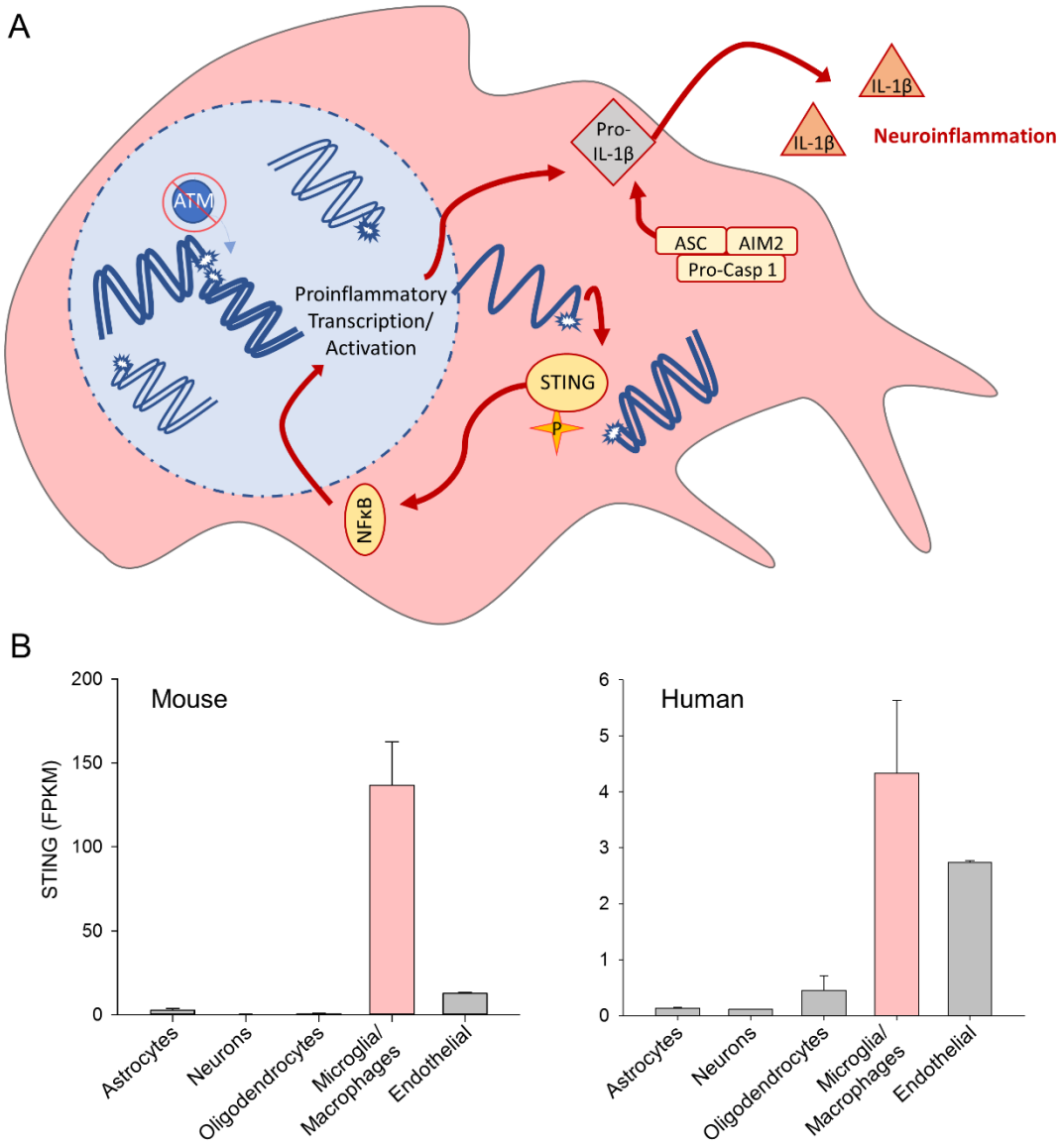

Figure 1. Microglia are key responders to cytoplasmic DNA accumulation through the STING antiviral pathway. (A) Proposed mechanism of innate immune response of microglia in A-T. Normally, ATM (ataxia atelangiectasia mutated) responds to DNA double strand (DS) breaks and aids in repair, while in A-T there is a reduction in the function of ATM and thus there is an accumulation of DNA breaks. Song et al., show that accumulation of DS breaks leads to the activation of the innate immune response in microglia, via accumulation of single strand and double stranded DNA in the cytoplasm. Cytoplasmic DNA then activates STING and AIM2 inflammasome leading to NF-κB activation and IL-1β release from microglia. This novel

pathway for overall increase in the activation state of microglia and subsequent neuroinflammation then contributes to and exacerbates the cell intrinsic degeneration of Purkinje neurons in the cerebellum. (B) Brain RNA-seq data indicates predominant expression of STING in microglia in both mice and humans[80]. Figure from Ferro et al., 2019[81].

Cytoplasmic nucleic acid recognition may be one of nature's oldest protective strategies, whereby detection of invading genetic material activates mechanisms to degrade the pathogen and destroy its ability to replicate. In A-T, deficient DNA repair leads to accumulation of cytoplasmic single and double stranded self-DNA that are recognized by this innate immune system resulting in microglial activation and secretion of neurotoxic cytokines. From a therapeutic perspective, these results suggest that targeting innate immune activation may ameliorate neurodegenerative aspects of this disease. Indeed, early targeting of innate immune pathways with anti-inflammatory drugs effectively inhibits development of disease phenotype in *ATM*-null mice[82]. Furthermore, the association of this microglial autoimmunity pathway and Purkinje cell death may, in part, explain the regional specificity of A-T neuropathology due to the hypervigilant state of cerebellar microglia, which include including genes involved in cytoplasmic DNA recognition such as *Zbp1*[83,83]. Furthermore, innate auto-immune dysfunction may also occur in other neurodegenerative diseases in which mutated proteins play a role in DNA repair, including but, not restricted to, Huntington's disease (HD), Spinocerebellar ataxia type 3 (SCA3) and Alzheimer's disease [84,85].

Therefore, the novel inflammatory cascade described by Song et al. may be a broadly applicable mechanism for neuroinflammatory induction in a variety of diseases. The pattern of inflammation induction and subsequent neural degeneration may be explained by the regional diversity of microglial alertness as well as the local mutant protein expression. Therefore neuroinflammation, and especially that of microglial

activation, could be an effective and broadly applicable therapeutic target if targeted early in disease.

1.4 Astrocyte, diversity and uniqueness of Bergmann glia

Another cell type that may is heavily implicated in the ataxias and other neurodegenerative disease is the astrocyte. Unlike microglia which derive from erythromyeloid progenitors from the yolk sac, astrocyte arise from ectodermal-derived radial glial stem cells through mostly symmetrical division (post-natal) and to a lesser extent asymmetrical division (early embryogenesis) and differentiation into intermediate glial progenitor cells[86]. Even though now well understood, the major developmental cascade (symmetrical division) which accounts for nearly half of the developed astrocytic population, had been proposed as early as 1913 by Santiago Ramon y Cajal, who observed astrocytes joined by the soma during development and aptly named them *"*astrocitos gemelos " (*English translation: astrocyte twins*)[87]. The subsequent astrocytic population in the adult human brain are estimated to account for near 40% of the number of total brain cells[88].

The symmetric division of radial glia into glial precursors in relation to neural development may contribute to a diversity of astrocyte of the brain, such as the distinction between fibrous, Müeller, velate, Bergmann, protoplasmic, and surface-associated astrocytes. Alongside the major distinctions between morphologies, such as the radial like Bergmann and Müeller astrocytes compared to the less polar and more ramified morphologies of protoplasmic and fibrous morphologies, there are differences in overall transcriptomics throughout CNS astrocytic populations and within brain regions[89–92]. These regional differences in transcriptomics are thought to be due to both the neural environment during development[93] as well as the continual release of factors such as sonic hedgehog from neighbor neurons[89].

Even though diverse, astrocyte share a wide array of normal functions in the developed brain. Astrocyte are known to perform many maintenance functions: 1) direct neurotransmitter reuptake and recycling (glutamate recovery and conversion to glutamate for neural reuse[94] and direct reuptake of GABA[95] and monoamines for recycling), 2) maintenance of synapse number via trophic support and indirect elimination through recruitment of microglia using the complement pathway[57,96], 3) regulation of extracellular space with regulation of ion concentration such as potassium via the potassium inward rectifier 4.1 (Kir4.1/*KCNJ10*)[97–99], 4) regulation of pH via the regulation of glutamate (excitatory amino acid transporter 1 (EEAT1) cotransport of protons and glutamate)[100] as well as the sodium bicarbonate cotransporter[101], 5) the maintenance of brain metabolism through the lactate shuttle[102], 6) as well as volume via the interactions of Aquaporin-4 (AQP4) and Kir4.1[103]. Astrocyte also exhibit more direct functions on overall neural function via direct gliotransmission[104] and through neurovascular coupling[105].

As one may expect, aging plays a crucial role in the ability of astrocyte to maintain these critical functions. Data from Dr. Allen's lab, where her group used an astrocyte specific ribonuclease tag as means of isolating actively transcribed RNAs from tissues for downstream RNA sequencing analysis[90,106]. When comparing 4 month (developed) and 2 year old (aged) mice, they found that the brain regions most affected by aging were the cerebellum which largely upregulated pro-inflammatory cascade genes such as *Caspase-1, -12*, and the chemokine *Cxcl15* yet downregulated key synaptic neurotrophic factors like *Thbs1*. Furthermore, pathway analysis indicated that the cerebellum underwent the largest increase in reactivity genes. This data corroborates the uniqueness of the cerebellum in aging as a hub for glial reactivity.

The cerebellar astrocyte reactivity is particularly important due to the age-dependent loss of Purkinje cells[47], with Bergmann glia being the most probable astrocyte subtype to contribute to this age-dependent degeneration. Bergmann glia are the

astrocytic subtype with the most prominent interaction with Purkinje cells and are the most abundant astrocyte cell type in the cerebellar cortex. In the cerebellar cortex, Bergmann glia outnumber Purkinje cells ~10:1 whereas Velate astrocytes, which are found in the granule cell layer, are outnumbered by granule neurons ~8:1 and each Bergmann glia sheaths 6,000-8,000 synapses[107,108]. The intimate relationship between Bergmann glia, Purkinje cells and parallel/climbing fiber inputs, can be seen both in their calcium responses to both network activity caused by behavioral engagement[109] as well as their ability to signal directly to Purkinje cells via glutamate release[110]. Furthermore, Bergmann glial inflammation is directly related to Purkinje cell health, as specific activation of the NF-κB canonical pro-inflammatory cascade in Bergmann glia can cause non-cell autonomous Purkinje cell degeneration[111]. Due to their intimate connection to Purkinje neurons, the overall pro-inflammatory/reactivity state of the cerebellum, and their overrepresentation compared to Velate astrocyte, it is hypothesized that Bergmann glia would exert the most prominent effect on Purkinje cells and therefore contribute specifically to the ataxias.

1.5 Astrocyte in neurodegenerative disease and the Ataxias

Like microglia, astrocytes are heavily implicated in neurodegenerative disease and have long been used as markers of neuroinflammation. Upon sensing an insult, like microglia, astrocyte profoundly alter both their morphological state and their overall transcriptomics. The classical activation state of astrocyte can be defined by an increase in glial fibrillary acidic protein (GFAP) and vimentin expression which coincides with thickening of the major processes resulting in cellular hypertrophy[112]. Astrocytic activation was suggested to result in either A1 (neurotoxic) or A2 (neuroprotective) phenotypes which can profoundly worsen or ameliorate the severity of the insult [113,114]. Importantly, similar to microglia, astrocytes in mouse models of neurodegeneration often have

decreased expression of genes involved in their homeostatic roles, such as *Kcnj10* and *EEAT1*, indicating reduction in neurosupportive functions [115,116,117,118].

For instance, astrocytes in mouse models of HD have reduced expression of the potassium inward rectifier 4.1 (Kir4.1) that results in perturbed ion concentration and as a consequence increased excitability of neurons[119]. Furthermore, rescue of Kir4.1 expression in the HD mouse model, was able to reduce motor behavioral deficits as well as extend life of the HD mice in comparison to vehicle treated controls[119]. The evidence of Kir4.1's importance was further supported by the first Kir4.1 knock-out model, which had similarly depolarized neurons that resulted in both an epileptic as well as an ataxic motor phenotype[97]. The ataxic and epileptic phenotype found in the Kir4.1 knockout model also mimics that of **E**pilepsy, **A**taxia, **S**ensorineural deafness, and (a renal salt-wasting) **T**ubulopathy (EAST) patients[120,121]. EAST syndrome is a recessive genetic disorder caused by mutations within the *KCNJ10* that reduce Kir4.1 function, causing severe cerebellar abnormalities resulting in the ataxia seen in a majority of patients[122].

Other evidence for the role of astrocyte in the neurodegenerative disease and specifically in the ataxias comes from SCA7, caused a polyQ expansion within the ATAXN-7 (ATXN7) protein. In the first transgenic mouse models of SCA7, they found that polyQ-expanded ATXN7 recapitulated the expected Purkinje cell atrophy and gross motor pathologies[123]. Yet upon further histological assessment, they found Purkinje cells were devoid of ATXN7 expression, suggesting a cell-nonautonomous degeneration caused by neighboring cells. The cell non-autonomous degeneration was elaborated upon via an astrocytic-directed expression of ATXN7 using the GFAP promoter, which resulted in motor performance deficits and a progressive Purkinje cell atrophy[124]. Bergmann glial ATXN7 caused decrease in the expression of glutamate transporter 1 *Slc1a2* (GLAST) which correlated with increases in extracellular glutamate and eventual excitotoxicity[124]. The importance of the cell non-autonomous effects on Purkinje cells was supported

through a directed knock-out experiment. Knocking out pathogenic ATXN7 from astrocyte resulted in a decrease in cerebellar pathology, further implicating Bergmann glia in Sca7[125].

Evidence for the role of astrocyte has also been found in SCA1. Pathological assessment of postmortem patient tissue shows gliosis as a prominent feature in both the cerebellum and medulla[126,127]. These data are corroborated in pathological and magnetic resonance spectroscopy (MRS) assessments in both the Purkinje cell specific *ATXN1[82Q]* and *Atxn1*$^{154Q/2Q}$ mouse models. Both models show prominent astrogliosis within the cerebellum, even before motor and Purkinje cell dysfunction[128]. MRS studies quantifying the putative gliosis metabolite myo-inositol, show increases in myo-inositol in the cerebella of *ATXN1[82Q]* mice, and that myo-inositol concentrations positively correlate with the severity of the ataxia and negatively correlate with reduction in molecular layer width of the cerebellar primary fissure[129]. Furthermore, increased myo-inositol is seen in a SCA1 patient population and myo-inositol levels can be used to predict SARA score, the clinical assessment measure of ataxia[129,130]. Therefore, data from both histological and MRS assessments suggest the predictive power of astrocytic activation to disease state.

This hypothesis was directly tested through manipulation of astrocyte activation in *ATXN1[82Q]* mice. Kim et al., (2018) used a cre-Lox approach to inhibit the activity of nuclear factor kappa (NFkB signaling) in astrocyte using an astrocyte-specific tamoxifen (TMX) inducible Cre line[131]. By doing so, they were able to effectively knock down astrocytic, NFκB mediated activation at an early or late stages of disease. Early inhibition of astrocytic inflammation caused a worsening of pathology, whereas late inhibition caused an improvement of pathology. These data suggest a biphasic role of astrocyte inflammation where early astrocytic inflammation is neuroprotective and later in disease, astrocytic inflammation is neurodestructive.

1.6 Crosstalk between Microglia and Astrocytes

There is emerging evidence that communication between microglia and astrocytes is extremely important for defining physiological and pathophysiological functional states of each cell type. For example, astrocyte expression of interleukin 33 (IL-33) during normal development is required for normal circuit formation and microglial synapse engulfment, a precursor to synapse pruning[132]. The communication between microglia and astrocytes during central nervous system insult has severe effects on the neural and glial environment. The neurotoxic astrocytic inflammatory phenotype can be driven by microglial signaling[57]. Likewise, aberrant microglial removal of synapses in AD is regulated by astrocytes[133].

In context of the ataxias though, the communication between microglia and astrocyte is less clear. For instance, Kim et al., (2018) suggested a biphasic effect of NF-κB signaling in astrocytes, saw a potential inversion of the cascade seen by the Barres group[131]. Again, reducing inflammatory NF-κB signaling in astrocytes prior to onset of motor symptoms exacerbated Purkinje neuron dysfunction and motor deficits. Intriguingly, reduced astrocytic inflammatory signaling early in SCA1 increased microglial reactivity and conversely, reduced astrocytic inflammatory signaling late in SCA1 decreased microglial reactivity[131].

While reduced astrogliosis correlates with increased microglial activity during early stages of SCA1, the reverse has not yet been demonstrated (i.e., modulation of microglial activation has not yet been shown to elicit detectable changes in astrocytic reactivity in SCA1)[74]. Although this may indicate that microglia do not modulate astrocytic phenotypes in SCA1, it is important to consider several restrictions of this study. Pharmacological approaches to reducing microglial density were not fully effective in the cerebellum. Pharmacological depletion, which was up to 99% effective in the cerebrum, was only 69%

effective in the cerebellum. The remaining 31% of microglia may be sufficient to mediate astrogliosis[57,74].

Hypothesis

With the normal and pathological states that both microglia and astrocyte may undertake in a spectrum of neurodegenerative disorders, I hypothesize that both cell types contribute to the overall disease state of SCA1. In particular, I hypothesize that microglia contribute to SCA1 disease progression via a NF-κB dependent inflammatory pathway that exacerbates the neuroinflammatory state. I will explore this hypothesis in chapter 2, exploring the interactions between microglia and pathology in the ATXN1[82Q] mouse model. The aim of this chapter is to determine the contribution of microglial NF-κB signaling, a canonical inflammatory pathway, to motor performance and overall Purkinje cell health. Through microglial specific knockout of IKKβ, the upstream activator of NF-κB, I hypothesized that we would reduce overall behavioral and neural pathologies in the ATXN1[82Q].

In chapter 3, I shift from studies on microglia to astrocyte in order to assess how potential astrocytic signaling pathways may contribute to SCA1. The aim of chapter 3 is to characterize astrocytic transcriptional changes and resolve whether expressional changes in the inward rectifier potassium channel Kir4.1/*Kcnj10* were due to cell non-autonomous effects of inflammation or cell-autonomous effects of polyQ expanded ATXN1 in astrocytes. The overall hypothesis is that astrocytic polyQ ATXN1 affects transcriptional regulation of *Kcnj10* in a cell autonomous manner which in turn affects SCA1 disease severity.

Chapter 2. Inhibition of NF-κB signaling in microglia causes motor deficits and does not alter pathogenesis of Spinocerebellar ataxia type 1

2.1 Introduction

With the accumulating evidence for the role of microglia in neurodegenerative disease states, we sought to further characterize the role of microglia in SCA1. Both postmortem pathological studies and longitudinal imaging studies on SCA1 patients as well as on mouse models of SCA1 demonstrated reactive cerebellar gliosis that correlated well with the progression of disease and neuronal loss. Moreover, we have previously demonstrated that cerebellar gliosis occurs prior to the onset of motor symptoms in mouse models of SCA1, indicating it may play a role in the pathogenesis during these early, pre-symptomatic stages of disease[134]. Gliosis is a process of profound morphological and functional changes by which glial cells, such as microglia and astrocytes, respond to brain injury[135,136]. While gliosis has been described in many neurodegenerative disease, its functional role remains unclear as both beneficial and harmful effects of gliosis have been reported[45,137–139].

Even though microglial activation is a key feature of many neurological disorders, including Amyotrophic Lateral Sclerosis (ALS), multiple sclerosis (MS), Huntington's disease (HD), Parkinson's disease (PD), and Alzheimer's disease (AD)[115,133,140,141], role of microglia in the disease is still debatable. This is mostly because there is evidence supporting both neuroprotective as well as neurotoxic effects of microglia in disease [142]. Neuroprotective functions are mostly accomplished by microglia secreting neurotrophic factors including brain-derived neurotrophic factor (BDNF) or by removing dying cells and extracellular aggregates[138]. Microglia can be neurotoxic by inappropriately removing synapses and thereby damaging the neuronal networks, and by inducing neuroinflammation. Neuroinflammation is largely mediated by cytokines, such as microglia-derived as tumor necrosis factor α (TNF- α) that was shown to worsen outcome in various neurological disorders, including AD, MS, and PD[51,143–145].

We tested the role of microglial neuroinflammation in the pathogenesis of SCA1 at the pre-symptomatic stage due to the findings that this stage has therapeutic potential to delay onset of disease and prevent neuronal loss. Moreover, because SCA1 is inherited disease pre-symptomatic treatments are possible. To modulate microglial neuroinflammation we decided to inhibit the activity of nuclear factor kappa (NFkB signaling) only in microglia using a Cre-Lox approach. NF-κB is a master transcriptional regulator of inflammation, and is well -known regulator of TNF-α expression[146]. Most of NF-κB is kept inactive in the cytoplasm by being bound to inhibitor of κB protein (IκB) proteins[147]. NF-κB is commonly activated through the classical pathway in which inducing stimuli trigger phosphorylation of catalytic unit of IκB kinase (IKK) complex, IKKβ subunit at Ser 180[148,149]. Activated IKKβ in turn phosphorylates IκB proteins leading to their ubiquitination and degradation[149], thus releasing NF-κB dimers to translocate to the nucleus and promote transcription of target genes.

To determine the role of pre-symptomatic microglial neuroinflammation in SCA1, we crossed IKKβF/F mice (in which exon 3 of IKKβ is surrounded by two loxP sites)[150] with LysM-Cre mice (that express Cre recombinase in microglia and macrophages)[150–152] and transgenic Purkinje neuron specific *ATXN1[82Q*] mice, that express mutant *ATXN1[82Q]* only in Purkinje neurons[43]. We have found that *ATXN1[82Q];IKKβF/F;LysM-Cre* mice had decreased density of microglia and expression of TNF-α compared to *ATXN1[82Q]* littermates suggesting that NF-κB pathway is the main regulator of microglial neuroinflammation in SCA1 mice. However, onset and severity of SCA1 pathogenesis were not altered in *ATXN1[82Q];IKKβF/F;LysM-Cre* mice. In addition, we have found that surprisingly, *IKKβF/F;LysM-Cre* mice exhibited motor deficits at 3 months of age.

2.2 NF-κB pathway contributes to microglial activation in SCA1 mice.

To alter microglial neuroinflammation in SCA1, we reduced the activation of the key transcriptional regulator NF-κB in microglia of SCA1 mice. To inhibit microglial NF-κB signaling, we deleted IKKβ specifically in microglia by using the LysMCre-LoxP system. For this we created triple transgenic *ATXN1[82Q];IKKBF/F;LysM-Cre* mouse line, in which microglia and macrophage specific Lysozyme M promoter drives the expression of Cre-recombinase[70,151] to delete the exon 3 of IKKβ (bordered by two loxP sequences)[150,153].

We examined the effect of NF-κB inhibition on microglial activation in SCA1 by performing immunohistochemistry for microglial marker ionic calcium binding protein (Iba1) (Fig 2A). We found significant reduction of Iba1-positive microglia in the *ATXN1[82Q];IKKBF/F;LysM-Cre* mice compared to *ATXN1[82Q]* control mice (Fig 2B, one-way ANOVA with Tukey's HSD test, $p<0.05$), suggesting that the canonical NF-κB pathway is involved in regulating microglia activation in SCA1, which is consisted with the previous studies. Furthermore, expression of pro-inflammatory cytokine TNF-α that we have previously shown is upregulated in SCA1 through microglia, was decreased in the cerebella of *ATXN1[82Q]; IKKβF/F;LysM-Cre* compared to *ATXN1[82Q]* mice. These results suggest that microglial NF-κB pathway regulates TNF-α in SCA1 (Fig 2C, *ATXN1[82Q]* 1.987, N= 5*, ATXN1[82Q]*; *IKKβF/F;LysM-Cre* 1.46, N= 4, P< 0.05, one-way ANOVA with Bonfferoni post-test).

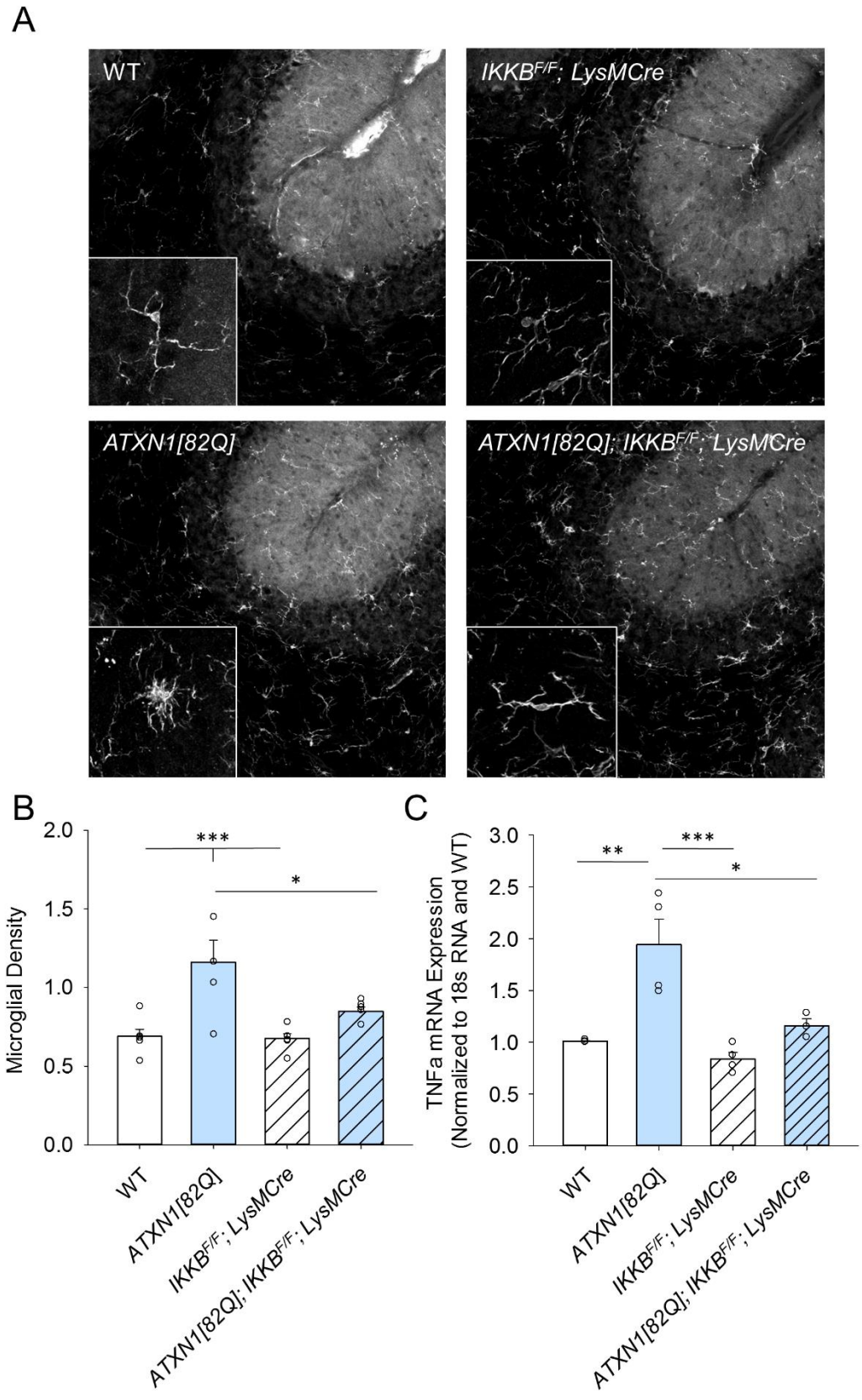
A
WT
IKKB^F/F; LysMCre
ATXN1[82Q]
ATXN1[82Q]; IKKB^F/F; LysMCre
B
Microglial Density
2.0
1.5
1.0
0.5
0.0
***
*
WT
ATXN1[82Q]
IKKB^F/F; LysMCre
ATXN1[82Q]; IKKB^F/F; LysMCre
C
TNFa mRNA Expression
(Normalized to 18s RNA and WT)
3.0
2.5
2.0
1.5
1.0
0.5
0.0
**
***
*
WT
ATXN1[82Q]
IKKB^F/F; LysMCre
ATXN1[82Q]; IKKB^F/F; LysMCre

Figure 2. Microglial density and TNF-α production in *ATXN1[82Q]; IKKβF/F;LysM Cre* mice. Cerebella of 3-month–old mice were used for IHC with Iba1-antibody. Representative image of microglia specific Iba-1 staining. Insets of higher magnification images illustrating microglial morphology. B. Quantification of microglial density in the molecular layer (N ≥ 4 per each genotype), one-way ANOVA followed by Tukey's HSD post-hoc test. * $P < 0.05$ C. RNA was extracted from the cerebella of 3-month–old mice and RT-qPCR was used to determine expression of TNF-α (with reference to control treated wild type and normalized to 18S RNA). Each dot represents one mouse, and values indicate mean ± SEM, one-way ANOVA followed by Bonfferoni post-hoc test. * $P < 0.05$, ** $P < 0.01$, *** $P < 0.0001$. Open bars are WT controls, light blue bars are *ATXN1[82Q]* mice, and hashed bars indicate the presence of IKKβF/F;LysM Cre. Figure from Ferro et al., 2018[154].

2.3 Inhibition of NF-κB causes motor deficits in IKKβF/F;LysM-Cre mice but does not alter pathogenesis in SCA1 mice

We next determined whether reducing activity of microglial NF-κB affects motor deficits characteristic for SCA1. One of the earliest symptoms of SCA1 is ataxia, which refers to a loss of motor control and balance. Ataxia in mice can be quantified by the accelerating rotating rod (rotarod) test[155]. In the rotarod test, mice are placed on rotating rod that accelerates and the time it takes for a mouse to fall is recorded (latency to fall). Mice that have cerebellar deficits, such as SCA1 mice, tend to fall off the rotating rod earlier due to reduced ability to balance and coordinate movements[156].

We performed the rotarod test at three months of age, the earliest age at which we can detect motor deficits in SCA1 mice. We found that both *ATXN1[82Q]* mice and *ATXN1[82Q]; IKKβF/F;LysM-Cre* mice performed poorly on rotarod compared to wild-type mice (Fig 3, WT mice 370 s N=11, *ATXN1[82Q]* mice 199.1s, N=11, *ATXN1[82Q]; IKKβF/F;LysM-Cre* 152.6s, N= 10, $p<0.05$, one-way ANOVA with Bonferroni post-test). However, because of its connection with inflammation, we were surprised to find that loss of IKKβ itself in normal brains in *IKKβF/F;LysM-Cre* mice caused significant impairment in

rotarod performance (Fig 3, WT mice 370 s N=11, *IKKβF/F;LysM-Cre* 198s, N= 10, P< 0.05, one-way ANOVA with Bonferroni post-test) . These results suggest that reducing canonical NF-κB pathway in *IKKβF/F;LysM-Cre* mice causes motor deficits.

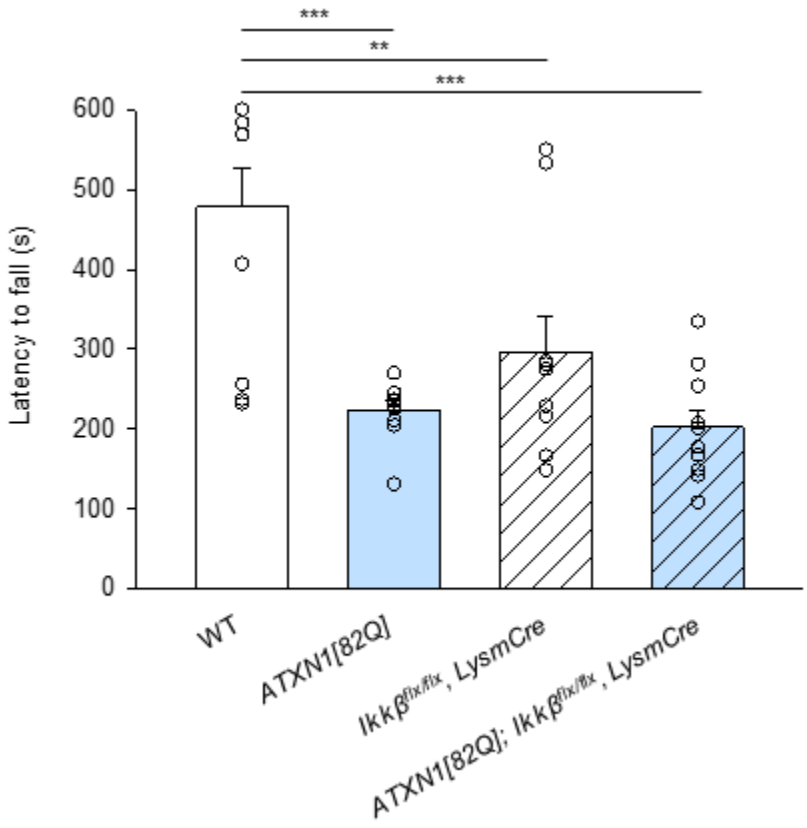

Figure 3. Motor performance of IKKβF/F;LysM Cre and *ATXN1[82Q]; IKKβF/F;LysM* Cre mice. Mice were tested on a rotarod at three months of age. Each dot represents one mouse, and values indicate mean ± SEM, one-way ANOVA followed by Bonfferoni post-hoc test. * P < 0.05, ** P < 0.01, *** P < 0.001. Open bars are WT controls, light blue bars are *ATXN1[82Q]* mice, and hashed bars indicate the presence of IKKβF/F;LysM Cre. Figure from Ferro et al., 2018[32].

We next determined whether microglial IKKβ depletion ameliorates the well-characterized pathological change in Purkinje neurons in SCA1 mice, such as atrophy of Purkinje neuron soma and dendrites[74,157]. To quantify dendritic atrophy, we used

immunofluorescence of parasagittal cerebellar slices with antibodies against calbindin, a marker of Purkinje neurons that labels well their cell bodies and processes. In SCA1 mice Purkinje neuron atrophy can be quantified as decrease in the calbindin intensity or decrease in the width of molecular layer[158]. Importantly neither the molecular layer width nor the intensity of calbindin staining were altered in *IKKβF/F; LysM-Cre* mice compared to control WT mice. As expected we found a reduced width of the molecular layer in *ATXN1[82Q]* mice compared to WT mice; yet this decrease was not significantly altered in *ATXN1[82Q]; IKKβF/F; LysM-Cre mice* (Fig 4A, normalized to N = 5 WT littermate controls *IKKβF/F; LysM-Cre* mice 0.96 ± 0.07, N = 5, *ATXN1[82Q]* mice 0.706 ±0.12, N = 5, *ATXN1[82Q]; IKKβF/F; LysM-Cre* mice 0.68 ± 0.1, N = 5). Similar results were obtained for the intensity of calbindin staining that was equally decreased in both *ATXN1[82Q]* and *ATXN1[82Q]; IKKβF/F; LysM-Cre* mice (Fig 4A, normalized to N = 5 WT littermate controls *IKKβF/F; LysM-Cre* mice 0.96 ± 0.07, N = 5, *ATXN1[82Q]* mice 0.706 ±0.12, N = 5, *ATXN1[82Q]; IKKβF/F; LysM-Cre* mice 0.68 ± 0.1, N = 5).

A recent study identified a set of genes that have reduced expression in Purkinje neurons in SCA1 mice that correlates well with disease progression[157]. As an additional way of testing for health of Purkinje neurons, we quantified the expression of subset of these genes in cerebellar extracts from each of our experimental mice using quantitative reverse transcriptase polymerase chain reaction (qRT-PCR). We have found a decrease in the expression of these genes in *ATXN1[82Q]* mice, as would be expected based on the published data[157]. While expression of these genes showed trend towards milder decrease in *ATXN1[82Q]; IKKβF/F; LysM-Cre* mice compared to *ATXN1[82Q]* littermates, it did not reach statistical significance. Importantly, *IKKβF/F; LysM-Cre* also showed a slight but not significant decrease in gene expression compared to control wild-type littermates (Fig 4C, for example expression of *Homer3* normalized to N = 5 WT littermate controls *in IKKβF/F; LysM-Cre* mice 0.896 ± 0.01, N = 5, *ATXN1[82Q]* mice 0.465 ± 0.06,

N = 5, *ATXN1[82Q]; IKKβF/F; LysM-Cre* mice 0.485 ± 0.07, N = 5, and for Regulator of G protein signaling (Rgs8) normalized to N = 5 WT littermate controls *IKKβF/F; LysM-Cre* mice 0.96 ± 0.11, N = 5, *ATXN1[82Q]* mice 0.41 ± 0.05, N = 5, *ATXN1[82Q]; IKKβF/F; LysM-Cre* mice 0.49 ± 0.07, N = 5). Thus, our results indicate that reducing microglial NF-κB activity early in disease is not sufficient to rescue atrophy of Purkinje neuron dendrites or disease associated gene expression changes.

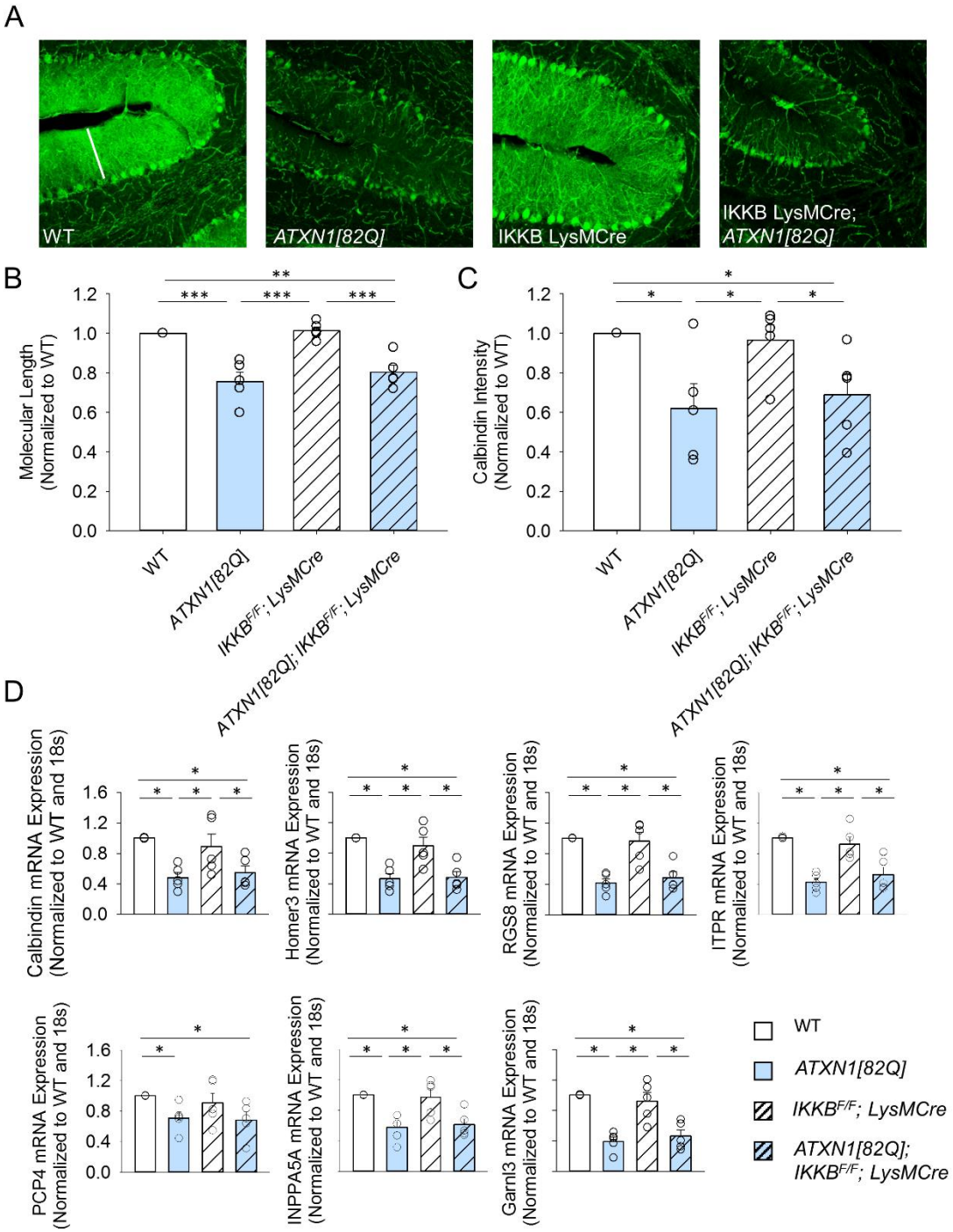

Figure 4. Cerebellar pathology in *IKKβF/F;LysM Cre* and *ATXN1[82Q]; IKKβF/F;LysM Cre* mice. A. Cerebella of 3-month-old mice stained with calbindin antibody, specific for Purkinje neurons. B.

Quantification of the width of the molecular layer,* P < 0.05, Kruskal-Wallis test with Dunn's test, N ≥ 4 per each genotype. C. Quantification of Calbindin intensity, * P < 0.05, Kruskal-Wallis test with Dunn's test, N ≥ 4 per each genotype. D. RNA was extracted from the cerebella of 3-month–old mice and RT-qPCR was used to determine expression of Purkinje neuron genes belonging to Magenta cluster (with reference to control treated wild type littermates and normalized to 18S RNA). N ≥ 3 per each genotype. Each dot represents one mouse, and values indicate mean ± SEM. * P < 0.05, ** P < 0.01, *** P < 0.0001. Open bars are WT controls, light blue bars are *ATXN1[82Q*] mice, and hashed bars indicate the presence of IKKβF/F;LysM Cre. Figure from Ferro et al., 2018 and data collected by Wenhui Qu [32].

2.4 Cerebellar astrogliosis in SCA1 mice is not altered with reduced microglial neuroinflammation

Astrocytes are another type of glial cells that are activated alongside microglia in brain injury[142,159]. Moreover, increasing evidence point to the importance of astrocyte microglial communication in the pathogenesis of neurodegenerative disease[15]. While we have found that both astrocytes and microglia are activated early in SCA1 mice, it is unclear if microglial activation is required or contributes to astrogliosis[114,133]. We thus next examined whether astrogliosis is altered in *ATXN1[82Q]; IKKβF/F;LysM-Cre* mice in which microglial activation is decreased. We determined the level of astrogliosis using immunohistochemistry of parasagittal cerebellar slices with the antibody against marker of astrogliosis, glial fibrillary acidic protein (GFAP)(Fig 5A)[45]. As we have previously demonstrated there was an increase in the intensity of GFAP staining in *ATXN1[82Q]* mice compared to their wild-type littermates. GFAP intensity was not significantly altered in *ATXN1[82Q];IKKβF/F;LysM-Cre* mice compared to *ATXN1[82Q]* mice, indicating that microglial activation is not required for SCA1 astrogliosis. Moreover, *IKKβF/F; LysM-Cre* mice were not different from control WT mice indicating that reduced NF-κB activity does

not cause astrogliosis (Fig 5B, normalized to N = 5 WT littermate *controls IKKβF/F;LysM-Cre* mice 1.04 ± 0.17, N = 5, *ATXN1[82Q]* mice 1.33 ± 0.18, N = 5, *ATXN1[82Q]; IKKβF/F;LysM-Cre* mice 1.39 ± 0.27, N = 6). Classically activated microglia have recently been found to induce expression of neurotoxic astrocytic A1 phenotype[57]. However, we have found only a trend towards lower expression of A1 astrocytic genes, such as decreased expression of complement C3 (*ATXN1[82Q]* mice 1.78 ± 0.28, N = 4, *ATXN1[82Q]; IKKβ$^{F/F}$;LysM Cre* mice 1.48 ± 0.21, N = 4 normalized to N = 4 WT littermate controls, data not shown, P > 0.05 one-way Kruskal-Wallis test with Dunn's test).

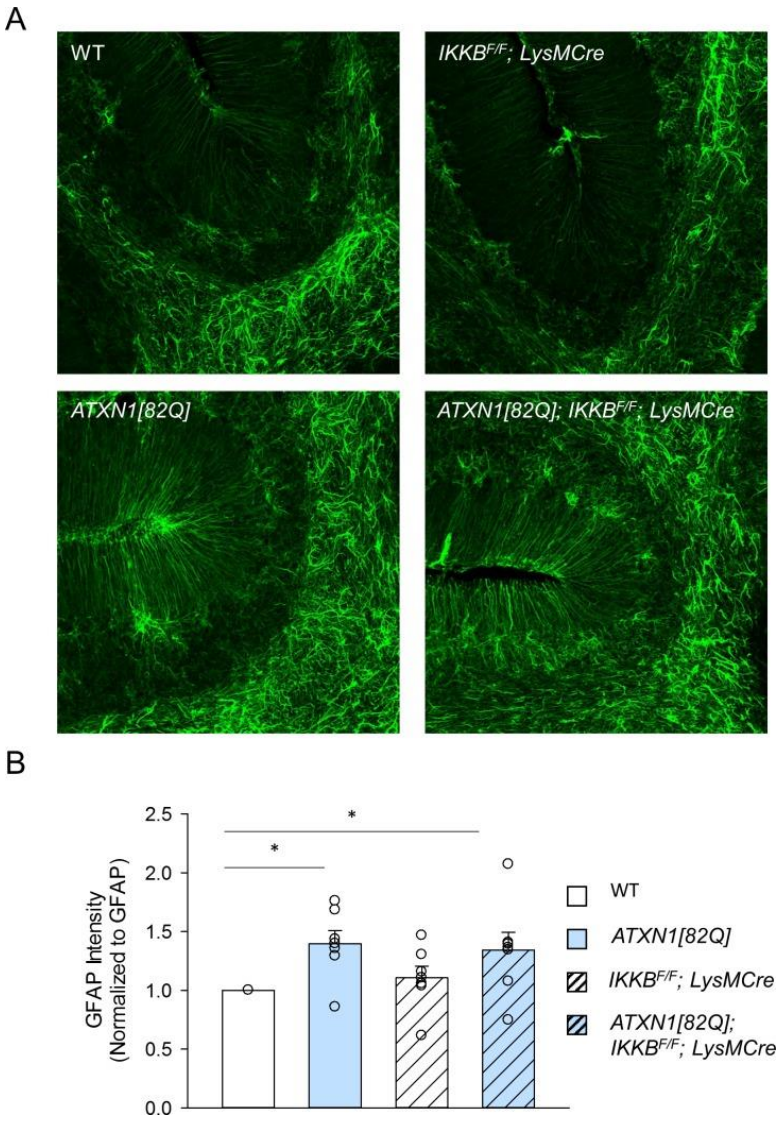

Figure 5. Astrocytic GFAP expression *in IKKβF/F;LysM Cre* and *ATXN1[82Q]; IKKβF/F;LysM* mice. A. Representative image of astrocyte specific GFAP staining B. Quantification of GFAP staining in the molecular layer of 3-month old mice, * indicates $P < 0.05$, Kruskal-Wallis test with Dunn's test, N = 6 per each genotype). Each dot represents one mouse and open bars are WT controls, light blue bars are *ATXN1[82Q]* mice, and hashed bars indicate the presence of *IKKβF/F;LysM Cre.* Figure from Ferro et al., 2018 and data collected by Wenhui Qu [154].

2.5 IKKβ depletion increases PN somatic synapse puncta

While *IKKβF/F;LysM-Cre* mice demonstrated profound motor deficits on rotarod (Fig 3), we did not detect any overt degeneration in Purkinje neurons or cerebellar astrogliosis. Since pharmacological depletion of microglia in adult mice did not cause any motor deficits[74], we reasoned that motor deficits seen in *IKKβF/F;LysM-Cre* mice may be due to developmental effect. Microglia are critical during development where they serve to remove apoptotic cells and synapses. Establishment of the appropriate synaptic connections during brain development is achieved by balancing synaptogenesis with synapse pruning and maturation[21,160]. In cerebellum, shortly after birth, there are multiple climbing fibers (CFs) that contact Purkinje neuron soma, while in adult cerebellum one CF contacts proximal dendrites but not soma of Purkinje neurons[30,161]. Thus, in adult cerebellum approximately only one CF contacts proximal dendrites but not the soma of Purkinje neurons[162,163]. Furthermore, previous studies have shown that reduced synaptic pruning during development and the persistence of somatic puncta on Purkinje neurons impairs motor coordination in mice[31,162].

Since LysM promoter is active from E7[155] it has potential to alter NF-κB –regulated gene expression in microglia and thus their normal function during this critical postnatal period of the cerebellar development. We therefore tested whether there is a retention of somatic puncta in IKKβF/F;LysM-Cre mice. To quantify PN somatic synapse puncta, we

co-stained cerebellar slices with Purkinje cell marker calbindin and a marker of climbing fiber terminals vesicular glutamate transporter 2 (VGLUT2). We found that both IKKβF/F;LysM-Cre mice had significantly more unpruned CF terminal puncta on the soma of Purkinje neurons than WT mice (Fig 6, WT 4.5 ± 0.6, N = 3, IKKβF/F; LysM-Cre mice 10.12 ± 0.24, N = 4, student's t-test, P = 0.0156). This result may suggest that the canonical NF-κB pathway in microglia has important role in pruning somatic synapses on Purkinje neurons during cerebellar development.

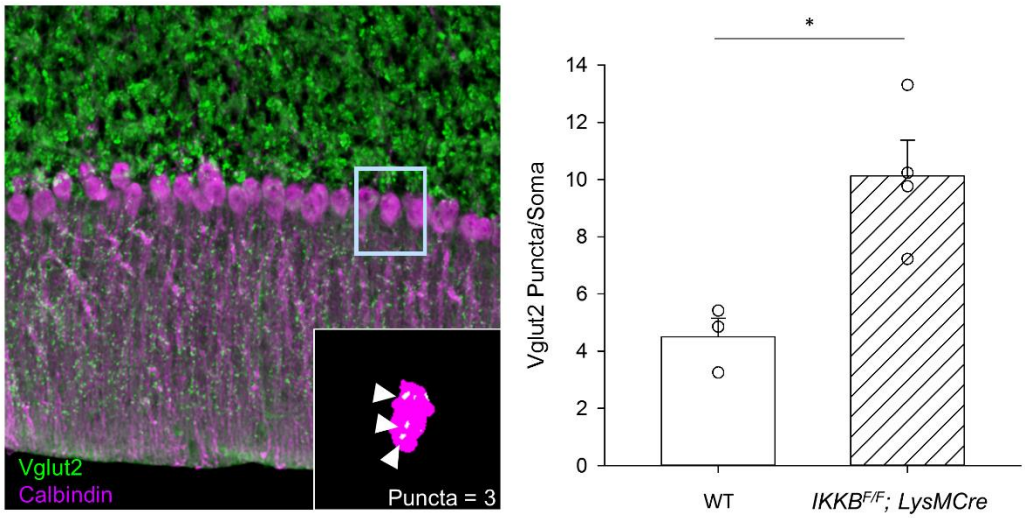

Figure 6. Quantification of the climbing fiber puncta on the soma of Purkinje neurons in *IKKβF/F;LysM Cre* mice. A. Cerebellar slices were co-stained with Calbindin (purple) and VGLUT2 (green). Inset An example of puncta counting. B. Average number of somatic puncta on Purkinje neurons. * P < 0.05, Student's t-test. Figure from Ferro et al., 2018.

2.6 LysM Cre is not selective for microglia

To test the specificity and efficiency of Cre activation in microglia, we crossed LysM Cre mice with reporter Gcamp6 mice[109]. These reporter mice have a floxed-STOP cassette preventing the transcription of the GFP protein. Therefore, LysM expressing mice

should express the GFP protein due to excision of the stop codon. Cerebellar slices from Gcamp6-LysmCre were analyzed with both Iba1 (microglial) and parvalbumin (PV) (inhibitor neuron) markers to determine the specificity and efficiency (Fig 7A). Surprisingly, only around 10-15% of cerebellar microglia expressed GFP, a low efficiency that has previously been demonstrated[164] and may have contributed to the low level effects seen in *ATXN1[82Q]; IKKβF/F* mice. Furthermore, we were surprised to detect ~20% GFP+ inhibitory neurons in both the molecular layer and Purkinje cell layer. We attempted to confirm these results with IKKβ immunohistochemistry on cerebellar slices but were unable to get good signal using several commercially available antibodies against IKKβ. Thus, it is possible that both pruning and motor deficits in *the IKKβF/F;LysmCre* mice may be caused by loss of IKKβ in cerebellar neurons.

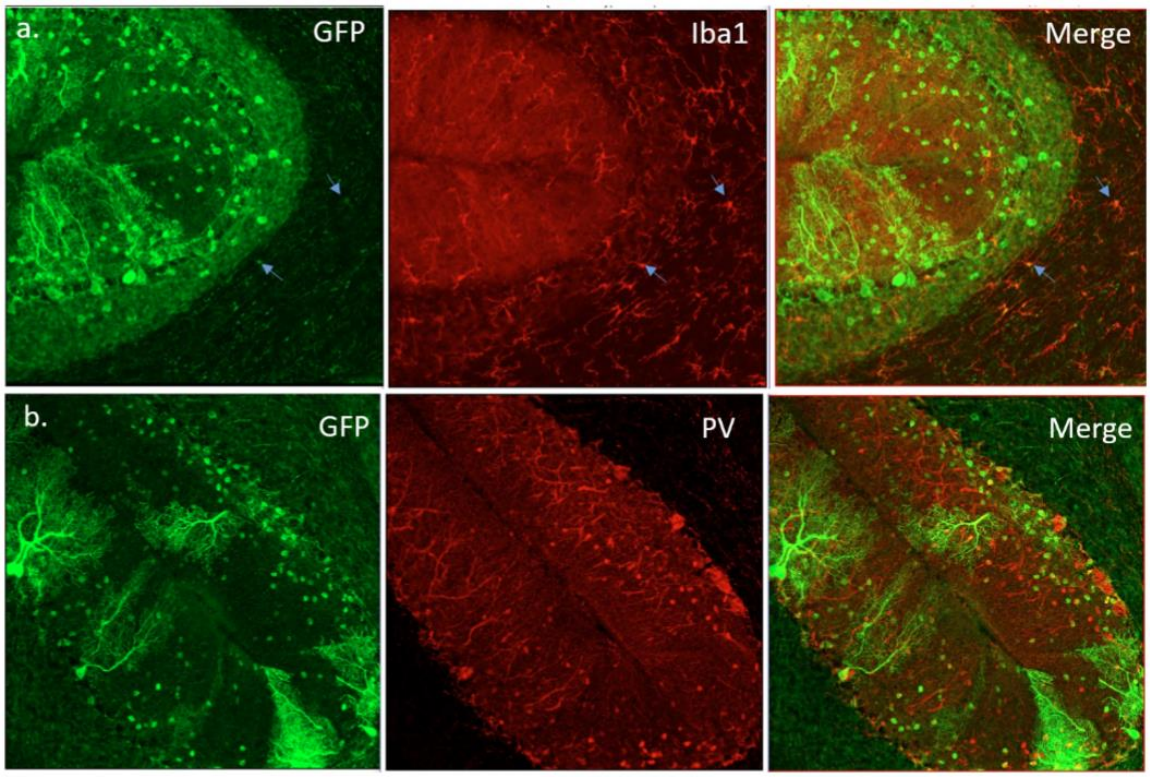

Figure 7. LysM Cre activity is not restricted to microglia cells. Cerebellar slices from *LysM-Cre GCamp6* mice were co-stained for GFP, indicating Cre activity and markers of microglia (Iba1) and

inhibitory interneurons [Parvalbumin (PV)]. A. Representative confocal images of GFP and Iba1 co-staining. Arrows indicate cells that are both GFP positive and Iba1 positive. Around 10% Iba1 positive cells are also GFP positive. B. Representative confocal images of GFP and PV co-staining. Around 20% PV-positive cells are also GFP positive. Figure from Ferro et al., 2018.

2.7 Discussion

We have found that *ATXN1[82Q];IKKβ$^{F/F}$;LysM Cre* mice have reduced microglial density and TNF-α expression in cerebellum, but undistinguishable motor and cerebellar neurological phenotype compared to *ATXN1[82Q]* mice. Moreover, we have found motor deficits in *IKKβ$^{F/F}$;LysM Cre* mice that were dissociated from overt Purkinje cell degeneration but instead, associated with abnormal retention of climbing fiber synapses on Purkinje soma. These results may indicate that microglial NF-κB signaling is important for pruning of immature surplus synapses during cerebellar development, but it is not critical to the pathogenesis of SCA1.

Microglia are the resident phagocytic cells of the brain that derive from primitive myeloid progenitors in yolk sac and populate the brain during early embryonic development. As such, microglia are well positioned to influence brain development and sculpt functional neuronal connections, including elimination of synapses and neurons. Pruning of immature surplus synapses is critical for the establishment of the appropriate synaptic connections during brain development[21,160]. In cerebellum, shortly after birth, there are multiple climbing fibers (CFs) that contact Purkinje neuron soma, while in adult cerebellum one climbing fiber contacts proximal dendrites but not soma of Purkinje neurons[159]. This change in wiring is achieved during postnatal days (P) 7–21 when one "winning" CF translocate synapses to the proximal dendrites of Purkinje neurons while CF synapses on the soma of Purkinje neurons are pruned[163]. Since previous studies have shown that reduced synaptic pruning during development and ensuing persistence of

somatic puncta on Purkinje neurons can impair motor coordination in mice[31,162], it is possible that observed persisting somatic CF synapses in Purkinje neurons in adult *IKKβ$^{F/F}$;LysM Cre* mice could contribute to motor deficits exhibited by these mice. While role of microglia in the cerebellar development is not well understood[165], our novel results may suggest that the canonical NF-κB pathway in microglia, typically considered as pro-inflammatory, is required for the removal of immature synapses during cerebellar development.

In chronic disease microglia are thought to be neurotoxic in part due to the increased production of pro-inflammatory cytokine TNF-α. TNF-α is one of the key microglial cytokines that modulates synaptic strength in response to neuronal activity in physiological conditions[166]. As different levels of TNF-α are known to increase or decrease synaptic strength, regulation of its expression in microglia is tightly regulated, in part through NF-κB signaling[167,168]. In our previous experiments we have demonstrated that microglial density is increased pre-symptomatically in SCA1 mice concurrent with increased production of TN-Fα[45]. Moreover, we have found that pharmacologically depleting microglia early in SCA1 reduced production of TNF-α[74], indicating that microglia produce most of TNF-α in SCA1 mice. However, despite the observed decrease in microglial density and expression of TNF-α, SCA1 motor and neurological pathology were not ameliorated in *ATXN1[82Q];IKKβ$^{F/F}$;LysM Cre* mice. While these results may suggest that microglia and TNF-α expression are not critical for the pathogenesis of SCA1 during early stages of disease, it is important to note that neither microglial density nor TNF-α expression were fully reversed.

One likely reason for the partial reduction of neuroinflammation and the lack of differences between *ATXN1[82Q]* and *ATXN1[82Q];IKKβ$^{F/F}$;LysM Cre* mice is the low efficiency of *LysM Cre* line. Using reporter mice we have found that approximately 15% of cerebellar microglia showed Cre activity as was previously demonstrated[164]. Thereby, it is

possible that inhibition of microglial NF-κB pathway is beneficial in SCA1, but that due to the low efficiency of Cre recombination in *LysM Cre* line, we did not reach the threshold of NF-κB inhibition necessary for the significant alteration of disease phenotype.

However, it is important to note that this low efficiency of *LysM Cre* line was sufficient to modulate pathogenesis is mouse models of several conditions, including AD[59,153], Rett syndrome[169], multiple sclerosis[170], ischemia[164], obesity[171], and depression[172]. For example, genetic deletion of IKKβ in microglia ameliorated neuronal loss in a mouse model of excitotoxicity and ischemic brain injury[164]. LysM Cre deletion of IKKβ in the microglia of mouse model of multiple sclerosis, experimental autoimmune encephalomyelitis (EAE) mice, delated the onset and alleviated the severity of EAE neurological symptoms, such as ataxia and paralysis of limbs[170]. Furthermore, *LysM Cre* mice were used to demonstrate that microglial progranulin deficiency increases plaque deposition and impairs phagocytosis in AD[59] and that targeted expression of MECP2 in myeloid cells, driven by *LysM Cre* promoter in an Mecp2-null background attenuated pathology in a mouse model of Rett syndrome[169]. Thus, because low efficiency of *LysM Cre* had a significant effect in these other diseases, it is also possible the role of microglia in pathogenesis may be specific to each disease or to the stage of disease[173]. For example, Liao et al. (2012) demonstrated that in mouse model of ALS microglia have neuroprotective role at disease onset, whereas at the end-stage of disease microglia have a neurotoxic role, supporting the transformation of microglial phenotype during disease progression.

In this study we have focused on the early stages on SCA1, due to their significant therapeutic potential. It is possible that role of microglial neuroinflammation in the pathogenesis of SCA1 may change as the extent of injury worsens with disease progression. Future studies testing the role of microglial NF-κB signaling in the late stage of SCA1 using inducible Cre-LoxP system are needed to address this question. However,

cerebellar microglia are not well studied, and it is also possible that cerebellar microglia may play a different role in disease than microglia in other brain regions. Genome-wide analysis of microglia from different brain regions demonstrated that cerebellar microglia exist in a more immune-vigilant state that is further augmented during aging[43]. Time-lapse in vivo imaging, found that cerebellar microglia have decreased parenchymal surveillance compared to cortical microglia[174]. Thus, our data may also indicate that cerebellar microglia and in particular NF-κB signaling behave differently in disease compared to microglia from other brain regions.

Another possible explanation for the observed lack of amelioration of disease phenotype in *ATXN1[82Q];IKKβ$^{F/F}$;LysM Cre* mice is that reactive astrocytes have a predominant role in contributing to the pathogenesis of SCA1. Astrocytes have numerous important functions in the brain, including structural and metabolic support of neurons, and regulation of extracellular ion and neurotransmitter homeostasis[175,176]. Similar to microglia, astrocytes also undergo activation in neurological diseases that results in morphological and functional changes, including enlarged cell bodies, thickening of cell processes, and alteration in their ability to maintain homeostasis and to provide neurotrophic support. Liddelow et al. demonstrated that LPS activated microglia induce neurotoxic phenotype of astrocyte though the secretion of pro-inflammatory cytokines, including TNF-α[57]. We have not detected a significant alteration of astrogliosis, measured as increased expression of GFAP and A1-associated genes in *ATXN1[82Q];IKKβ$^{F/F}$;LysM Cre* cerebella, indicating that reduced microglial density and TNF-α expression may not be sufficient to affect astrogliosis and its possible neurotoxic effects in SCA1 mice.

Finally, when interpreting disease phenotype in *ATXN1[82Q]; IKKβ$^{F/F}$;LysM Cre* mice we need to consider specificity of the *LysM Cre* line[59,155,177,178]. We examined the cerebellar cell specificity of the *LysM Cre* line, by crossing them with the reporter line[109], and were surprised to find evidence of Cre recombination not only in microglia as

expected, but also in neuronal cells including Purkinje neurons and parvalbumin (PV) positive interneurons. Thus, it is possible that a decrease in microglial NF-κB and neuroinflammation in the cerebellum may have a beneficial effect on SCA1 pathogenesis, but this is masked by a negative effects of decreased NF-κB in Purkinje neurons[53]. Similarly, while the observed retention of climbing fiber puncta on the soma of Purkinje neurons is sufficient to cause motor deficits in *IKKβ$^{F/F}$;LysM Cre* mice, it is possible that decreased NF-κB activity in Purkinje neurons contributes to the these motor deficits.

In addition, while efficiency of LysM Cre mediated deletion may be higher in the cerebellum compared to the other regions of the brain[179], it is by no means limited to the cerebellum. Thus, it is possible that loss of IKKβ in other brain regions contributes to the impaired motor phenotype of *IKKβ; LysM Cre* mice. We have not found any change in microglial density or morphology in the striatum, a brain region involved in the control of movement, but we cannot exclude subtle changes in microglial function. To resolve these issues of cell and region specificity of IKKβ depletion future studies using more selective Cre lines or AAV viruses expressing Cre recombinase to selectively target cerebellar microglia, Purkinje neurons or PV interneurons are needed. Moreover, previous studies, including the comprehensive evaluation of several myeloid-expressing Cre strains, have demonstrated LysM-Cre mediated deletion in macrophages, neutrophils, and monocytes[180,181]. Thus, while depletion of IKKβ in microglia may be beneficial in the context of SCA1 (e.g. by lowering neuroinflammation), it is possible that loss of IKKβ in these other myeloid cells may negatively impact on the motor function in mice and thereby contribute to the unaltered disease severity in *ATXN1[82Q];IKKβ$^{F/F}$;LysM Cre* mice or to the motor deficits in *IKKβ$^{F/F}$;LysM Cre* mice. Importantly this study strongly cautions against using *LysM Cre* mice to study microglia specific effects and calls for considering neuronal and myeloid cell recombination when re-interpreting previous CNS studies using these mice.

2.4 Materials and Methods

Mouse lines

ATXN1[82Q], *IKKβ*$^{F/F}$ and *LysM Cre* mice were generated as previously described[70,155,171]. Because our previous studies have detected no sex-specific effects in SCA1, we have used an equal mix of animals of both sexes for our experiments. All animal experiments were performed in compliance with the National Institutes of Health's Guide for the Care and Use of Laboratory Animals and the University of Minnesota Institutional Animal Care and Use Committee.

The protocol was approved by the University of Minnesota Institutional Animal Care and Use Committee (protocol number 1511-33160A).

Rotating rod test

Motor deficits were assessed using rotarod assay at the age of 3 months. The rotarod test was performed as previously described[182]. Briefly, mice were placed on the rotarod apparatus (Ugo Basile) that accelerates from a speed of 4 rotations per minute (rpm) to 40 rpm over a 5-minute period. We recorded the time it takes for a mouse to fall off rotarod, to a maximum of 10 minutes. Mice were subjected to four trials per day for four consecutive days, with at least ten minutes of rest between each trial. Data for the performance on day 4 was analyzed using one-way ANOVA with Bonferroni post-hoc test. Significance was assumed at $P < 0.05$. All tests were performed blinded with respect to the genotype.

Immunohistochemistry

Mouse brains were fixed overnight in 4% formaldehyde, incubated in 30% sucrose, and cut into 45 μm sections on cryostat (Leica, CM 1850). Sections were washed three times in cold Phosphate Buffered Saline (PBS), and incubated in blocking buffer (3% Normal

Donkey Serum in PBST (1% Triton X-100 PBS) for 1 hr. at room temperature (RT). This was followed by an overnight incubation at 4°C in blocking buffer containing the relevant primary antibody [anti-GFAP (Z0334, DAKO), anti-Iba1 (019–19741, WAKO), anti-Calbindin-D-28K (C9848, Sigma Aldrich), anti-VGLUT2 (MAB5504, Millipore), anti-ataxin1 (11NQ, a gift from Dr. Harry Orr)]. After incubation with primary antibody we washed samples three times with PBS, and incubated them overnight at 4°C with the relevant fluorescently labeled secondary antibody (Alexa, Invitrogen). We mounted stained sections on slides with Vectashield mounting media containing DAPI (Vector Laboratories) for imaging at 20X magnification under the confocal microscope (Olympus FV1000). For each mouse, we imaged at least six different, randomly selected cerebellar lobules. Each image consisted of 20 µm Z-stacks, composed of 1µm thick image slices. Images were analyzed using FIJI (ImageJ, NIH) software. For analysis of calbindin length and intensity, we drew a straight line extending from the middle of Purkinje cell body to the end of the molecular layer in at least two places for each lobule. We then used the Measure function in ImageJ to quantify the length of the line to obtain measurement of the width of the molecular layer, and the average intensity along the line to obtain calbindin intensity. For GFAP staining, we used the Measure function in ImageJ to quantify the intensity of signal in the molecular layer that was then normalized to the average intensity in the control group (wild-type mice). For microglial Iba1 staining, we counted the Iba1 positive cells and to obtain microglial density we divided the number of Iba1 positive cells by the area in which they were counted. Staining, microscopy, and image analysis were performed blinded to the experimental groups. Data was analyzed using ANOVA with Bonferroni post-hoc test using GraphPad Prism software (GraphPad software).

For counting puncta, tissue was stained in the same manner using antibodies against calbindin and VGLUT2 and then imaged at 60X magnification (20 µm Z stack, 1 µm Z

step). Images were then processed using an in-house written ImageJ macro that would segment the calbindin and VGLUT2 signals, and procedurally count VGLUT2 puncta (minimum size 1.4 μm^3, maximum μm^3 70.3 size filter for puncta) on somata of Purkinje cells, defined by volume segmentation (minimum/maximum volume 281.3 and 7,031.3 μm^3 respectively). Resultant images of segmented somata and counts were filtered by hand to remove artefactual somata. Counts were compared using a student's t test.

Quantitative real time RT-PCR

Total RNA was isolated from cerebella using TRIzol (Invitrogen) and treated with DNAse (TURBO Dnase, Thermo Fisher Scientific). Complementary DNA (cDNA) synthesis was performed in duplicate, using Superscript III First-Strand Synthesis SuperMix (Invitrogen) and random hexamer primers. The expression level of each gene was determined on a Light Cycler 480 II (Roche) using Light Cycler 480 SYBR Green PCR I Master mix (Roche). Cycling conditions were: 5 min at 95°C, followed by 40 cycles of 95°C for 15 sec, 56°C for 1 min. Samples were analyzed in triplicate and a melting curve analysis was performed in each sample at the end of the qPCR reaction to confirm specificity of reaction. Expression levels of mouse 18S RNA (forward primer: 5'AGT CCC TGC CCT TTG TAC ACA 3' and reverse primer: 5' CGA TCC GAG GGC CTC ACT A -3') were used as internal controls. Primers used for the Purkinje neuron's Magenta cluster genes (*calbindin*, *ITPR*, *INPP5a*, *Garnl3*, *Pcp4*, *Homer3* and *Rgs8*) were from Ingram et al. (2016), and primers used for astrocytic genes (*Kir4.1*, *EAAT1*, *P2RY*, *Aqp4*, *C3*, *S100*, and *Glul)* and microglial gene (*TNF-α*) were PrimeTime qPCR primers (IDT). Relative gene expression was determined by the $2^{-\Delta\Delta Ct}$ method[128]. The threshold cycle (Ct) value was determined for target genes and the endogenous internal controls (18S RNA) in each sample. The difference between target gene and 18S RNA control Ct values was determined for each sample, resulting in the ΔCt value. The ΔCt of a calibrator, a wild type

sample, was subtracted from each sample's ΔCt to yield the ΔΔCt value. Relative fold change was calculated as $2^{-\Delta\Delta Ct}$. Data was analyzed using ANOVA with Bonferroni post-hoc test using GraphPad Prism software (GraphPad software).

Western blotting

Cerebella were dissected from mice and lysed in RIPA lysis buffer [50mM Tris HCl, pH7.4, 150mM NaCl, 1% sodium deoxycholate, 1% NP-40, 0.2% SDS, phosphatase (Sigma) and protease inhibitors cocktail (Roche)]. After three cycles of freeze and thaw, proteins were separated on a 12% or 15% SDS-PAGE gel and transferred onto a nitrocellulose membrane. The following primary antibodies were used: anti-ATXN1 (rabbit 11NQ, Orr lab), anti-PSD95 (Biolegend), and alpha-tubulin (mouse, Sigma). Signals from secondary antibodies linked to horseradish peroxidase (HRP) (GE Healthcare) were detected using Amersham ECL Western Blotting Detection Reagent (GE Healthcare) and ImageQuant LAS 4000 imager (GE Healthcare); protein levels were quantified using ImageQuant (GE healthcare) and ImageJ. Data was analyzed with one-way ANOVA followed by Bonferroni post-hoc test.

Statistical analysis

Statistical tests were performed with GraphPad Prism or R. For rotarod, we have used one-way ANOVA followed by either Tukey's HSD or Bonferroni post-hoc test. For IHC, qRT-PCR, and Western blot quantification, we have also used Kruskal-Wallis test with Dunn's test or one-way ANOVA followed by Bonferroni post-hoc test.

Chapter 3. The role of Astrocyte in Ataxias

3.1 Introduction

The predominant hypothesis of SCA1 neuropathology is that ATXN1's transcriptional and splicing regulatory activity becomes dysfunctional upon polyQ expansion[157]. This ATXN1 neurodegenerative pathway has been well characterized in cerebellar Purkinje neurons using both the *Atxn1*$^{154Q/2Q}$ and the Purkinje cell specific *PCP2-ATXN1[82Q]* (*ATXN1[82Q]*) mouse models of SCA1. In the *ATXN1[82Q]* mouse model, it has been shown that polyQ expanded ATXN1 requires nuclear localization for Purkinje cell pathology and the associated motor deficits[183–185]. Furthermore, polyQ expanded ATXN1 requires its nuclear binding partner Capicua (CIC), a transcriptional repressor, for cerebellar degeneration[186]. Lastly, there is major transcriptional dysregulation in both the cerebellum and medulla in the *Atxn1*$^{154Q/2Q}$ mouse model that suggests that the abhorrent transcriptional and splicing activity of ATXN1 is contributing factor to SCA1 pathology[1,13].

One aspect of SCA1 that has been overlooked until recently is the role of other cell types within the brain, such as astrocytes and microglia. Both are reactive in both mouse models of SCA1, and prominent astrogliosis is seen in the medullary nuclei and cerebellum of SCA1 patients[32,45,129]. Even so, we have recently observed only minor contributions of microglia to cerebellar pathology in microglial depletion studies, and nuclear factor kappa b (NF-κB) inhibition studies[32]. However, we have shown that in the *ATXN1[82Q]* mouse model that astrocytic activation NF-κB has a biphasic effect on SCA1, where early cell non-autonomous activation is beneficial to overall neural health, and late N-FκB activation is neurodestructive suggesting a cell non-autonomous effect of astrocytes due to the restricted expression of pathogenic ATXN1 to Purkinje cells[131]. Yet, due to the directed expression of ATXN1, has limited previous studies to the cell non-autonomous effects of astrocytes.

The Purkinje cell specific expression of ATXN1 in the *ATXN1[82Q]* is especially problematic when looking at endogenous *Atxn1* expression. Recently, Barres group published an RNA-seq database of the expression patterns of brain cells using purified cortical suspensions (http://www.brainrnaseq.org/)[80]. Using this resource to observe cell-type specific expression of *Atxn1* shows that mouse cortical astrocytes (FPKM = 2.4531 ± 0.2061) express *Atxn1* at a near equal level to that of neurons (FPKM = 3.1594 ± 0.6083)(Fig 8). Furthermore, it has recently been reported in a brain region and disease stage RNAseq comparison study that overall gene transcription alterations differ between the *ATXN1[82Q]* and the *Atxn1*$^{154Q/2Q}$ mouse model. The differential gene transcription alongside astrocytic expression of *Atxn1* suggests polyQ expanded ATXN1s differential effect on a variety of cell types[1].

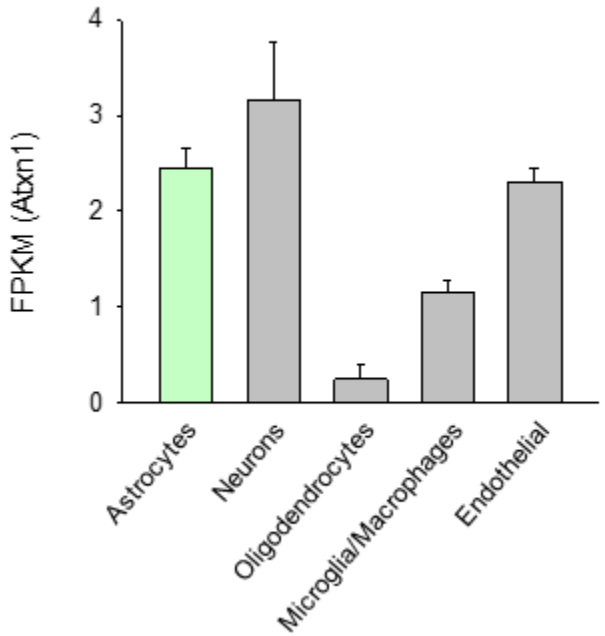

Figure 8. Cortical cell type purification RNAseq shows ATXN1 expression is found in both astrocytes and neurons.

Therefore, in this chapter, we aim to determine the cell autonomous effect of ATXN1 and its underlying contribution to SCA1 pathology in various knock-in models of SCA1. Here we show that astrocytes downregulate their expression of the potassium inward rectifier 4.1, otherwise known as Kir4.1 or *Kcnj10*, in multiple knock-in mouse models including the *Atxn1*$^{154Q/2Q}$ mouse model of SCA1. Kir4.1 has recently been implicated as an astrocytic disease associated gene[119–121,187]. Here I show the downregulation of Kir4.1 is dependent on both the endogenous expression of ATXN1, the expansion of the polQ domain, and the intracellular trafficking of ATXN1. Using the novel conditional humanized model of SCA1, humanized *ATXN1*$^{146Qfloxed/2Q}$, we found that astrocyte expression of polyQ expanded ATXN1 is potentially required for downregulation of Kir4.1.

3.2 Prominent downregulation of Kcnj10 in disease associated brain regions

One prominent function of astrocytes is the maintenance of the extracellular space, where they regulate the concentration of neurotransmitters and ions including potassium. The main mediator of potassium buffering is *Kcnj10*, otherwise known as the potassium inward rectifier 4.1, which is required for maintenance of both the astrocyte and neuron resting membrane potential[97,98]. Due to *Kcnj10*'s apparent function in multiple neurodegenerative disorders, including cerebellar ataxias and polyQ disorders, we sought to quantify *Kcnj10* expression in both the *ATXN1[82Q]* transgenic and the *Atxn1*$^{154Q/2Q}$ knock-in mouse models of SCA1. Using reverse transcriptase quantitative PCR (RT-qPCR) we found a severe downregulation of *Kcnj10* in the cerebellum of *Atxn1*$^{154Q/2Q}$ mice (n = 3, 0.717± 0.0534) when compared to wild-type (WT)(n = 4, 1 ± 0.0558) mice ($p<0.001$, $t = 6.753$, $df = 5$), but not in the cerebellum of the *ATXN1[82Q]* mice(WT: n = 5, 1.000 ± 0.0299; *ATXN1[82Q]*: n = 6, 0.964 ± 0.0716)(p=0.321)(Fig. 9A,B; Appendix Fig 1,2). The clear downregulation in *Kcnj10* was not restricted to the cerebellum, and was also present

in the medulla at 15 (WT: n = 4, 1.000 ± 0.0461; *Atxn1*$^{154Q/2Q}$: n = 3, 0.677 ± 0.0489; p = 0.00515) and 26W (WT: n = 4, 1.000 ± 0.0619; *Atxn1*$^{154Q/2Q}$: n = 3, 0.716 ± 0.0815; p = 0.0365). (Fig. 9B). Furthermore, when looking through multiple RNAseq datasets of various brain regions, we found that *Kcnj10* is downregulated throughout the brain (Table 1) with the medulla having the most significant downregulation[1,13].

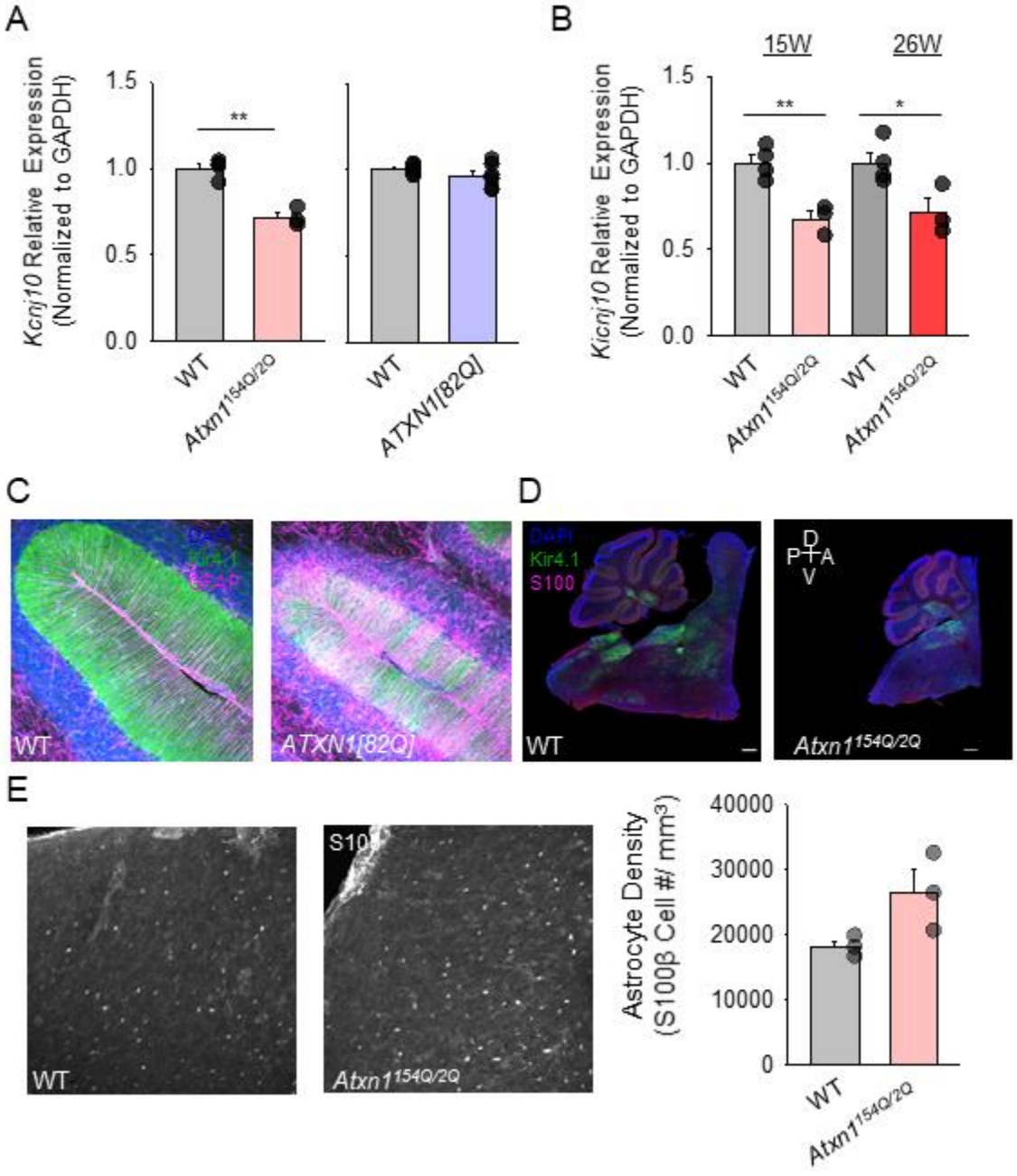

Figure 9. Astrocytes alter their expression of *Kcnj10* in the *ATXN1*^{154Q2Q} mouse line. (A) RT-qPCR of Kir4.1 (*Kcnj10*) in 26W *Atxn1*$^{154Q/2Q}$ (p <0.001. *t* = 6.753, *df* = 5) and *ATXN1[82Q]* (p > 0.05, t = 1.050, *df* = 9) cerebella relative to age matched WT controls. (B) RT-qPCR of KCNJ10 in the medulla of *Atxn1*$^{154Q/2Q}$ and age matched WT mice at 15 (WT: n = 4, 1.000± 0.0923; *Atxn1*$^{154Q/2Q}$: n = 3, 0.677± 0.0847; p = 0.00515) and 26W (WT: n = 4, 1.000± 0.124; *Atxn1*$^{154Q/2Q}$: n = 3, 0.716± 0.141; p = 0.0365) (C-D) Immunofluorescent confocal imaging of Kir4.1 and astrocyte markers at 20X and 40X. (E) Counts of astrocytes within the lateral vestibular nuclei (WT n = 3, *Atxn1*$^{154Q/2Q}$ n = 3; p = 0.0797, *t* = -2.336, *df* = 4). Data represented as mean ± S.E.M. and analyzed with student t-test.

Brain Region	LogFC	q Value
Cerebellum	-0.53	2.58E-03
Cortex	-1.42	1.83E-06
Striatum	-0.57	4.71E-07
Hippocampus	-0.51	2.25E-08
Medulla	-0.88	1.39E-40

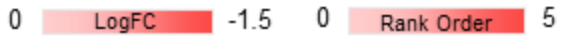

Table 1. RNAseq reveals that Kir4.1 downregulation is a global occurrence in the *Atxn1*$^{154Q/2Q}$ mice at 26W, where q is the adjusted p value (GSE114674)[13].

Astrocyte Marker	Log2 Fold Change	Adjusted p value
Gfap	-0.27	0.148354
Slc1a3	0.03	0.999663
Glul	-0.24	0.555308
Glt1d1	0.04	0.999663
Aldh1l1	-0.07	0.999663

Table 2. RNAseq reveals that astrocytic markers in the inferior olive of *Atxn1*$^{154Q/2Q}$ mice at 12W are unchanged when compared to WT controls (GSE122099)[1].

It is possible that the downregulation of *Kcnj10* could be due to the death of medullary astrocytes, and therefore we assessed astrocyte number using immunofluorescent confocal imaging of *Atxn1*$^{154Q/2Q}$ at 15W of age. At this time point, astrocyte numbers within the lateral vestibular nucleus of the medulla, an easily identifiable nucleus within the medulla, are not statistically different between the *Atxn1*$^{154Q/2Q}$ (n = 3, 1.8085x10^4 ± 9.2451x10^2 astrocytes/mm^3) and WT (n = 3, 2.6423x10^4 ± 3.4474x10^3 astrocytes/mm^3) mice *Atxn1*$^{154Q/2Q}$ mice ($p = 0.0797$, $t = -2.336$, $df = 4$) (Fig1E). Yet, when looking at RNAseq data from a later stage of disease progression (26W), astrocyte cell death may account for some of the downregulation (Tables 2 and 3), and we are missing this overt glial death near the 15 week timepoint (Table 2). Therefore, the downregulation of *Kcnj10* at 14W of age does not seem to be due to astrocytic death, and if anything, the trending increase in astrocytic number may suggest a greater downregulation per astrocyte.

Astrocyte Marker	Log2 Fold Change	Adjusted p value
Gfap	-0.78	7.32E-13
Slc1a3	-0.08	0.38
Glul	-0.71	3.41E-19
Glt1d1	-0.02	0.91
Aldh1l1	-0.36	6.41E-06

Table 3. RNAseq reveals that many astrocytic markers in the medulla of *Atxn1*$^{154Q/2Q}$ mice at 26W are largely downregulated, suggesting astrocyte death may be occurring at this age.

3.3 Kcnj10 downregulation is dependent on Atxn1 polyQ tract length and the endogenous promoter

We next wanted to determine if the apparent effect of polyQ expanded ATXN1 on Kir4.1 was a gain or loss of the normal function of ATXN1. Therefore, we probed *Kcnj10* expression in cerebella of both the *ATXN1-/-* knockout mice and the *Atxn1*$^{82Q/2Q}$ knock-in

in mice. We found that at 7W of age, there was no significant effect of knocking out ATXN1 on *Kcnj10* ($p > 0.05$, $t = 0.603$, $df = 5$)(Fig 10A). The lack of effect of ATXN1 knockout on *Kcnj10* suggesting that any effect on *Kcnj10* expression is not due to loss of function. Rather, when we probed the $Atxn1^{82Q/2Q}$ knock-in in mice, we found that there was non-significant effect of the effect on *Kcnj10* caused by the non-pathogenic expanded polyQ allele (Two tailed Student T test, $p = 0.0919$, $t = 2.081$, $df = 5$)(Fig 10B). The lack of effect of the knock-in line with the clear lack of affect caused by the ATXN1 knockout suggests the requirement of polyQ expanded ATXN1, driven by its endogenous promoter, to observe *Kcnj10* expression. This data, alongside the lack of a cell non-autonomous effect seen in the *ATXN1[82Q]* mice therefore would suggest a cell autonomous interaction of *ATXN1* and *Kcnj10* expression. Furthermore, the lack of affect due to ATXN1 knockout suggests that this interaction is a gain of function mutation that is dependent on the polyQ tract.

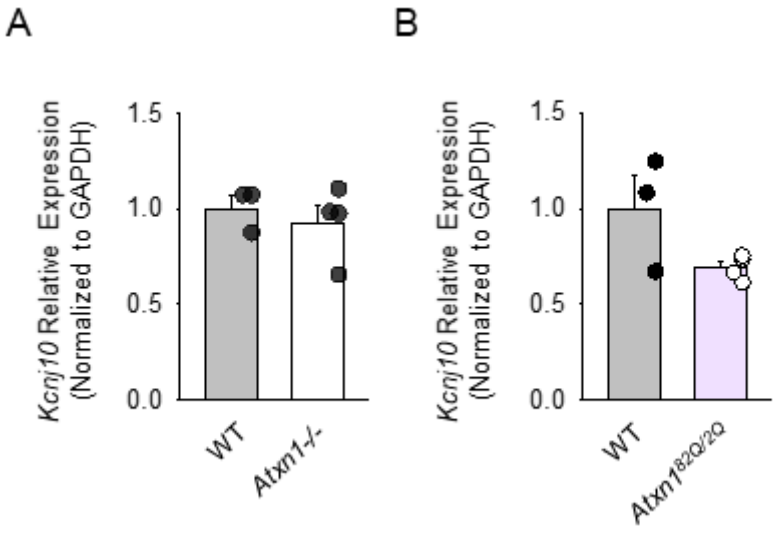

Figure 10. Cerebellar Kir4.1 expression is not affected in *Atxn1* null mice at 7W, but trends towards downregulation in the $Atxn1^{82Q/2Q}$ knock-in mice. Two tailed student t-test ($p > 0.05$, $t = 0.603$, $df = 5$) and ($p = 0.0919$, $t = 2.081$, $df = 5$) respectively.

3.4 Disruption of Atxn1^{154Q}'s nuclear localization sequence reduces KCNJ10 downregulation

With evidence for a cell-autonomous effect of ATXN1 on astrocytic transcription of *Kcnj10*, we next asked if ATXN1 nuclear localization is required. To test this, we used the novel nuclear localization knock-in *Atxn1*$^{154Q\text{-}K772T/2Q}$ mouse model recently created by the Orr lab (personal communication). To create this model, the lysine residue at 772 was replaced with a threonine via CRISPR/Cas9 directed recombination (*in preparation*; data not shown). Previously, this K772T mutation had been used in the Purkinje cell specific *ATXN1[82Q]* transgenic model to show that Purkinje cell degeneration, and subsequent motor dysfunction, required nuclear ATXN1 protein[185]. Preliminary data on the knock-in K772T model suggests that, similarly to the *ATXN1[82Q]-K772T* model, mutating the nuclear localization sequence of ATXN1 can reduce overall motor pathology (*in preparation*; data not shown). Furthermore, *Atxn1*$^{154Q\text{-}K772T/2Q}$ have a reduced early lethality, extending mean lifespan of these mice by 21.71 weeks, suggesting that the nuclear localization sequence also contributes to medullar pathology (*in preparation*; data not shown).

Therefore, we hypothesized that like Purkinje cells, ATXN1 nuclear localization in astrocytes would be required for ATXN1 mediated transcriptional changes and therefore *Kcnj10* downregulation. Yet, when comparing the medullar transcriptome of the *Atxn1*$^{154Q\text{-}K772T/2Q}$ animals against WT controls and *Atxn1*$^{154Q/2Q}$ mice at 27 weeks using bulk RNAseq. We found that *Kcnj10* downregulation had been attenuated, but not fully ameliorated. There was a significant increase in *Atxn1*$^{154Q\text{-}K772T/2Q}$ *Kcnj10* relative to *Atxn1*$^{154Q/2Q}$ (adjusted $p < 0.001$), yet there was still a significant downregulation found in *Atxn1*$^{154Q\text{-}K772T/2Q}$ mice relative to WT mice (adjusted $p < 0.001$) (Fig 11A). This was confirmed using RT-qPCR, which demonstrated a significant downregulation of *Kcnj10* only when

comparing *Atxn1*$^{154Q/2Q}$ (n = 4) and WT (n = 8) mice (ANOVA: $p < 0.001$, $F = 14.061$, $df = 17$; Tukey post hoc $p < 0.001$)(Fig 11B).

3.5 Knockdown of Atxn1 using ASOs ameliorates Kcnj10 expression

Recently, the Orr lab had developed one of the first possible therapeutics to treat SCA1 patients using an antisense oligonucleotide (ASOs) RNA suppression approach that had previously shown promise in a variety of neurodegenerative diseases including the ataxias[188,189,190]. By targeting *Atxn1* transcripts for degradation, they were able to significantly downregulate ATXN1 mRNA in the cerebellum, medulla, cortex and pons resulting in the attenuation of motor dysfunction progression and early mortality of *Atxn1*$^{154Q/2Q}$ mice[13]. To further confirm the effect of polyQ expanded ATXN1 on astrocytes, we used the previously published RNAseq datasets from the ASO treatment study (GSE114674) to assess relative *Kcnj10* expression[13]. When mining the medullar RNAseq dataset from 28-week *Atxn1*$^{154Q/2Q}$ mice either treated with *Atxn1* targeting ASO or a vehicle control, there was a significant amelioration of *Kcnj10* expression in the ASO treated group, which brought expression back to WT levels (Fig 11C). I attempted to confirm this finding using RT-qPCR on triple injected ASO mice yet was unable to find a similar affect in either the cerebellum or medulla, possibly due to the age of the RNA and subsequent RNA degradation (Fig 11D).

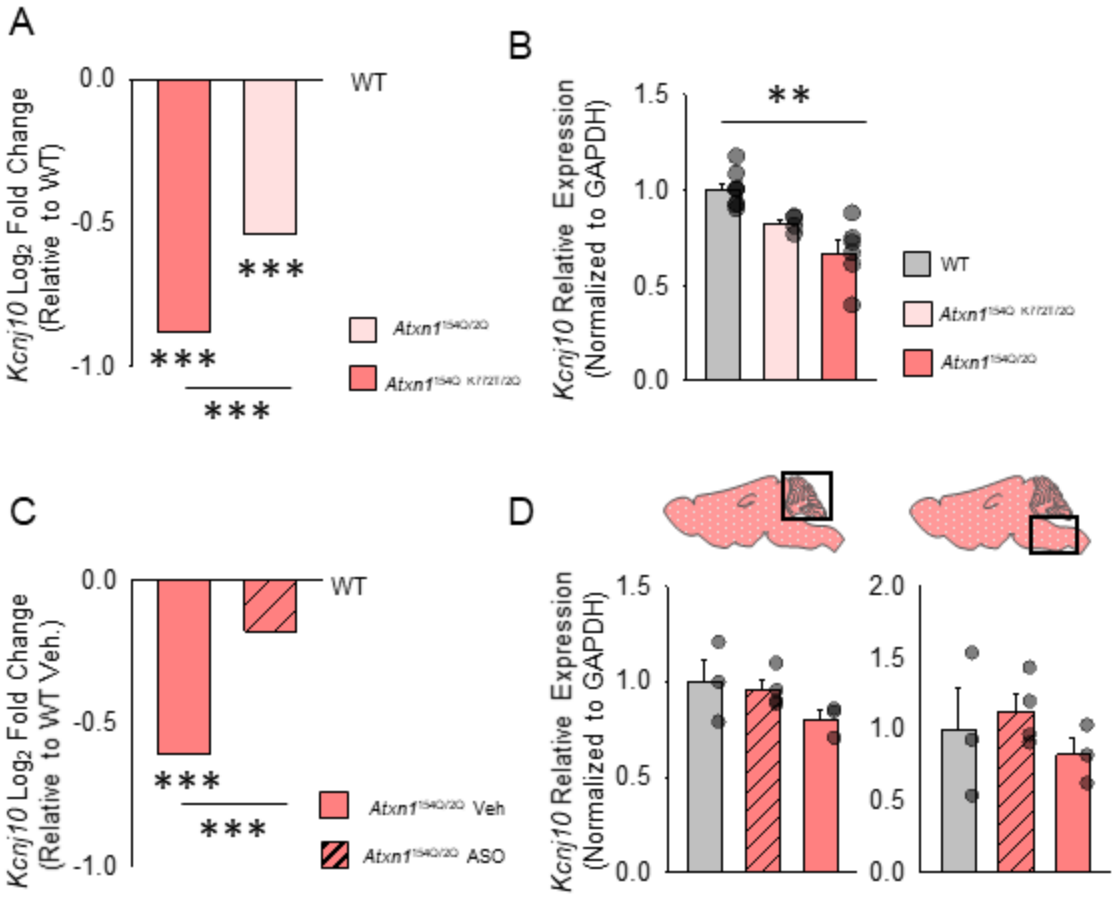

Figure 11. Altering ATXN1 expression as well as cellular trafficking reduces downregulation of *Kcnj10*. (A). RNA-seq data shows that modifying ATXN1's nuclear localization sequence also ameliorates *Kcnj10* expression at 27W in the medulla. Mouse line created by Hillary Handler of the Orr lab. (B) Replication of RNA-seq data using qPCR with way ANOVA (WT: n = 8, 1.000± 0.0325; *Atxn1*$^{154Q\text{-}K772T/2Q}$: n = 4, 0.821± 0.0216; *Atxn1*$^{154Q/2Q}$: n = 6, 0.668± 0.0663; ANOVA: $p < 0.001$, $F = 14.061$, $df = 17$) with Tukey post hoc comparisons. (C) RNA-seq data from 26W medulla of mice treated with ASO or vehicle shows significant amelioration of *Kcnj10* downregulation with ASO treatment ($q < 0.001$). (E) qPCR of 26W medullar (left) (WT: n = 3, 1.000± 0.291; *Atxn1*$^{154Q/2Q}$-ASO: n = 4, 1.126± 0.121; *Atxn1*$^{154Q/2Q}$-Veh: n = 3, 0.826± 0.118; ANOVA: $p = 0.962$, $F = 0.704$, $df = 9$) and cerebellar (WT: n = 3, 1.000± 0.121; *Atxn1*$^{154Q/2Q}$-ASO: n = 4, 1.126± 0.0486; *Atxn1*$^{154Q/2Q}$-Veh: n = 3, 0.826± 0.0483; ANOVA: $p = 0.234$, $F = 1.803$, $df = 9$) (right) RNA. Data represented as mean

of RNAseq Log 2 fold change, and mean ± S.E.M. and analyzed with DEseq2, student t-test and one-way ANOVA with Tukey, where appropriate. $p < 0.05$ = *, <0.001 = **, <0.0001 = ***.

3.6 The novel humanized ATXN1$^{146Qfloxed/2Q}$ mouse line recapitulates pathologies of the Atxn1$^{154Q/2Q}$ mouse model

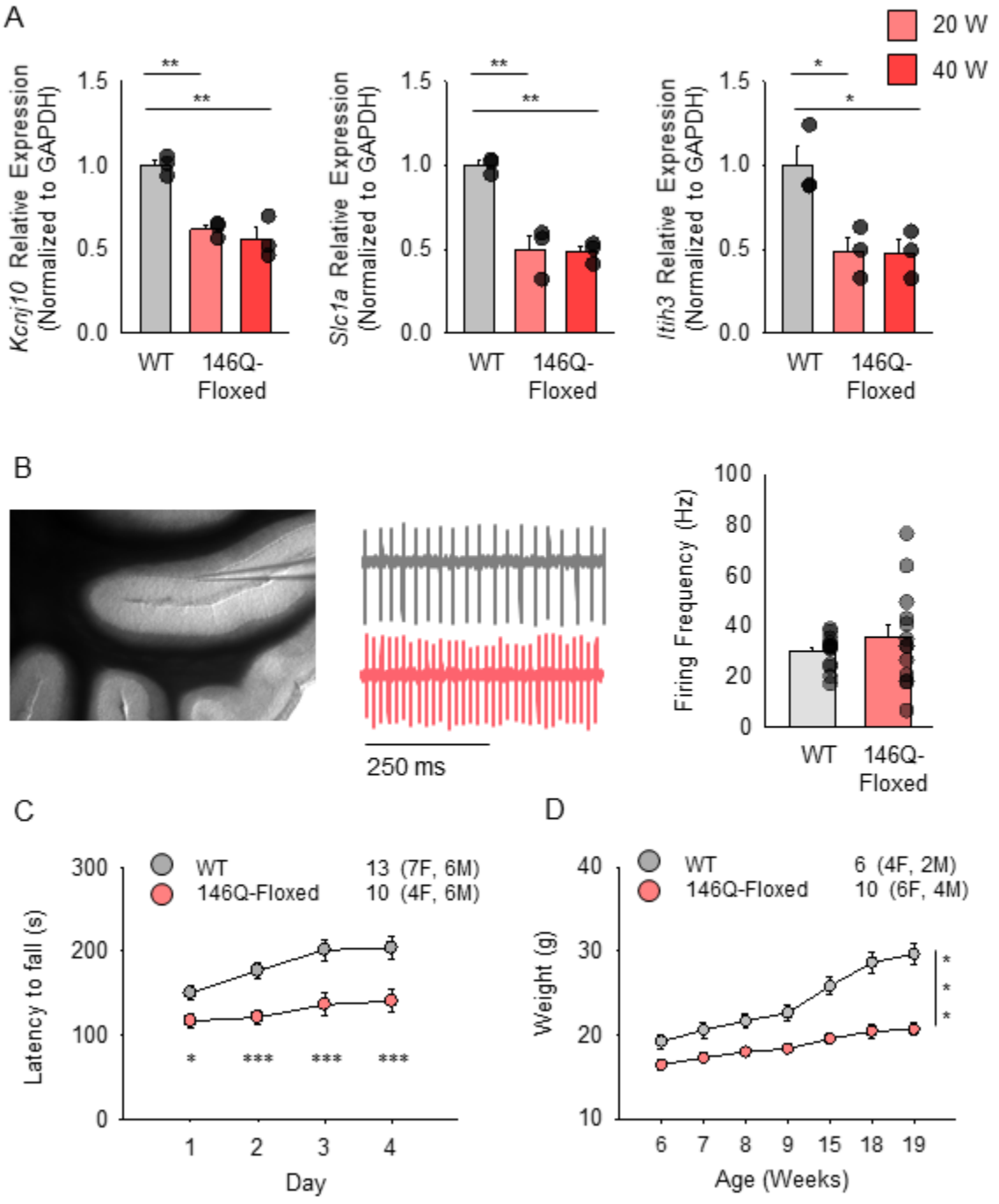

Figure 12. The humanized *ATXN1*$^{146QFloxed/2Q}$ recapitulates phenotypes of other models of SCA1. (A) At both 20 and 40W of age, the *ATXN1*$^{146QFloxed/2Q}$ (146Q-Floxed) mice downregulate both *Kcnj10* and the brown module genes *Slc1a* and *Itih3* in the cerebellum. (B) Even with the downregulation of magenta module genes and *Kcnj10*, Purkinje cells maintain their basal firing frequency at 24W (WT and *ATXN1*$^{146QFloxed/2Q}$: n_{cell} = 13, n_{mouse} = 3)($p > 0.05$) . (C) The *ATXN1*$^{146QFloxed/2Q}$ have a rotarod performance deficit by 12W genotype $p < 0.001$; $F = 45.379$, $df = 1$; day $p = 0.003$, $F = 5.027$, $df = 3$). (D) *ATXN1*$^{146Q/2Q\ Floxed/Floxed}$ mice retain a failure to gain weight (Genotype X Age: $p < 0.001$; $F = 8.221$, $df = 6$; Genotype X sex: $p < 0.001$, $F = 23.071$, $df = 1$; statistical significance via Tukey Post hoc of genotype within day). ANOVA, Student T-Test, Two-way ANOVA and Three-way ANOVA with Tukey post hoc where applicable. $p < 0.05$ = *, <0.001 = **, <0.0001 = ***.

To probe the relationship between polyQ expanded ATXN1 and *Kcnj10*, we employed the novel humanized *ATXN1*$^{146Qfloxed/2Q}$ mouse line created by the Orr and Koob labs (*in preparation*). The humanized *ATXN1*$^{146Qfloxed/2Q}$ mouse line was created using a targeted knock-in strategy, inserting the coding regions of human exons 8 and 9 containing a polyQ region of 146 CAGs in tandem repeat into the homologous region in the mouse genome while simultaneously knocking out the homologous mouse sequences. Furthermore, the coding region of the humanized, polyQ expanded allele are flanked by loxN sites allowing for site and temporal specific knockdown of the of the pathogenic region of ATXN1 while also retaining its endogenous expression.

The humanized *ATXN1*$^{146Qfloxed/2Q}$ model also reproduces key pathologies seen in the *Atxn1*$^{154Q/2Q}$ knock-in model. Using RT-qPCR to quantify both *Kcnj10* and two genes associated with medullar *Atxn1*$^{154Q/2Q}$ pathology, I found that humanized *ATXN1*$^{146Qfloxed/2Q}$ mice show similar reductions previously seen in *Atxn1*$^{154Q/2Q}$. Specifically, *Kcnj10* (p <

0.001, *F* = 24.34, *df* = 8), *Slc1a* (p < 0.001, *F* = 27.098, *df* = 8) and *Itih3* (p = 0.014, *F* = 9.385, *df* = 8), were downregulation in the medulla (Fig 12A) at both 20 and 40 weeks of age when compared to 30 week old WT mice (Friedrich et al., 2018).

Furthermore, the humanized *ATXN1*$^{146Qfloxed/2Q}$ mice recapitulate gross pathologies that are found in the *Atxn1*$^{154Q/2Q}$ mouse model, such as motor performance deficits and failure to gain weight[71]. Assessment of motor performance on the accelerating rotarod (5-50 rpm over 300 s) showed that humanized *ATXN1*$^{146Qfloxed/2Q}$ (n = 10) mice perform worse than WT (n = 13) controls at 12 weeks of age (Two way ANOVA: genotype; p < 0.001; *F* = 45.379, *df* = 1) where humanized *ATXN1*$^{146Qfloxed/2Q}$ mice performed worse on each day (Tukey Post Hoc: Day 1 p = 0.042, Days 2-4 p < 0.001)(Fig 12C). This motor performance deficit also was not due to a failure to learn, as both the WT and humanized *ATXN1*$^{146Qfloxed/2Q}$ mice improved performance over each day (day: p = 0.003, *F* = 5.027, *df* = 3). Alongside this motor performance deficit, humanized *ATXN1*$^{146Qfloxed/2Q}$ mice also exhibited a failure to gain weight over 6 to 19 weeks (genotype: p < 0.001, *F* = 272.967, *df* = 1) where humanized *ATXN1*$^{146Qfloxed/2Q}$ mice weighed less at every timepoint (Week 6, p = 0.003, Weeks 7-19, p < 0.001)(Fig 12D).

To assess Purkinje cell dysfunction in the humanized *ATXN1*$^{146Qfloxed/2Q}$ mouse line, I employed voltage clamp experiments. Patching Purkinje cells in anterior lobules 4/5 in cell attached voltage clamp mode revealed that humanized *ATXN1*$^{146Qfloxed/2Q}$ (n_{cell} = 13, n_{mouse} = 3) do not have a classical spontaneous firing frequency deficit at 6 months of age when compared to age matched controls (n_{cell} = 13, n_{mouse} = 3)(p > 0.05, *t* = -0.970, *df* = 24) like that found in the *ATXN1[82Q]* (Fig 12B)[191]. Even so, the humanized *ATXN1*$^{146Qfloxed/2Q}$ do occupy a greater rate space (σ = 19.440) when compared to WT Purkinje cells (σ = 6.546) and fails the Brown-Forsythe equal variance test (p < 0.05). The lack of clear firing rate deficit may be a result of the differences between the Purkinje cell specific transgenic line, which is largely used in electrophysiological studies, to knock-in

models. Despite not seeing a clear Purkinje cell firing deficit, I continued to utilize the humanized *ATXN1*$^{146Qfloxed/2Q}$ as it recapitulated both behavioral and transcriptomic changes, including *Kcnj10* downregulation.

3.7 Deletion of ATXN1^{146Q} *from astrocytes did not affect SCA1-associated phenotypes*

To test the cell-autonomous effects of pathogenic ATXN1 on astrocytes, we used the humanized *ATXN1*$^{146Qfloxed/2Q}$ mouse line bred to the astrocyte specific and tamoxifen inducible Glast-CreERT2[192]. This strategy allows for the temporal and cell type-specific deletion of pathogenic *ATXN1* from astrocytes, while avoiding off target effects of other Cre lines[192]. At 4-6* weeks of age mice were either injected with a sunflower oil control (Oil) or the exogenous estrogen analog tamoxifen (TMX), to direct Cre translocation and subsequent *ATXN1* knockout in astrocytes throughout the brain (Fig 13A,B). The subsequent four groups of mice, WT-Oil (n = 6), WT-TMX (n = 10), humanized *ATXN1*$^{146Qfloxed/2Q}$-Oil (146Q-Oil; n = 7) and humanized *ATXN1*$^{146Qfloxed/2Q}$ astrocyte knock out mice(146Q-TMX; n = 11) were then tested for motor pathology using the accelerating rotarod at 14, 18 and 21 weeks of age (Fig 13C).

I used a Three-way ANOVA to compare the influences of genotype, treatment and age over the entirety of motor assessment in order to compare learning over the time course of the experiment as well as compare the effects of both treatment and genotype over the entire behavioral assessment. In this analysis, sex was not accounted for as sex as a factor has not been our previous studies have detected no sex-specific effects in SCA1. As expected, there was a significant effect of genotype (WT-Oil n =6; WT-TMX = 10; 146Q-Oil n = 7; 146Q TMX n = 11)($p < 0.001$, $F = 328.575$, $df = 1$) and day ($p < 0.001$, $F = 5.799$, $df = 11$) and but not treatment ($p = 0.956$, $F = 0.00301$, $df = 1$). Yet, there was

both a significant interaction between genotype and treatment ($p < 0.001$, $F = 33.434$, $df = 1$) (Appendix Table 1). Therefore, to see the effects on treatment with genotype, I ran a subsequent Two-way ANOVA to compare the factors of both group and age over the entirety of motor assessment. As expected, there was a significant effect of group (WT-Oil n =6; WT-TMX = 10; 146Q-Oil n = 7; 146Q TMX n = 11)($p < 0.001$, $F = 145.869$, $df = 3$), day ($p < 0.001$, $F = 5.811$, $df = 11$) and an interaction between day and group ($p < 0.001$, $F = 2.741$, $df = 33$). Within each group, mice increased their performance between day 1 and all subsequent days of assessment. Yet, when looking within each day, 146Q-TMX mice had an decreased rotarod performance on day 1 compared to 146Q-Oil treated mice ($p = 0.023$), whereas for the rest of observation there was no significant differences between either treatment group ($p > 0.05$ for all days other than day 1) (See appendix table 2). Whereas there was a continual and significantly lower motor performance of both *ATXN1*$^{146Qfloxed/2Q}$ treatment groups between both WT treatment groups (days 7+ $p < 0.05$).

Similarly, at both 18 and 21 weeks, we found no significant effect of astrocytic knockdown of humanized polyQ expanded ATXN1 on weight pathologies at 18W (Treatment: $p = 0.764$, $F = 0.0921$, $df = 1$, Genotype: $p < 0.001$, $F = 56.946$, $df = 1$, and Sex: $p < 0.001$, $F = 50.068$, $df = 1$) nor at 21W (Treatment: $p = 0.0832$, $F = 0.0921$, $df = 1$, Genotype: $p < 0.001$, $F = 67.566$, $df = 1$, and Sex: $p < 0.001$, $F = 59.341$, $df = 1$)(Fig 13D). Furthermore, at these time points, there was no significant interaction between genotype and treatment.

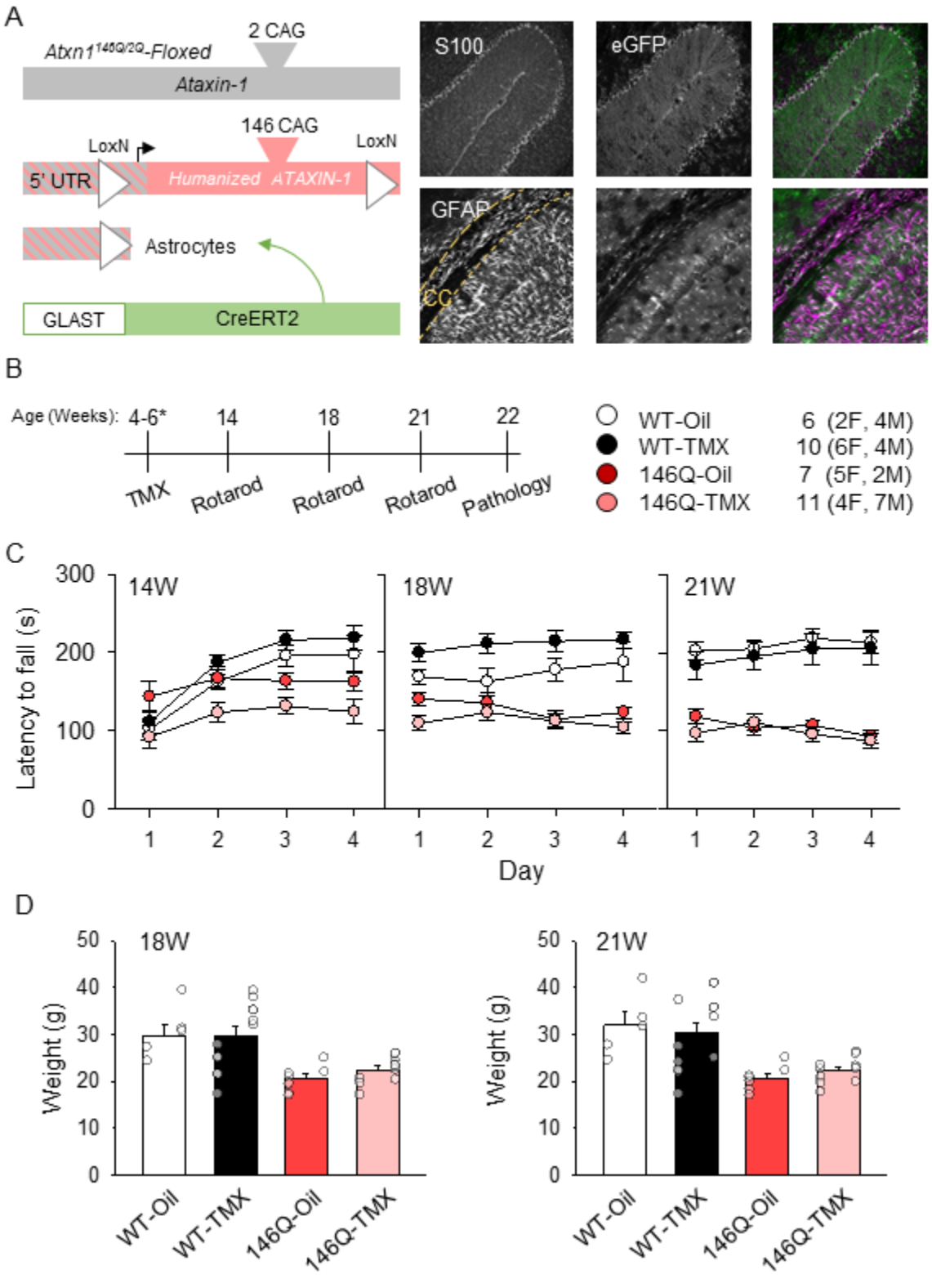
A
Atxn1146Q/2Q-Floxed
2 CAG
Ataxin-1
146 CAG
LoxN
LoxN
5' UTR
Humanized ATAXIN-1
Astrocytes
GLAST
CreERT2
S100
eGFP
GFAP
cc
B
Age (Weeks): 4-6* 14 18 21 22
TMX
Rotarod
Rotarod
Rotarod
Pathology
WT-Oil 6 (2F, 4M)
WT-TMX 10 (6F, 4M)
146Q-Oil 7 (5F, 2M)
146Q-TMX 11 (4F, 7M)
C
14W
18W
21W
Latency to fall (s)
300
200
100
0
1 2 3 4 1 2 3 4 1 2 3 4
Day
D
18W
21W
Weight (g)
50
40
30
20
10
0
WT-Oil
WT-TMX
146Q-Oil
146Q-TMX

Figure 13. PolyQ expanded ATXN1 in astrocytes does not affect the SCA1 like phenotypes. (A) Using the humanized *ATXN1*$^{146QFloxed/2Q}$ mice bred to the *Glast-Cre*^{ERt2} mouse line allows for temporal and sight specific excision and knockdown of the 146Q allele. Immunofluorescent confocal images using a stop-eGFP reporter as proof of principal of this knockdown strategy. (B) Experimental timeline of 146Q allele knockdown and behavioral pathology with experimental groups. * Range of initial excision due to COVID-19. (C) Rotarod performance over these 12 timepoints show that all groups were able to learn (day; $p < 0.001$, $F = 5.811$, $df = 11$) yet there was no lasting effect of astrocytic *ATXN1* knockout on rotarod performance. (D) There was no significant effect of astrocytic *ATXN1*^{146Q} on the failure to gain weight phenotype (left data points = females, right data points = males of each group).

3.8 Astrocytic knockout of humanized Atxn^{146Q} *trends towards ameliorating Kcnj10 expression.*

To examine if the lack of gross phenotypic changes was due to faulty recombination, I confirmed the targeted deletion of the humanized polyQ expanded ATXN1. Using a stop floxed GFP reporter line, I tested the recombination efficiency within both the cerebellum and medulla of mice from the behavioral cohort via immunofluorescent reactivity (Fig 14A). At 22 weeks (17 weeks ±1 week post TMX injection) the cerebellum of oil treated control mice had a large portion of Bergmann glia that were eGPF+ yet to a lesser degree than TMX treated mice. Supporting the gross examination, eGFP fluorescence intensity of the cerebellum of Oil (n = 3) treated mice was significantly lower than in TMX treated mice (n = 3)($p = 0.00466$, $t = -5.706$, $df = 4$). (Fig 14B). Further, when probing for excision of the pathogenic region of *hATXN1* using RT-qPCR against a human region that should be knocked out upon TMX treatment, we did not find an significant difference in *hATXN1* expression between Oil (n = 3) and TMX (n = 3)($p = 0.708$, $t = 0.402$, $df = 4$) treated mice (Fig 14C). The observation of a large population of eGFP+ Bergmann glia in oil treated controls suggests some leaky

recombination in these high *Glast* expressing cells[86]. This high level of recombination within cerebella of 146Q-Oil mice may have affected the lack of behavioral change in the cerebellar learning based rotarod experiments.

Even so, the apparent leaky recombination was restricted to cerebellar Bergmann glia. The medulla of Oil treated mice had no visibly eGFP+ cells yet there was a large population of eGFP+ astrocytes in TMX treated mice (Fig 14E). Like in the cerebellum, fluorescence intensity of the medulla of Oil (n = 3) treated mice was significantly lower than in TMX treated mice (n = 3)(p = 0.0358, t = -3.113, df = 4) (Fig 14E). With this cleaner recombination, we found significant effects of astrocytic knockout of humanized polyQ expanded ATXN1 (Fig 14E-G). Specifically, quantification of *hATXN1* expression showed that there was a significant downregulation when comparing 146Q-TMX (n = 3) to 146Q-Oil controls (n = 3)(p = 0.0265, t = 3.430, df = 4)(Fig 14F). Furthermore, when probing *Kcnj10* expression within the medulla, only 146Q-Oil (n = 4) mice significantly down regulated *Kcnj10* when compared to WT (n = 7) and 146Q-TMX (n = 3) mice (ANOVA; p = 0.007, F = 7.971, df = 13; WTvs146Q-TMX: p = 0.009, q = 5.269)(Fig 14G). Even though not significant, the cerebellum trended towards the same effect of TMX on *Kcnj10* expression (ANOVA; p = 0.146, F = 2.267, df = 14)(Fig 14D). Taken together, these data suggest polyQ expanded ATXN1 within astrocytes interact with transcriptional regulation of *Kcnj10* but require further study in order to confirm ATXN1's effect on *Kcnj10* regulation.

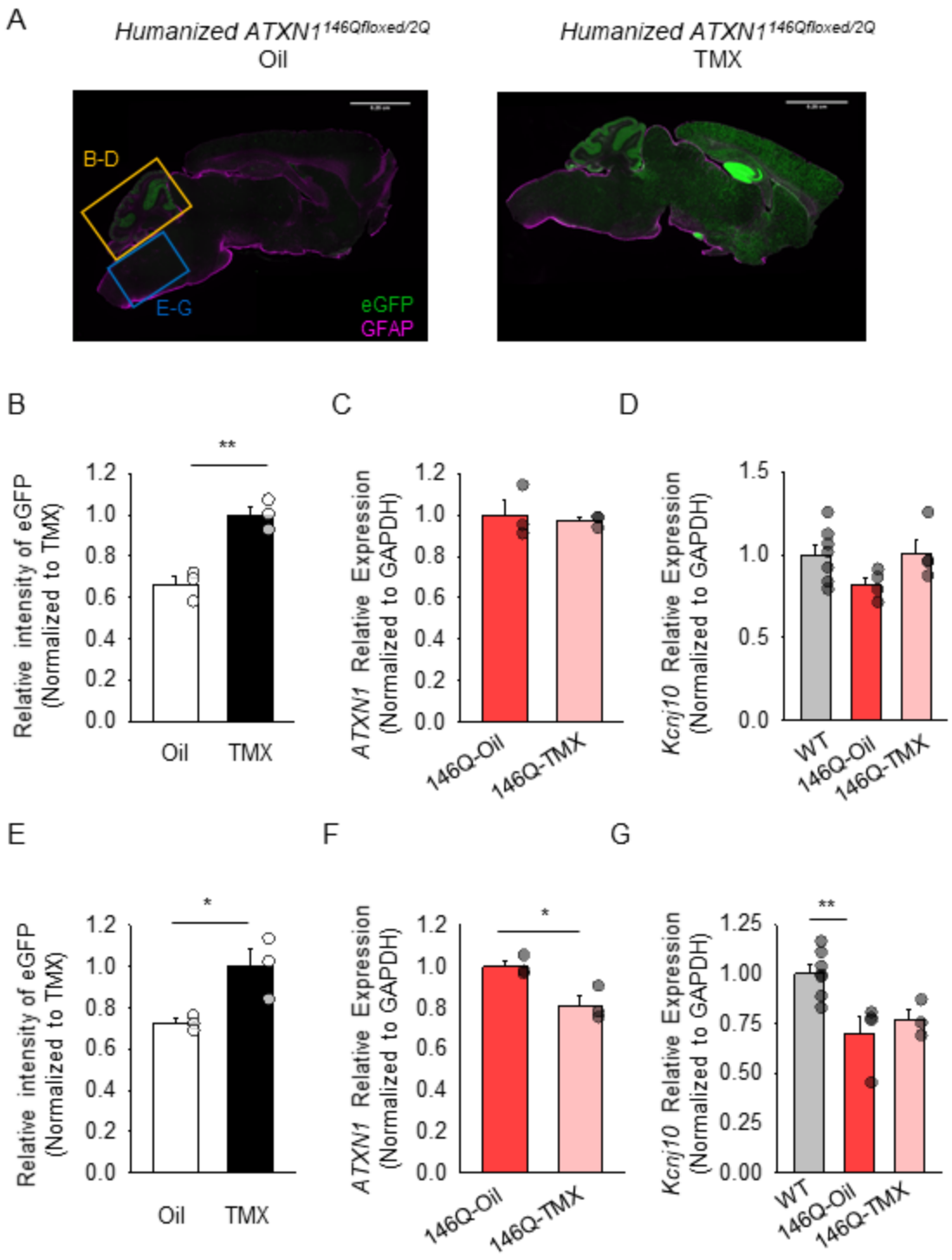

Figure 14. Astrocytic knockout of humanized *ATXN1*^{146Q} trends towards ameliorating *Kcnj10* expression. (A) Representative widefield images of *hATXN1*$^{146QFloxed/2Q}$ –Glast-CreERT2 mice treated with Oil or TMX. Inserts represent analysis performed in B-G where B-D are within the

cerebellum and E-G are within the medulla. (B) eGFP intensity is greater in TMX treated mice than oil controls (p = 0.00466, *t* = -5.706, *df* = 4). (C) There is no significant difference between oil and TMX treated *ATXN1*$^{146QFloxed/2Q}$ expression of *hATXN1* in the cerebellum (p = 0.708, *t* = 0.402, *df* = 4). (D) There is no significant, but a trending rescue of *Kcnj10* caused by astrocytic knockout of *hATXN1* in the cerebellum (ANOVA: p = 0.146, *F* = 2.267, *df* = 14). (E) Medullar intensity of eGFP is greater in TMX treated *ATXN1*$^{146QFloxed/2Q}$ mice than Oil controls (p = 0.0358 *t* = -3.113, *df* = 4). There was a significant decrease in *hATXN* expression in TMX treated *ATXN1*$^{146QFloxed/2Q}$ mice than Oil controls (p = 0.0265, *t* = 3.430, *df* = 4). (G) Correspondingly, there was only a significant downregulation of *Kcnj10* when comparing oil treated *ATXN1*$^{146QFloxed/2Q}$ mice to WT controls in the medulla (ANOVA: p = 0.007, *F* = 7.971, *df* = 13; Tukey post hoc: p = 0.009). p < 0.05 = *, <0.001 = **.

3.9 Discussion

In this chapter I combine astrocyte transcriptomics, behavior, and pathology with mouse genetics to determine the effects of astrocytic ATXN1. Here, I confirm the global downregulation of *Kcnj10* throughout the brain and specifically in the cerebellum and medulla. Both brain regions are particularly relevant to SCA1 as they are associated with both motor pathologies and premature lethality found in both mouse models and SCA1 patients[126,127]. Furthermore, I show that this downregulation of *Kcnj10* occurs in a polyQ-dependent manner, only in SCA1 models in which pathogenic ATXN1 was being expressed by the endogenous promoter. Indeed, both the *Atxn1*$^{154Q/2Q}$ and the humanized *ATXN1*$^{146Qfloxed/2Q}$ models showed significant *Kcnj10* downregulation, whereas it was absent from the Purkinje cell specific *ATXN1[82Q]* transgenic model. The non-significant change in *Kcnj10* in the *Atxn1*$^{82Q/2Q}$ mice further suggested the dependency of a pathogenically expanded polyQ region on *Kcnj10* downregulation and showed a relationship between the pathogenicity and change in astrocytic transcription. The lack of

Kcnj10 downregulation in the *Atxn1-/-* mouse model suggests that ATXN1's effect on *Kcnj10* expression is due to a gain, and not loss of function, of the normal function of either ATXN1's mRNA or protein.

Additionally, I found that disruption of ATXN1's pathogenicity, either through directed knockdown with ASO or disruption of ATXN1's nuclear localization sequence via the *K772T* mutation, can reduce the ATXN1-associated downregulation of *Kcnj10*. In relation to experiments in the *Atxn1*$^{154Q\text{-}K772T/2Q}$ model, it is possible that nuclear localization in cell types outside of Purkinje cells is reduced rather than completely inhibited, as *Atxn1*$^{154Q\text{-}K772T/2Q}$ mice retain some amount of nuclear localized ATXN1 outside of the cerebellum (data not shown). The reduced, and not fully inhibited, nuclear entry of ATXN1 therefore may explain the incomplete rescue of *Kcnj10* rescue. When considering the ASO work in a recent study by, McLoughlin et al. (2018), they show similar effects of an ASO targeting *ATXN3* in a SCA3 model to ASO studies with SCA1[190]. They show that ASOs targeting *ATXN3* were able to ameliorate transcriptional and behavioral pathologies, and furthermore noted the astrocytic and oligodendrocyte uptake of ASOs. In particular, oligodendrocyte expression of *ATXN3* has recently been shown to have a toxic gain of function on oligodendrocyte transcription, again highlighting the underappreciated cell-autonomous effect of SCA genes on glia[193]. Yet both experiments do not differentiate between a direct or indirect effect of ATXN1. It is possible that ATXN1 is functioning to indirectly effect *Kcnj10* expression by effecting regulators of *Kcnj10*. Further work is required to see if any ATXN1's nuclear binding partners can be found in regulatory regions of *Kcnj10* to parse if this is a direct ATXN1 affect.

Using the conditional deletion of the humanized *ATXN1*^{146Qfloxed} allele from astrocytes, we were unable to see improvements in gross motor pathologies or the failure to gain weight phenotype of the model. One possible reason for the lack of rotarod performance changes is due to the leaky recombination in oil treated *ATXN1*$^{146Qfloxed/2Q}$

mice. The accelerating rotarod is a classical motor performance paradigm that is designed to test cerebellar learning that has been classically used to test SCA1 like motor pathologies[194–196]. Therefore, it is possible that we are missing the effect of ATXN1 astrocytic knockout due to the study lacking a true intact *ATXN1*$^{146Qfloxed/2Q}$ control.

The lack of improvement on both rotarod and weight could also be due to a missed therapeutic window or due to ending behavioral assessment too early. In a recent study by Dr. Michelle Gray's group, her group employed a similar targeted astrocytic deletion of mutant Huntington (HTT) in the BACHD mouse model. In their study, they did not see behavioral improvement on the rotarod at 8 weeks of age, but only found behavioral effects of astrocytic knockout of mHTT until 24 weeks[197]. Furthermore, the behavioral improvement on motor performance, assessed with rotarod, was greater at 48 weeks, suggesting a slowing of progression caused by the astrocytic deletion[197]. One key difference between Dr. Gray's and my own is that Dr. Gray's group employed a CreERT2 driven by a GFAP promoter, possibly resulting in different levels or populations of astrocytes that underwent deletion. Even so, this time course for behavioral outcome may be similarly delayed in the SCA1 mice. In support of this hypothesis, ASO driven knockdown of ATXN1, in both neurons and glia, was unable to cause rotarod performance improvements in the *Atxn1*$^{154Q/2Q}$ model until 21 weeks of age[13]. Furthermore, ASO treatment did not affect failure to gain weight, and data presented here agrees with previous work suggesting that this phenotype may be due to pathologies in the periphery. Yet, the leakiness of the *Glast-CreERT2* needs to be resolved to see if astrocytic ATXN1 would affect rotarod performance.

Though we did not observe any behavioral outcomes following astrocytic deletion of the polyQ humanized *ATXN1*^{146Qfloxed} allele, this is the first study to report a cell-autonomous effect of ATXN1 on astrocytic transcription. In particular, we found that deletion of polyQ expanded, human *ATXN1* was able to reduce *Kcnj10* downregulation

within the medulla, with a similar, trending pattern in the cerebellum. Downregulation and or miss-regulation of *Kcnj10* has been linked to a variety of neurological disorders. Kir4.1, the protein product of *Kcnj10*, is an astrocytic potassium channel predominantly expressed by astrocyte[80]. Kir4.1 mediates both astrocytic membrane potential, neuronal cell excitability through its action as a potassium sink, as well as regulation of synaptic and extra synaptic glutamate concentrations via its interaction with glutamate transporters[198–200]. Allelic variations in human kir4.1, as well as Kir4.1 knockouts in mice produce motor dysfunction including seizures and ataxia like phenotypes in both mice and humans highlighting its importance to overall brain health[199,201]. Similar maladaptive astrocytic phenotypes have been found in the R6/2 HD mouse model. Astrocyte in the R6/2 model downregulate Kir4.1 during disease progression, which causes substantial increases in the potassium concentration in the extracellular space [K^+_o] of the striatum[8]. The resultant increase in [K^+_o] resulted in medium spiny neuron (MSN) depolarization and rescue of Kir4.1 expression attenuated MSN potential, ataxic like motor pathologies, and the early onset death seen in untreated R6/2 mice. *Kcnj10*/Kir4.1 expression, therefore, is highly correlated with overall brain health particularly in polyQ disorders.

The amelioration of *Kcnj10* downregulation caused by astrocytic deletion of the polyQ humanized *ATXN1*^{146Qfloxed} allele is the first evidence of ATXN1 affecting astrocytic transcriptomics in a cell-autonomous manner. One aspect of the ATXN1-astrocytic interaction that remains unknown is the pathway that may cause this transcriptional effect. One mechanism of action could be ATXN1 is interacting directly with regulators of *Kcnj10* expression to cause this transcriptional effect on *Kcnj10* as has been seen with CIC and its transcriptional targets. Another possible mechanism could be that polyQ ATXN1 is causing an indirect inflammatory transcriptional response. These two mechanisms could be disentangled using the inflammatory inhibition model *IKKβ*$^{F/F}$ with an astrocytic specific Cre in the *Atxn1*$^{154Q/2Q}$ model. In either case, epigenetic remodeling of *Kcnj10* could also

account for *Kcnj10* downregulation. Recent data suggests that *Kcnj10* regulation during brain insult is via hypermethylation of specific CpG islands throughout the gene[202]. Due to the relative stability of epigenetic remodeling, early hypermethylation caused by developmental polyQ ATXN1 in astrocytes may explain the incomplete rescue of expression.

In conclusion, even though the cell-autonomous impact of astrocytic ATXN1 on astrocytes on behavioral outcomes such as motor performance, failure to gain weight and early onset mortality is unresolved, these data provide evidence for a previously unexplored astrocytic-ATXN1 pathological pathway.

3.10 Methods

Animals

All mice were housed and managed by Research Animal Resources under specific pathogen–free conditions in an Association for Assessment and Accreditation of Laboratory Animal Care International–approved facility. Mice were housed in a reverse 12-12 light dark cycle with food and water *ad libitum*. For all experiments, both male and females were used in equal numbers when possible. For tissue analyses, mice were harvested via CO2 euthanasia and brains were dissected to isolate the cortex, cerebellum, and medulla. For conditional Cre-recombinase expression, mice were injected with 0.1 mg/g/mouse or equivalent volumes of sunflower oil for 5 days at 4-6W of age. For all experiments, mice were sex matched to the best ability.

Rotarod

Motor deficit was assessed at 14, 18, and 21 weeks of. Briefly, mice were placed onto the apparatus (Ugo Basile) that accelerates from 5 RPM to 50 RPM over 300 seconds. Latency to fall was recorded as either A) when the mouse fell from the apparatus, B) the

mouse completed the 300 second trial or C) when the mouse was unable to continue running and rotated on the rod for two rotations. Mice were subjected to four trials per day, with at least a 10 minute rest between trials, over 4 consecutive days of testing. Data is represented as the mean of each mouse over the day's four trials. Averaged day data was analyzed using Three-way ANOVA, with genotype (*Atxn1*$^{2Q/2Q}$ vs. humanized *ATXN1*$^{146Qfloxed/2Q}$, treatment (Vehicle vs. Tamoxifen [TMX]), and day with an alpha held at $p < 0.05$, and then using a two-way ANOVA, with group and day (alpha held at $p < 0.05$). In both cases, Tukey-Post hoc comparisons were used (appendix table 1,2). Data was presented as mean ∓ S.E.M. Mice were weighed on day four of each weeks rotarod.

Immunofluorescence Imaging

Mouse brains were fixed overnight in 4% formaldehyde, incubated in 30% sucrose, and cut into 45 µm sections on cryostat (Leica, CM 1850). Sections were washed three times in cold Phosphate Buffered Saline (PBS), and incubated in 1% Triton in PBS, before blocking in blocking buffer (10% Normal Goat Serum [NGS] in 0.3% triton-x100 PBS) for 1 hour at room temperature. Slices were then incubated in relevant primary antibodies (anti-S100β: ab41548 Abcam; anti-Kir4.1: AGP012AN0202 Alamone Labs; anti-calbindin-D-28k: C9848, Sigma Aldrich; anti-GFAP Z0334, DAKO, anti-GFP: A10262 Invitrogen) diluted in low serum blocking solution (1% NGS in 0.3% triton-x100 PBS). After washing 3X in PBS, slices were incubated in relevant secondary antibodies in a low serum blocking solution (3 hours at room temperature), before being washed 3X in PBS and mounted onto slides in DI water. Slides were coverslipped with Vectashield mounting media containing DAPI (Vector Laboratories) for confocal imaging (Olympus FV1000). Images were quantified using ImageJ software where mean gray intensity of specified channels or cell counting was performed. Each mouse ($n \geq 3$) had at least 4 images (each from a separate stained section) per quantification with the mean of the quantification being

represented as a single data point. All imaging data is either presented as cell number per volume, or the mean intensity normalized to appropriate controls and presented as mean ∓ S.E.M.

RT-qPCR

One half of each brain region from each mouse was homogenized in 500 µL Trizol (Thermo Fisher Scientific, 15596026). RNA isolation was done per the manufacturer's instructions. cDNA was synthesized in duplicate using 500 ng RNA in 10 µl iScript ADV (172-5038) reactions and then diluted 1:5 in water. qPCR was performed using 2 µl cDNA in 10 µl Roche Probes Master (04707494001) reactions on a Roche 480 Lightcycler. Target gene (KCNJ10; tccgggtttaagagtcttgg, cttagcgaccgacgtcatct, with probe-FAM) and reference gene (Roche mGAPD; 05046211001) reactions were amplified in separate wells under cycling conditions: 95°C for 10 seconds, 60°C for 20 seconds for 35 cycles. Cq values were determined using the Roche Second Derivative Max calculation. Relative quantification was done using standard relative fold expression calculations.

Cerebellar slice preparation

Mice were sacrificed via decapitated, and the brains were extracted before sectioning (250 µm) cerebellar slices using a vibratome (Leica VT1200S). Cerebella were parasagitally sectioned in ice cooled sucrose cutting solution (in mM: Sucrose 189, glucose, 10, sodium hydrogen carbonate 26, potassium chloride 3, magnesium sulfateheptahydrate 5, calcium chloride 0.2, sodium phosphate monobasic monohydrate 1.25) before recovering at room temperature for >30 min in oxygenated ACSF containing (in mM): NaCl 124, KCl 2.69, KH2PO4 1.25, $MgSO_4$ 2, $NaHCO_3$ 26, $CaCl_2$ 2, ascorbic acid 0.4, and glucose 10, and continuously bubbled with carbogen (95% O2 and 5% CO_2) (pH 7.3). Slices were then

transferred to an immersion recording chamber and superfused (2 mL/min) with oxygenated ACSF.

Electrophysiology

Using vermal sections of parasagittal sliced cerebella, Purkinje cells were were visualized under 40x water immersion objective using differential interface contrast (DIC) in an Olympus microscope. Purkinje cells and Bergmann glia within lobule 4/5 were selectively patched and recorded with loose cell attached recordings in voltage clamp mode. Patch pipettes were pulled from thick-walled borosilicate glass (1.5 mm outer diameter) on a Sutter Instruments P-1000 puller. Pipettes (3–8 MΩ) were filled with either ACSF (for cell attached recordings) as not to alter the established electrochemical gradient, or internal solution (whole cell recordings) that contained (in mM): K-Gluconate 135, KCl 10, HEPES 10, MgCl2 1, ATP-Na2 2 (pH = 7.3 adjusted with KOH; osmolality 280–290 mOsm/L). Recordings were obtained and filtered (1KHz) by PC-ONE amplifiers (Dagan Instruments, Minneapolis, MN). Signals were fed to a Pentium-based PC through a DigiData 1440A interface board. The pCLAMP 10.2 (Axon Instruments) software was used for data display, acquisition and storage.

For cell attached experiments, Purkinje cells were patched (R-seal >100 M Ω) and recorded under voltage clamp conditions such that baseline currents = 0 pA and spiking was recorded for 2-10 minutes. Basal firing frequency was quantified using Spike2 (Cambridge Electronic Design) where the signal was filtered with a DC removal (time constant 0.01) and the SD of the signal between two action potentials multiplied by 5 was used as either a falling or rising threshold for spike counting. Basal firing frequency was taken from the first 90 s of the recordings.

For whole cell Bergmann glial recordings, Bergmann glia were patched and held at -80 in voltage clamp mode. After establishment of a stable membrane and axis resistance (ΔΩ

< 20% baseline) currents were recorded for 3 minutes before perfusion of ACSF with 100 µM Barium Chloride. Bergmann glia currents were recorded for 20 minutes and resultant currents were subtracted from baseline currents to obtain the barium sensitive currents using pCLAMP 10.2 (Axon Instruments).

Chapter 4. Major Findings, Conclusions and Future Directions

4.1 Major Findings

Here, I present my thesis work concerning the role of both microglia and astrocyte in the pathogenesis of SCA1. Both cell types play crucial roles throughout the brain and have specialized functions and phenotypes that can alter disease progression. Particularly, in both normal and disease states astrocyte and microglia are further specialized and sensitized in brain regions that are most severely affected in SCA1. Due to their potential as druggable therapeutic targets, understanding of the role of glial inflammation and cell intrinsic effects of ATXN1 on non-neuronal cells is critical for drug discovery and for our understanding of SCA1 disease progression.

In order to determine the role of microgliosis in SCA1, I used the *LysM;NF-κB* inhibition model. There, I discovered that Inhibition of NF-κB signaling in LysM positive cells did not alter pathogenesis of *ATXN1[82Q]* mice. Even though LysM driven inhibition was capable of attenuating microgliosis, cerebellar astrogliosis was unchanged alongside key pathologies of Purkinje cells and resultant motor performance pathologies. Furthermore, the Inhibition of NF-κB signaling in non-SCA1 mice caused reduced motor performance on the rotarod. This motor pathology was accompanied by pathological innervation of climbing fibers onto Purkinje cell somas, suggesting that basal NF-κB signaling is required for correct cerebellar wiring[203].

This work illustrates the importance of basal NF-κB activity in cerebellar development. The deficiencies of climbing fiber synaptic pruning on Purkinje cell somas suggest that cerebellar synaptic refinement requires a basal level of NF-κB signaling. Yet due to the lack of selectivity, it is inconclusive if this is specific to microglial or other cerebellar/ inferior olive cells' NF-κB signaling.

Furthermore, these data corroborate previous work on the *ATXN1[82Q]* model and microglia[74]. Even when reducing microglial density by 69%, there was only a small (% difference = 16.52 between *ATXN1[82Q]*-PLX and *ATXN1[82Q]* mice; % difference = 49.0

between *ATXN1[82Q]* and WT mice) yet significant increase in motor performance. This low impact of microglia on SCA1 phenotype accompanied with the low efficiency of recombinase activity (10-15%) in microglia may explain the lack of behavioral effect of LysM;NF-κB inhibition in the *ATXN1[82Q]* model. One aspect that we did observe was the lack of effect on cerebellar astroglioisis, and therefore it may be that astrocyte may have a greater impact on SCA1.

When looking at astrocyte in SCA1, I found a possible cell-autonomous effect of ATXN1 on astrocytic transcription. I found that polyQ expanded ATXN1 may affect the expression of *Kcnj10* in a cell autonomous manner in both the $Atxn1^{154Q/2Q}$ and the novel humanized $ATXN1^{floxed\ 146Q/2Q}$ mouse model. This was confirmed by a lack of expressional changes in the *ATXN1[82Q]* transgenic model and the trending decrease in the $Atxn1^{82Q/2Q}$ model. The expression data derived from the mouse models used, as well as the *ATXN1-/-* mouse model suggests a polyQ dependent gain of function of ATXN1 on *Kcnj10* regulation. Using the conditional deletion of the 146Q allele with an astrocytic specific Cre, I further show that astrocytic polyQ expanded ATXN1 does not directly affect acquisition of motor pathologies or failure to gain weight by 21W of age. Yet, even so I do show that astrocytic polyQ expanded ATXN1 does indeed affect expression of Kir4.1, therefore suggesting a direct, cell-autonomous affect.

4.2 Future directions

This work provides evidence for the importance of microglia in cerebellar development, the communication between astrocyte and microglia, and a possible cell-autonomous effect of mutant ATXN1 on astrocyte; yet these data provide many avenues for future explorations.

Due to the lack of microglial specificity of *Lysm-Cre;IKKβ* mice, the data is inconclusive concerning the role of microglia in synaptic pruning and in SCA1. The Lysm-

Cre line had been previously used and described as specific to myeloid, and therefore microglia, cells, yet we and others clearly observed off-target recombination in neurons[203]. This has been an issue with microglial specific Cre lines, where the more modern Cx3cr1-cre has been shown to have both neural and astrocytic activity[204]. Further experimentation using a more specific microglial Cre line, including the novel Tmem119-CreERT2 may be the optimal choice for future work [205]. The Tmem119-CreERT2 with the floxed IKKβ, would be able to resolve the shortcomings of this work. In the context of either the *ATXN1[82Q]* or the *Atxn1*$^{154Q/2Q}$ SCA1 mouse models, the effects of microglial reactivity could be resolved. Furthermore, the Tmem119-CreERT2 with the floxed IKKβ line would be able to resolve the role of microglia in cerebellar development to test if NF-KB activity specifically in microglia contributes to pruning of climbing fiber synapses on Purkinje cell somas. This set of experiments could be coupled with a floxed stop constitutively active IKKβ, that may show an increase in climbing fiber-Purkinje cell synaptic pruning.

Yet, in either case, if the *ATXN1[82Q]* mouse line is used, it should be noted that any cell autonomous effects could be missed when assessing the contribution of microglial activation to SCA1 pathology. This is of particular importance due to the recent findings of how double strand breaks and STING interact with A-T, as well as the importance of non-neuronal cells in SCA3[78,190,206,207]. With the expression pattern of STING in microglia and their reactivity in knock-in lines of SCA1, it would be interesting to see if cytoplasmic DNA induced by double strand breaks is translatable and a contributing factor to SCA1 pathology.

Concerning the astrocyte specific knockout of humanized polyQ expanded ATXN1, there are still many avenues for exploration. One aspect of the presented study is the limited scope and less than ideal numbers of mice that were used due to the COVID-19 pandemic. As usual, it would be beneficial to increase the n of mice used for behavioral experimentation. Increasing the sample size in a more sex matched manner would further

allow to test for any sex specific differences, which have recently been observed in both the *ATXN1[82Q]* transgenic line as well as in the patient population[208]. Furthermore, this has been seen in the BACHD mouse model of HD, where astrocytic knockout of pathogenic HTT had a small sex effect[197].

Other than increasing sample size, another limitation of the presented work was its temporal scope. Using multivariant analysis on rotarod performance showed a significant effect of treatment on day 1 rotarod between oil and TMX treated *ATXN1*$^{146QFloxed/2Q}$ mice (Fig 13C at 14W). Therefore, it would be crucial to see if there was an early effect of astrocytic knockout of *ATXN1* not only on motor performance but also *Kcnj10* transcription. The temporal effect of astrocyte on disease progression has already been seen in the *ATXN1[82Q]* transgenic model, and therefore looking at earlier timepoints would be of great importance[131]. Furthermore, extending the behavioral assay to later timepoints would be critical to ensure any late effects were not missed. Recently, when Dr. Gray's group used the astrocytic deletion of pathogenic HTT, they did not see behavioral attenuations until 6 months of age, and the effect of astrocytic knockdown only became greater with increased time[197]. In addition, it would be important to conduct a survival assay to determine whether astrocytic *ATXN1* contributes to premature lethality in SCA1 mice.

One aspect of the data that may interact with the premature lethality is the trending attenuation of *Kcnj10* downregulation. *Kcnj10* downregulation in the R6/2 model of HD has been shown to contribute not only to medium spiny neuron degeneration, as well as premature lethality[40]. The importance of *Kcnj10* in premature lethality phenotypes in HD, as well as how the downregulation is found in the medulla, a brain region associated with lethality in SCA1, should not be overlooked. The downregulation was not region specific, and this is the first work to expressly show the global downregulation of *Kcnj10* throughout the brain in the *Atxn1*$^{154Q/2Q}$ model. A viral rescue strategy could be done concurrently with

electrophysiological analysis of *Atxn1*$^{154Q/2Q}$ and or *ATXN1*$^{146QFloxed/2Q}$ mice to observe whether the downregulation of *Kcnj10* mRNA expression results in a decrease in barium sensitive currents[40,199].

The trending attenuation of *Kcnj10* downregulation is further indication of the cell autonomous effect of *ATXN1* on astrocyte, which is found in other SCAs[123]. Yet, due to the low observed impact of *ATXN1* knockout on *Kcnj10* expression, the methylation state of *Kcnj10* should be compared between astrocytic *ATXN1* knockout mice (TMX), intact astrocytic *ATXN1* mice (oil) and WT mice. It remains unknown if the downregulation is caused by a direct ATXN1 effect, and it is possible that early insult caused by polyQ ATXN1 could cause epigenetic remodeling. If this occurs at an early enough state, (ie before ATXN knockout), it could explain only trending attenuation of *Kcnj10* downregulation. Therefore, measuring the methylation state could reveal an epigenetic mechanism for *Kcnj10* downregulation that could be stable due to the timeline of knockout. Furthermore, data from such an experiment would corroborate methylation as a common regulatory mechanism of *Kcnj10* in brain injury[202].

Even though both my own and data from the Barres' lab suggests astrocytic expression of ATXN1 (Fig 8 and 14F-G), it has yet to be conclusively shown that astrocyte express functional ATXN1. Due to correlative nature of the eGFP signal with *hATXN1* expression, it would be necessary to confirm *ATXN1* expression in astrocyte. One possible approach would be to use RNAscope in combination with immunofluorescent histology(Fig 15A)[209,210]. With our already available eGFP stop floxed mouse line, we would probe both GFAP and *hATXN1* transcripts to get single transcript expression resolution on a cell by cell basis. The combinatorial approach would not only be able to elucidate on astrocytic *ATXN1* expression, but also provide a better understanding of the recombination efficiency and specificity of our Glast-CreERT2 line, particularly with the concerns due to leakiness.

My qPCR data from the astrocytic knockout was suggestive of attenuation of *Kcnj10* downregulation. In the cerebellum, there was only trends for the normally observable downregulation, and subsequent rescue, of *Kcnj10*. This lack of downregulation may be due to a large portion of Bergmann glia, an astrocyte subtype that highly expresses *Kcnj10* within the cerebellum, having undergone recombination. Therefore, the 146Q-Oil mice should be considered as a partial deletion group, rather than a true control, and it would be of great interest to see how both 146Q-TMX, and 146Q-Oil mice would compare to intact *ATXN1*$^{146Qfloxed/2Q}$ mice. In the medulla though, only 146Q-Oil and WT mice were significantly different, while also being a cleaner system for study.

Yet, in both cases, it is unknown how astrocytic knockout of ATXN1 may have had a cell non-autonomous effect on other brain cells, particularly the affected neurons. One first step to take would be to immunhistologically assess the tissue, to quantify neural pathologies, microgliosis, and astrogliosis, particularly within the medulla due to the cleaner recombination. Also, with the mice used in the presented work, I have harvested tissue from the cerebellum, medulla, hippocampus, cortex and striatum (Fig 15B). The banked tissues could be used for RNAseq experiments to assess effects of pathogenic ATXN1 astrocyte knockout on non-astrocytic transcription. As astrocytes are key mediators of the neuroinflammatory state, quantifying levels of inflammation and downstream neural health, would be of great interest. Comparisons between *ATXN1*$^{146Q/2Q}$ with and without astrocytic knockdown would reveal the cell non-autonomous effects on non-astrocytic transcription. Furthermore, we can compare differentially expressed genes between brain regions to see if astrocytic effects of mutant ATXN1 are brain region dependent (Fig 15B)[1].

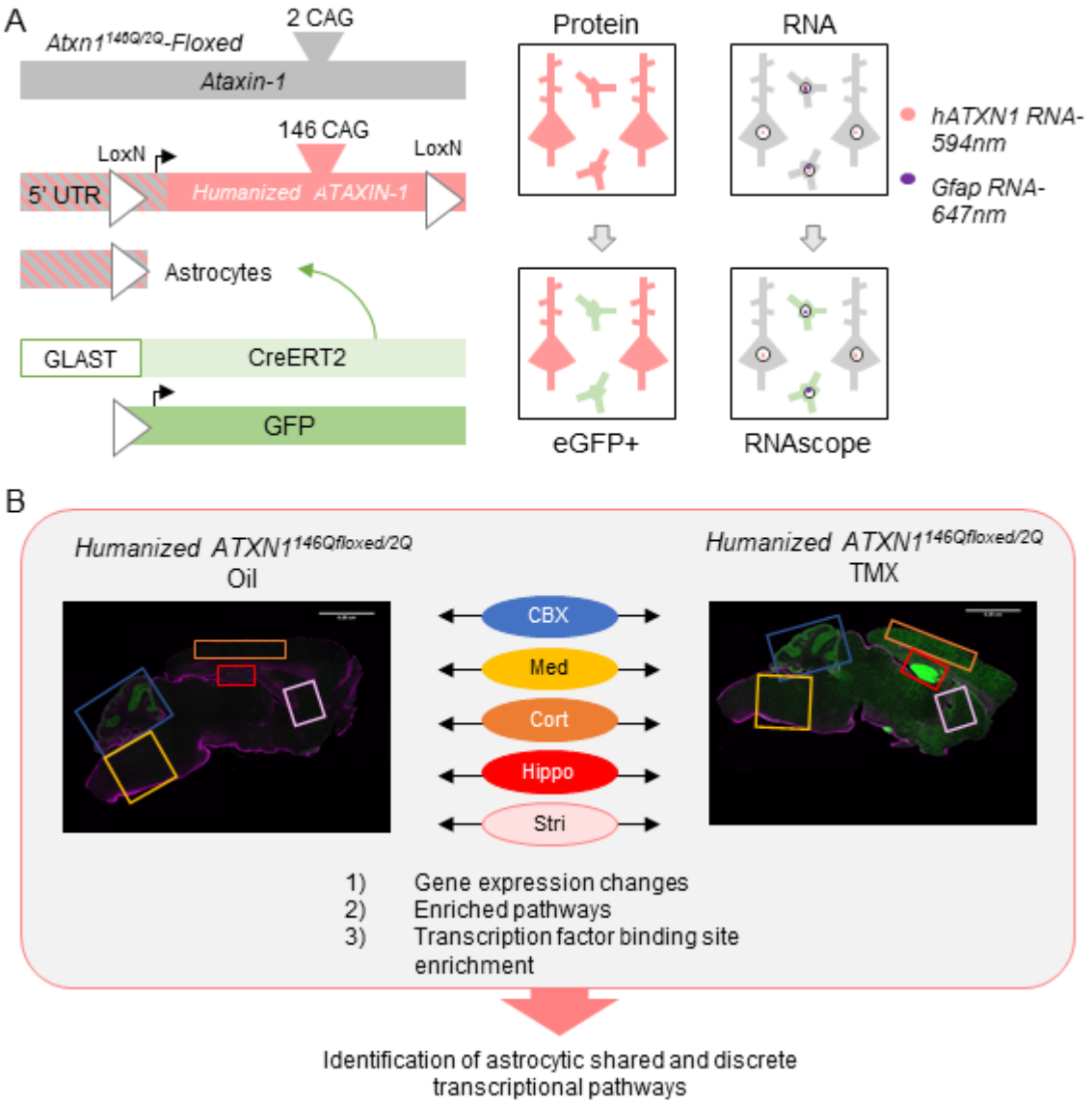

Figure 15. Future directions for the astrocytic conditional SCA1 model. (A) Confirmation of *ATXN1* astrocyte specific knockout using both the stop floxed eGFP reporter in combination with RNAscope. By using both approaches discreetly and in combination to provide further evidence for astrocytic ATXN1 and subsequent knockout. (B) RNAseq strategy for determining region specific (CBX = cerebellum, Med. = medulla, Cort. = Cortex, Hippo = hippocampus and Stri = striatum) transcriptional alterations caused by astrocytic knockout of polyQ ATXN1. Using a region specific RNAseq approach would give us the most power to determine the effect of astrocytic polyQ ATXN1

on SCA1 related transcriptional pathways and reveal the effect of astrocytic polyQ ATXN1 on astrocyte specific transcription.

In conclusion, my thesis work concerning the role of both microglia and astrocyte in the pathogenesis of SCA1 has revealed the importance of NFκB signaling in cerebellar development as well as the potential cell-autonomous effect of polyQ ATXN1 on astrocytes.

Bibliography

1. Driessen, T. M., Lee, P. J. & Lim, J. Molecular pathway analysis towards understanding tissue vulnerability in spinocerebellar ataxia type 1. *Elife* **7**, (2018).
2. Akbar, U. & Ashizawa, T. Ataxia. *Neurol Clin* **33**, 225–248 (2015).
3. Teive, H. A. G. & Ashizawa, T. Primary and secondary ataxias. *Current Opinion in Neurology* **28**, 413–422 (2015).
4. Abele, M., Minnerop, M., Urbach, H., Specht, K. & Klockgether, T. Sporadic adult onset ataxia of unknown etiology. *J. Neurol.* **254**, 1384–1389 (2007).
5. Klockgether, T. Ataxias. *Park. Relat. Disord.* **13**, S391-4 (2007).
6. Teive, H., Munhoz, R. P. & Werneck, L. C. Acquired cerebellar ataxia due to statin use. *Arq Neuropsiquiatr.* **70**, 152 (2012).
7. Pandolfo, M. & Manto, M. Cerebellar and Afferent Ataxias. *Contin. Lifelong Learn. Neurol.* **19**, 1312–1343 (2013).
8. Zoghbi, H. Y. & Orr, H. T. Glutamine repeats and neurodegeneration. *Annual Review of Neuroscience* **23**, 217–247 (2000).
9. Sun, Y.-M., Lu, C. & Wu, Z.-Y. Spinocerebellar ataxia: relationship between phenotype and genotype - a review. *Clin. Genet.* **90**, 305–314 (2016).
10. Rüb, U. *et al.* Clinical features, neurogenetics and neuropathology of the polyglutamine spinocerebellar ataxias type 1, 2, 3, 6 and 7. *Progress in Neurobiology* **104**, 38–66 (2013).
11. Mouro Pinto, R. *et al.* Patterns of CAG repeat instability in the central nervous system and periphery in Huntington's disease and in spinocerebellar ataxia type 1. *Hum. Mol. Genet.* **29**, 2551–2567 (2020).
12. Ferro, A. *et al.* Short-term succinic acid treatment mitigates cerebellar mitochondrial OXPHOS dysfunction, neurodegeneration and ataxia in a Purkinje-specific spinocerebellar ataxia type 1 (SCA1) mouse model. *PLoS One* **12**, e0188425 (2017).
13. Friedrich, J. *et al.* Antisense oligonucleotide-mediated ataxin-1 reduction prolongs survival in SCA1 mice and reveals disease-associated transcriptome profiles. *JCI insight* **3**, (2018).
14. Salter, M. W. & Stevens, B. Microglia emerge as central players in brain disease. *Nat. Med.* **23**, 1018–1027 (2017).
15. Crotti, A. *et al.* Mutant Huntingtin promotes autonomous microglia activation via myeloid lineage-determining factors. *Nat. Neurosci.* **17**, 513–521 (2014).
16. Efthymiou, A. G. & Goate, A. M. Late onset Alzheimer's disease genetics implicates microglial pathways in disease risk. *Mol. Neurodegener.* **12**, 43 (2017).
17. Sierra, A., Gottfried-Blackmore, A. C., Mcewen, B. S. & Bulloch, K. Microglia derived from aging mice exhibit an altered inflammatory profile. *Glia* **55**, 412–424 (2007).
18. Ginhoux, F. *et al.* Fate mapping analysis reveals that adult microglia derive from primitive macrophages. *Science (80-.).* **330**, 841–845 (2010).
19. Ginhoux, F., Lim, S., Hoeffel, G., Low, D. & Huber, T. Origin and differentiation of microglia. *Frontiers in Cellular Neuroscience* (2013). doi:10.3389/fncel.2013.00045
20. Marín-Teva, J. L. *et al.* Microglia Promote the Death of Developing Purkinje Cells. *Neuron* **41**, 535–547 (2004).
21. Schafer, D. P. *et al.* Microglia Sculpt Postnatal Neural Circuits in an Activity and Complement-Dependent Manner. *Neuron* **74**, 691–705 (2012).
22. Matcovitch-Natan, O. *et al.* Microglia development follows a stepwise program to regulate brain homeostasis. *Science (80-.).* **353**, (2016).
23. Thion, M. S. *et al.* Microbiome Influences Prenatal and Adult Microglia in a Sex-Specific Manner. *Cell* **172**, 500-516.e16 (2018).

24. Hammond, T. R. *et al.* Single-Cell RNA Sequencing of Microglia throughout the Mouse Lifespan and in the Injured Brain Reveals Complex Cell-State Changes. *Immunity* **50**, 253-271.e6 (2019).
25. Hickman, S. E. *et al.* The microglial sensome revealed by direct RNA sequencing. *Nat. Neurosci.* **16**, 1896–1905 (2013).
26. ten Donkelaar, H. J., Lammens, M., Wesseling, P., Thijssen, H. O. & Renier, W. O. Development and developmental disorders of the human cerebellum. *J. Neurol.* **250**, 1025–1036 (2003).
27. Leto, K. *et al.* Consensus Paper: Cerebellar Development. *Cerebellum* **15**, 789–828 (2016).
28. Manto, M. U. & Jissendi, P. Cerebellum: links between development, developmental disorders and motor learning. *Front. Neuroanat.* **6**, (2012).
29. Nakayama, H. *et al.* Microglia permit climbing fiber elimination by promoting GABAergic inhibition in the developing cerebellum. *Nat. Commun.* **9**, 2830 (2018).
30. Hashimoto, K., Ichikawa, R., Kitamura, K., Watanabe, M. & Kano, M. Translocation of a “Winner” Climbing Fiber to the Purkinje Cell Dendrite and Subsequent Elimination of “Losers” from the Soma in Developing Cerebellum. *Neuron* **63**, 106–118 (2009).
31. Chen, C. *et al.* Impaired motor coordination correlates with persistent multiple climbing fiber innervation in PKCγ mutant mice. *Cell* **83**, 1233–1242 (1995).
32. Ferro, A. *et al.* Inhibition of NF-κB signaling in IKKβF/F;LysM Cre mice causes motor deficits but does not alter pathogenesis of Spinocerebellar ataxia type 1. *PLoS One* **13**, (2018).
33. Serra, H. G. *et al.* RORα-Mediated Purkinje Cell Development Determines Disease Severity in Adult SCA1 Mice. *Cell* **127**, 697–708 (2006).
34. Barnes, J. A. *et al.* Abnormalities in the climbing fiber-Purkinje cell circuitry contribute to neuronal dysfunction in ATXN1[82Q] mice. *J. Neurosci.* **31**, 12778–89 (2011).
35. Li, Y., Du, X., Liu, C., Wen, Z. & Du, J. Reciprocal Regulation between Resting Microglial Dynamics and Neuronal Activity In Vivo. *Dev. Cell* **23**, 1189–1202 (2012).
36. Davalos, D. *et al.* ATP mediates rapid microglial response to local brain injury in vivo. *Nat. Neurosci.* **8**, 752–758 (2005).
37. Davalos, D. *et al.* Fibrinogen-induced perivascular microglial clustering is required for the development of axonal damage in neuroinflammation. *Nat. Commun.* **3**, (2012).
38. Madry, C. *et al.* Microglial Ramification, Surveillance, and Interleukin-1β Release Are Regulated by the Two-Pore Domain K+ Channel THIK-1. *Neuron* **97**, 299-312.e6 (2018).
39. Wake, H., Moorhouse, A. J., Jinno, S., Kohsaka, S. & Nabekura, J. Resting Microglia Directly Monitor the Functional State of Synapses In Vivo and Determine the Fate of Ischemic Terminals. *J. Neurosci.* **29**, 3974–3980 (2009).
40. Tong, X. *et al.* Astrocyte Kir4.1 ion channel deficits contribute to neuronal dysfunction in Huntington’s disease model mice. *Nat. Neurosci.* **17**, 694–703 (2014).
41. Baroni, F. & Mazzoni, A. Heterogeneity of heterogeneities in neuronal networks. *Front. Comput. Neurosci.* **8**, (2014).
42. Ayata, P. *et al.* Epigenetic regulation of brain region-specific microglia clearance activity. *Nat. Neurosci.* **21**, 1049–1060 (2018).
43. Grabert, K., Michoel, T., Karavolos, M., … S. C.-N. & 2016, undefined. Microglial brain region− dependent diversity and selective regional sensitivities to aging. *nature.com*
44. Lawson, L. J., Perry, V. H., Dri, P. & Gordon, S. Heterogeneity in the distribution and morphology of microglia in the normal adult mouse brain. *Neuroscience* **39**, 151–170 (1990).
45. Cvetanovic, M., Ingram, M., Orr, H. & Opal, P. Early activation of microglia and astrocytes in mouse models of spinocerebellar ataxia type 1. *Neuroscience* **289**, 289–299 (2015).
46. Morterá, P. & Herculano-Houzel, S. Age-related neuronal loss in the rat brain starts at the

end of adolescence. *Front. Neuroanat.* **6**, (2012).
47. Woodruff-Pak, D. S. *et al.* Differential effects and rates of normal aging in cerebellum and hippocampus. **107**, 1624–1629 (2010).
48. Cartier, N., Lewis, C.-A., Zhang, R. & Rossi, F. M. V. The role of microglia in human disease: therapeutic tool or target? *Acta Neuropathol.* **128**, 363–380 (2014).
49. Hanisch, U. K. & Kettenmann, H. Microglia: Active sensor and versatile effector cells in the normal and pathologic brain. *Nature Neuroscience* **10**, 1387–1394 (2007).
50. Cunningham, C. Microglia and neurodegeneration: The role of systemic inflammation. *Glia* **61**, 71–90 (2013).
51. Ransohoff, R. M. A polarizing question: do M1 and M2 microglia exist? *Nat. Neurosci.* **19**, 987–91 (2016).
52. Lawrence, T. The nuclear factor NF-kappaB pathway in inflammation. *Cold Spring Harbor perspectives in biology* **1**, a001651–a001651 (2009).
53. Mincheva-Tasheva, S. & Soler, R. M. NF-κB Signaling Pathways. *Neurosci.* **19**, 175–194 (2013).
54. Matsusaka, T. *et al. Transcription factors NF-IL6 and NF-KB synergistically activate transcription of the inflammatory cytokines, interleukin 6 and interleukin 8 (C/EBP/protein-protein interaction/acute-phase reaction)*. *Proc. Natl. Acad. Sci. USA* **90**, (1993).
55. Santa-Cecília, F. V. *et al.* Doxycycline Suppresses Microglial Activation by Inhibiting the p38 MAPK and NF-kB Signaling Pathways. *Neurotox. Res.* **29**, 447–459 (2016).
56. Wyss-Coray, T. & Rogers, J. Inflammation in Alzheimer Disease — A Brief Review of the Basic Science and Clinical Literature. *Cold Spring Harb. Perspect. Biol.* 1–24 (2012). doi:10.1101/cshperspect.a006346
57. Liddelow, S. A. *et al.* Neurotoxic reactive astrocytes are induced by activated microglia. *Nature* **541**, 481–487 (2017).
58. Czirr, E. *et al.* Microglial complement receptor 3 regulates brain Aβ levels through secreted proteolytic activity. *J. Exp. Med.* **214**, 1081–1092 (2017).
59. Minami, S. S. *et al.* Progranulin protects against amyloid β 2 deposition and toxicity in Alzheimer's disease mouse models. *Nat. Med.* **20**, 1157–1164 (2014).
60. Yuan, P. *et al.* TREM2 Haplodeficiency in Mice and Humans Impairs the Microglia Barrier Function Leading to Decreased Amyloid Compaction and Severe Axonal Dystrophy. *Neuron* **90**, 724–739 (2016).
61. Hong, S., Dissing-Olesen, L. & Stevens, B. New insights on the role of microglia in synaptic pruning in health and disease. *Current Opinion in Neurobiology* **36**, 128–134 (2016).
62. Hong, S. *et al.* Complement and microglia mediate early synapse loss in Alzheimer mouse models. *Science (80-.).* **352**, 712–716 (2016).
63. Lian, H. *et al.* NFκB-Activated Astroglial Release of Complement C3 Compromises Neuronal Morphology and Function Associated with Alzheimer's Disease. *Neuron* **85**, 101–115 (2015).
64. Wolf, S. A., Boddeke, H. W. G. M. & Kettenmann, H. Microglia in Physiology and Disease. *Annual Review of Physiology* **79**, 619–643 (2017).
65. Aikawa, T. *et al.* Loss of MyD88 alters neuroinflammatory response and attenuates early Purkinje cell loss in a spinocerebellar ataxia type 6 mouse model. *Hum. Mol. Genet.* **24**, 4780–4791 (2015).
66. Seki, T. *et al.* Lysosomal dysfunction and early glial activation are involved in the pathogenesis of spinocerebellar ataxia type 21 caused by mutant transmembrane protein 240. *Neurobiol. Dis.* **120**, 34–50 (2018).
67. Shen, Y. *et al.* Frataxin deficiency promotes excess microglial DNA damage and inflammation that is rescued by PJ34. *PLoS One* **11**, (2016).
68. Quek, H. *et al.* A rat model of ataxia-telangiectasia: evidence for a neurodegenerative

phenotype. *Hum. Mol. Genet.* **26**, ddw371 (2016).
69. Nykjær, C. H., Brudek, T., Salvesen, L. & Pakkenberg, B. Changes in the cell population in brain white matter in multiple system atrophy. *Mov. Disord.* **32**, 1074–1082 (2017).
70. Burright, E. N. *et al.* SCA1 transgenic mice: a model for neurodegeneration caused by an expanded CAG trinucleotide repeat. *Cell* **82**, 937–48 (1995).
71. Watase, K. *et al.* A Long CAG Repeat in the Mouse Sca1 Locus Replicates SCA1 Features and Reveals the Impact of Protein Solubility on Selective Neurodegeneration. *Neuron* **34**, 905–919 (2002).
72. Ebner, B. A. *et al.* Purkinje Cell Ataxin-1 Modulates Climbing Fiber Synaptic Input in Developing and Adult Mouse Cerebellum. *J. Neurosci.* **33**, 5806–5820 (2013).
73. Elmore, M. R. P. *et al.* Colony-stimulating factor 1 receptor signaling is necessary for microglia viability, unmasking a microglia progenitor cell in the adult brain. *Neuron* **82**, 380–397 (2014).
74. Qu, W. *et al.* Inhibition of colony-stimulating factor 1 receptor early in disease ameliorates motor deficits in SCA1 mice. *J. Neuroinflammation* **14**, 107 (2017).
75. Petersen, A. J., Rimkus, S. A. & Wassarman, D. A. ATM kinase inhibition in glial cells activates the innate immune response and causes neurodegeneration in Drosophila. *PNAS* **109**, E656–E664 (2012).
76. Hui, C. W. & Herrup, K. Individual Cytokines Modulate the Neurological Symptoms of ATM Deficiency in a Region. *eNeuro* **2**, e00032 (2015).
77. Quek, H. *et al.* Rats with a missense mutation in Atm display neuroinflammation and neurodegeneration subsequent to accumulation of cytosolic DNA following unrepaired DNA damage. *J. Leukoc. Biol* **101**, 927–947 (2017).
78. Song, X., Ma, F. & Herrup, K. Accumulation of Cytoplasmic DNA Due to ATM Deficiency Activates the Microglial Viral Response System with Neurotoxic Consequences. *J. Neurosci.* **39**, 6378–6394 (2019).
79. Zhang, Y. *et al.* An RNA-Sequencing Transcriptome and Splicing Database of Glia , Neurons , and Vascular Cells of the Cerebral Cortex. *J. Neurosci.* **34**, 11929–11947 (2014).
80. Zhang, Y. *et al.* An RNA-sequencing transcriptome and splicing database of glia, neurons, and vascular cells of the cerebral cortex. *J. Neurosci.* **34**, 11929–11947 (2014).
81. Ferro, A., Sheeler, C., Rosa, J. G. & Cvetanovic, M. Role of Microglia in Ataxias. *Journal of Molecular Biology* **431**, 1792–1804 (2019).
82. Hui, C. W., Song, X., Ma, F., Shen, X. & Herrup, K. Ibuprofen prevents progression of ataxia telangiectasia symptoms in ATM-deficient mice. *J. Neuroinflammation* **15**, 308 (2018).
83. Grabert, K. *et al.* Microglial brain region − dependent diversity and selective regional sensitivities to aging. *Nat Neurosci* **19**, 504 (2016).
84. Gao, R. *et al.* Mutant huntingtin impairs PNKP and ATXN3, disrupting DNA repair and transcription. *Elife* **8**, (2019).
85. Chapman, T. P. *et al.* Ataxin-3 Links NOD2 and TLR2 Mediated Innate Immune Sensing and Metabolism in Myeloid Cells. *Front. Immunol.* **10**, Article 1495 (2019).
86. Verkhratsky, A. & Nedergaard, M. Physiology of Astroglia. *Physiol. Rev.* **98**, 239–389 (2018).
87. Cajal, S. y. Contribucion al conocimiento de la neuroglia del cerebro humano. (1913).
88. von Bartheld, C. S., Bahney, J. & Herculano-Houzel, S. The search for true numbers of neurons and glial cells in the human brain: A review of 150 years of cell counting. *J. Comp. Neurol.* **524**, 3865–3895 (2016).
89. Farmer, W. T. *et al.* Neurons diversify astrocytes in the adult brain through sonic hedgehog signaling. *Science* **351**, 849–54 (2016).
90. Boisvert, M. M., Erikson, G. A., Shokhirev, M. N. & Allen, N. J. The Aging Astrocyte

Transcriptome from Multiple Regions of the Mouse Brain. *Cell Rep.* **22**, 269–285 (2018).
91. Batiuk, M. Y. *et al.* Identification of region-specific astrocyte subtypes at single cell resolution. *Nat. Commun.* **11**, 1220 (2020).
92. Chai, H. *et al.* Neural Circuit-Specialized Astrocytes: Transcriptomic, Proteomic, Morphological, and Functional Evidence. *Neuron* **95**, 531-549.e9 (2017).
93. Tsai, H. H. *et al.* Regional astrocyte allocation regulates CNS synaptogenesis and repair. *Science (80-.).* **337**, 358–362 (2012).
94. Rival, T. *et al.* Decreasing glutamate buffering capacity triggers oxidative stress and neuropil degeneration in the Drosophila brain. *Curr. Biol.* **14**, 599–605 (2004).
95. Oland, L. A., Gibson, N. J. & Tolbert, L. P. Localization of a GABA transporter to glial cells in the developing and adult olfactory pathway of the moth Manduca sexta. *J. Comp. Neurol.* **518**, 815–838 (2010).
96. Takarada, T. *et al.* Possible neuroprotective property of nicotinic acetylcholine receptors in association with predominant upregulation of glial cell line-derived neurotrophic factor in astrocytes. *J. Neurosci. Res.* **90**, 2074–2085 (2012).
97. Djukic, B., Casper, K. B., Philpot, B. D., Chin, L.-S. & McCarthy, K. D. Conditional Knock-Out of Kir4.1 Leads to Glial Membrane Depolarization, Inhibition of Potassium and Glutamate Uptake, and Enhanced Short-Term Synaptic Potentiation. *J. Neurosci.* **27**, (2007).
98. Kofuji, P. & Newman, E. A. Potassium buffering in the central nervous system. *Neuroscience* **129**, 1043–1054 (2004).
99. Nwaobi, S. E., Cuddapah, V. A., Patterson, K. C., Randolph, A. C. & Olsen, M. L. The role of glial-specific Kir4.1 in normal and pathological states of the CNS. *Acta Neuropathologica* **132**, (2016).
100. Theparambil, S. M., Naoshin, Z., Thyssen, A. & Deitmer, J. W. Reversed electrogenic sodium bicarbonate cotransporter 1 is the major acid loader during recovery from cytosolic alkalosis in mouse cortical astrocytes. *J. Physiol.* **593**, 3533–3547 (2015).
101. Deitmer, J. W. & Rose, C. R. pH regulation and proton signalling by glial cells. *Progress in Neurobiology* **48**, 73–103 (1996).
102. Newman, E. A. Glial cell regulation of neuronal activity and blood flow in the retina by release of gliotransmitters. *Philos. Trans. R. Soc. B Biol. Sci.* **370**, 1–9 (2015).
103. Haj-Yasein, N. N. *et al.* Aquaporin-4 regulates extracellular space volume dynamics during high-frequency synaptic stimulation: A gene deletion study in mouse hippocampus. *Glia* **60**, 867–874 (2012).
104. Covelo, A. & Araque, A. Neuronal activity determines distinct gliotransmitter release from a single astrocyte. *Elife* **7**, (2018).
105. Attwell, D. *et al.* Glial and neuronal control of brain blood flow. *Nature* **468**, 232–243 (2010).
106. Sanz, E. *et al.* Cell-type-specific isolation of ribosome-associated mRNA from complex tissues. *Proc. Natl. Acad. Sci. U. S. A.* **106**, 13939–13944 (2009).
107. Grosche, J. *et al.* Microdomains for neuron-glia interaction: Parallel fiber signaling to Bergmann glial cells. *Nat. Neurosci.* **2**, 139–143 (1999).
108. Grosche, J., Kettenmann, H. & Reichenbach, A. Bergmann glial cells form distinct morphological structures to interact with cerebellar neurons. *J. Neurosci. Res.* **68**, 138–149 (2002).
109. Paukert, M. *et al.* Norepinephrine controls astroglial responsiveness to local circuit activity. *Neuron* **82**, 1263–1270 (2014).
110. Cervetto, C. *et al.* Calcium-permeable AMPA receptors trigger vesicular glutamate release from Bergmann gliosomes. *Neuropharmacology* **99**, 396–407 (2015).
111. Lattke, M. *et al.* Transient IKK2 activation in astrocytes initiates selective non-cell-autonomous neurodegeneration. *Mol. Neurodegener.* **12**, 1–20 (2017).

112. Zamanian, J. L. *et al.* Genomic analysis of reactive astrogliosis. *J. Neurosci.* **32**, 6391–410 (2012).
113. Liddelow, S. A. & Barres, B. A. Reactive Astrocytes: Production, Function, and Therapeutic Potential. *Immunity* **46**, 957–967 (2017).
114. Liddelow, S. A. *et al.* Neurotoxic reactive astrocytes are induced by activated microglia. *Nature* **541**, 481–487 (2017).
115. Ilieva, H., Polymenidou, M. & Cleveland, D. W. Non-cell autonomous toxicity in neurodegenerative disorders: ALS and beyond. *Journal of Cell Biology* **187**, 761–772 (2009).
116. Jiang, R., Diaz-Castro, B., Looger, L. L. & Khakh, B. S. Dysfunctional Calcium and Glutamate Signaling in Striatal Astrocytes from Huntington's Disease Model Mice. *J. Neurosci.* **36**, 3453–3470 (2016).
117. Cvetanovic, M. Decreased Expression of Glutamate Transporter GLAST in Bergmann Glia Is Associated with the Loss of Purkinje Neurons in the Spinocerebellar Ataxia Type 1. *Cerebellum* **14**, 8–11 (2015).
118. Mellesmoen, A., Sheeler, C., Ferro, A., Rainwater, O. & Cvetanovic, M. Brain Derived Neurotrophic Factor (BDNF) Delays Onset of Pathogenesis in Transgenic Mouse Model of Spinocerebellar Ataxia Type 1 (SCA1). *Front. Cell. Neurosci.* **12**, 509 (2019).
119. Tong, X. *et al.* Astrocyte Kir4.1 ion channel deficits contribute to neuronal dysfunction in Huntington's disease model mice. *Nat. Neurosci.* **17**, 694–703 (2014).
120. Reichold, M. *et al.* KCNJ10 gene mutations causing EAST syndrome (epilepsy, ataxia, sensorineural deafness, and tubulopathy) disrupt channel function. *Proc. Natl. Acad. Sci. U. S. A.* **107**, 14490–14495 (2010).
121. Abdelhadi, O., Iancu, D., Stanescu, H., Kleta, R. & Bockenhauer, D. EAST syndrome: Clinical, pathophysiological, and genetic aspects of mutations in KCNJ10. *Rare Dis.* **4**, e1195043 (2016).
122. Cross, J. H. *et al.* Neurological features of epilepsy, ataxia, sensorineural deafness, tubulopathy syndrome. *Dev. Med. Child Neurol.* **55**, 846–856 (2013).
123. Garden, G. A. *et al.* Polyglutamine-Expanded Ataxin-7 Promotes Non-Cell-Autonomous Purkinje Cell Degeneration and Displays Proteolytic Cleavage in Ataxic Transgenic Mice. *J. Neurosci.* **22**, 4897–4905 (2002).
124. Custer, S. K. *et al.* Bergmann glia expression of polyglutamine-expanded ataxin-7 produces neurodegeneration by impairing glutamate transport. *Nat. Neurosci.* **9**, 1302–1311 (2006).
125. Furrer, S. A. *et al.* Spinocerebellar ataxia type 7 cerebellar disease requires the coordinated action of mutant ataxin-7 in neurons and glia, and displays non-cell-autonomous bergmann glia degeneration. *J. Neurosci.* **31**, 16269–16278 (2011).
126. Seidel, K. *et al.* Brain pathology of spinocerebellar ataxias. *Acta Neuropathol.* **124**, 1–21 (2012).
127. Rüb, U. *et al.* Spinocerebellar ataxia type 1 (SCA1): New pathoanatomical and clinico-pathological insights. *Neuropathol. Appl. Neurobiol.* **38**, 665–680 (2012).
128. Cvetanovic, M. Decreased Expression of Glutamate Transporter GLAST in Bergmann Glia Is Associated with the Loss of Purkinje Neurons in the Spinocerebellar Ataxia Type 1. *The Cerebellum* **14**, 8–11 (2015).
129. Öz, G. *et al.* Neurochemical alterations in spinocerebellar ataxia type 1 and their correlations with clinical status. *Mov. Disord.* **25**, 1253–1261 (2010).
130. Deelchand, D. K. *et al.* Sensitivity of Volumetric Magnetic Resonance Imaging and Magnetic Resonance Spectroscopy to Progression of Spinocerebellar Ataxia Type 1. *Mov. Disord. Clin. Pract.* **6**, 549–558 (2019).
131. Kim, J. H., Lukowicz, A., Qu, W., Johnson, A. & Cvetanovic, M. Astroglia contribute to the pathogenesis of spinocerebellar ataxia Type 1 (SCA1) in a biphasic, stage-of-disease

specific manner. *Glia* **66**, 1972–1987 (2018).
132. Vainchtein, I. D. *et al.* Astrocyte-derived interleukin-33 promotes microglial synapse engulfment and neural circuit development. *Science (80-.).* **359**, 1269–1273 (2018).
133. Lian, H. *et al.* Astrocyte-microglia cross talk through complement activation modulates amyloid pathology in mouse models of alzheimer's disease. *J. Neurosci.* **36**, 577–589 (2016).
134. Matilla-Dueñas, A., Goold, R. & Giunti, P. Clinical, genetic, molecular, and pathophysiological insights into spinocerebellar ataxia type 1. *Cerebellum* **7**, 106–114 (2008).
135. Zoghbi, H. Y. & Orr, H. T. Pathogenic mechanisms of a polyglutamine-mediated neurodegenerative disease, Spinocerebellar ataxia type 1. *Journal of Biological Chemistry* **284**, 7425–7429 (2009).
136. Nino, H. E. *et al.* A family with hereditary ataxia: Hla typing. *Neurology* **30**, 12–20 (1980).
137. Thameem Dheen, S., Kaur, C. & Ling, E.-A. Microglial Activation and its Implications in the Brain Diseases. *Curr. Med. Chem.* **14**, 1189–1197 (2007).
138. Prinz, M. & Mildner, A. Microglia in the CNS: Immigrants from another world. *Glia* **59**, 177–187 (2011).
139. Ginhoux, F. *et al.* Fate mapping analysis reveals that adult microglia derive from primitive macrophages. *Science (80-.).* **330**, 841–845 (2010).
140. Wyss-Coray, T. *et al.* TGF-β1 promotes microglial amyloid-β clearance and reduces plaque burden in transgenic mice. *Nat. Med.* **7**, 612–618 (2001).
141. Wang, X., Chen, S., Ma, G., Ye, M. & Lu, G. Involvement of proinflammatory factors, apoptosis, caspase-3 activation and Ca2+ disturbance in microglia activation-mediated dopaminergic cell degeneration. *Mech. Ageing Dev.* **126**, 1241–1254 (2005).
142. Burda, J. E. & Sofroniew, M. V. Reactive gliosis and the multicellular response to CNS damage and disease. *Neuron* **81**, 229–248 (2014).
143. Glass, C. K., Saijo, K., Winner, B., Marchetto, M. C. & Gage, F. H. Mechanisms Underlying Inflammation in Neurodegeneration. *Cell* **140**, 918–934 (2010).
144. Aguzzi, A., Barres, B. A. & Bennett, M. L. Microglia: Scapegoat, saboteur, or something else? *Science* **339**, 156–161 (2013).
145. Brambilla, R. *et al.* Inhibition of soluble tumour necrosis factor is therapeutic in experimental autoimmune encephalomyelitis and promotes axon preservation and remyelination. *Brain* **134**, 2736–2754 (2011).
146. Li, R. *et al.* Tumor Necrosis Factor Death Receptor Signaling Cascade Is Required for Amyloid-β Protein-Induced Neuron Death. *J. Neurosci.* **24**, 1760–1771 (2004).
147. He, P. *et al.* Deletion of tumor necrosis factor death receptor inhibits amyloid β generation and prevents learning and memory deficits in Alzheimer's mice. *J. Cell Biol.* **178**, 829–841 (2007).
148. Sriram, K. *et al.* Deficiency of TNF receptors suppresses microglial activation and alters the susceptibility of brain regions to MPTP-induced neurotoxicity: role of TNF-α 1 . *FASEB J.* **20**, 670–682 (2006).
149. Liu, H. *et al.* TNF-α Gene Expression in Macrophages: Regulation by NF-κB Is Independent of c-Jun or C/EBPβ. *J. Immunol.* **164**, 4277–4285 (2000).
150. Zandi, E., Rothwarf, D. M., Delhase, M., Hayakawa, M. & Karin, M. The IκB kinase complex (IKK) contains two kinase subunits, IKKα and IKKβ, necessary for Iκb phosphorylation and NF-κB activation. *Cell* **91**, 243–252 (1997).
151. Hayden, M. S. & Ghosh, S. Shared Principles in NF-κB Signaling. *Cell* **132**, 344–362 (2008).
152. Zhong, H., May, M. J., Jimi, E. & Ghosh, S. The phosphorylation status of nuclear NF-κB determines its association with CBP/p300 or HDAC-1. *Mol. Cell* **9**, 625–636 (2002).
153. Cho, S. H. *et al.* SIRT1 deficiency in microglia contributes to cognitive decline in aging

and neurodegeneration via epigenetic regulation of IL-1β. *J. Neurosci.* **35**, 807–818 (2015).
154. Ferro, A. *et al.* Inhibition of NF-κB signaling in IKKβF/F;LysM Cre mice causes motor deficits but does not alter pathogenesis of Spinocerebellar ataxia type 1. *PLoS One* **13**, (2018).
155. Clausen, B. E., Burkhardt, C., Reith, W., Renkawitz, R. & Förster, I. Conditional gene targeting in macrophages and granulocytes using LysMcre mice. *Transgenic Res.* **8**, 265–277 (1999).
156. Khoshnan, A. *et al.* Activation of the IκB kinase complex and nuclear factor-κB contributes to mutant huntingtin neurotoxicity. *J. Neurosci.* **24**, 7999–8008 (2004).
157. Ingram, M. *et al.* Cerebellar Transcriptome Profiles of ATXN1 Transgenic Mice Reveal SCA1 Disease Progression and Protection Pathways. *Neuron* **89**, 1194–207 (2016).
158. Duvick, L. *et al.* SCA1-like disease in mice expressing wild-type Ataxin-1 with a serine to aspartic acid replacement at residue 776. *Neuron* **67**, 929–935 (2010).
159. Haim, L. Ben, Carrillo-de Sauvage, M. A., Ceyzériat, K. & Escartin, C. Elusive roles for reactive astrocytes in neurodegenerative diseases. *Frontiers in Cellular Neuroscience* **9**, 278 (2015).
160. Stephan, A. H., Barres, B. A. & Stevens, B. The complement system: An unexpected role in synaptic pruning during development and disease. *Annual Review of Neuroscience* **35**, 369–389 (2012).
161. Hashimoto, K. & Kano, M. Postnatal development and synapse elimination of climbing fiber to Purkinje cell projection in the cerebellum. *Neurosci. Res.* **53**, 221–228 (2005).
162. Hashimoto, K. & Kano, M. Functional differentiation of multiple climbing fiber inputs during synapse elimination in the developing cerebellum. *Neuron* **38**, 785–796 (2003).
163. Letellier, M., Willson, M. L., Gautheron, V., Mariani, J. & Lohof, A. M. Normal adult climbing fiber monoinnervation of cerebellar Purkinje cells in mice lacking MHC class I molecules. *Dev. Neurobiol.* **68**, 997–1006 (2008).
164. Cho, I. H. *et al.* Role of microglial IKKβ in kainic acid-induced hippocampal neuronal cell death. *Brain* **131**, 3019–3033 (2008).
165. Perez-Pouchoulen, M., VanRyzin, J. W. & McCarthy, M. M. Morphological and phagocytic profile of microglia in the developing rat cerebellum. *eNeuro* **2**, (2015).
166. Stellwagen, D. & Malenka, R. C. Synaptic scaling mediated by glial TNF-α. *Nature* **440**, 1054–1059 (2006).
167. Lewitus, G. M. *et al.* Microglial TNF-α Suppresses Cocaine-Induced Plasticity and Behavioral Sensitization. *Neuron* **90**, 483–491 (2016).
168. Sedger, L. M. & McDermott, M. F. TNF and TNF-receptors: From mediators of cell death and inflammation to therapeutic giants - past, present and future. *Cytokine and Growth Factor Reviews* **25**, 453–472 (2014).
169. Derecki, N. C. *et al.* Wild-type microglia arrest pathology in a mouse model of Rett syndrome. *Nature* **484**, 105–109 (2012).
170. Lee, M. J. *et al.* lKKβ-mediated inflammatory myeloid cell activation exacerbates experimental autoimmune encephalomyelitis by potentiating Th1/Th17 cell activation and compromising blood brain barrier. *Mol. Neurodegener.* **11**, (2016).
171. Arkan, M. C. *et al.* IKK-β links inflammation to obesity-induced insulin resistance. *Nat. Med.* **11**, 191–198 (2005).
172. Kwon, S. H. *et al.* Dysfunction of microglial STAT3 alleviates depressive behavior via neuron-microglia interactions. *Neuropsychopharmacology* **42**, 2072–2086 (2017).
173. Liao, B., Zhao, W., Beers, D. R., Henkel, J. S. & Appel, S. H. Transformation from a neuroprotective to a neurotoxic microglial phenotype in a mouse model of ALS. *Exp. Neurol.* **237**, 147–152 (2012).
174. Stowell, R. D. *et al.* Cerebellar microglia are dynamically unique and survey Purkinje

neurons in vivo. *Dev. Neurobiol.* **78**, 627–644 (2018).
175. Pekny, M. *et al.* Astrocytes: a central element in neurological diseases. *Acta Neuropathologica* **131**, 323–345 (2016).
176. Sofroniew, M. V. & Vinters, H. V. Astrocytes: Biology and pathology. *Acta Neuropathologica* **119**, 7–35 (2010).
177. Greten, F. R. *et al.* IKKβ links inflammation and tumorigenesis in a mouse model of colitis-associated cancer. *Cell* **118**, 285–296 (2004).
178. Li, Z.-W., Omori, S. A., Labuda, T., Karin, M. & Rickert, R. C. IKKβ Is Required for Peripheral B Cell Survival and Proliferation. *J. Immunol.* **170**, 4630–4637 (2003).
179. Orthgiess, J. *et al.* Neurons exhibit *Lyz2* promoter activity in vivo: Implications for using LysM-Cre mice in myeloid cell research. *Eur. J. Immunol.* **46**, 1529–1532 (2016).
180. Abram, C. L., Roberge, G. L., Hu, Y. & Lowell, C. A. Comparative analysis of the efficiency and specificity of myeloid-Cre deleting strains using ROSA-EYFP reporter mice. *J. Immunol. Methods* **408**, 89–100 (2014).
181. Ye, M. *et al.* Hematopoietic stem cells expressing the myeloid lysozyme gene retain long-term, multilineage repopulation potential. *Immunity* **19**, 689–699 (2003).
182. Cvetanovic, M., Patel, J. M., Marti, H. H., Kini, A. R. & Opal, P. Vascular endothelial growth factor ameliorates the ataxic phenotype in a mouse model of spinocerebellar ataxia type 1. *Nat. Med.* **17**, 1445–1447 (2011).
183. Serra, H. G. *et al.* Gene profiling links SCA1 pathophysiology to glutamate signaling in Purkinje cells of transgenic mice. *Hum. Mol. Genet.* **13**, 2535–2543 (2004).
184. Emamian, E. S. *et al.* Serine 776 of ataxin-1 is critical for polyglutamine-induced disease in SCA1 transgenic mice. *Neuron* **38**, 375–387 (2003).
185. Klement, I. A. *et al.* Ataxin-1 nuclear localization and aggregation: Role in polyglutarnine-induced disease in SCA1 transgenic mice. *Cell* **95**, 41–53 (1998).
186. Rousseaux, M. W. C. *et al.* ATXN1-CIC Complex Is the Primary Driver of Cerebellar Pathology in Spinocerebellar Ataxia Type 1 through a Gain-of-Function Mechanism. *Neuron* **97**, 1235-1243.e5 (2018).
187. Abdelhadi, O., Iancu, D., Stanescu, H., Kleta, R. & Bockenhauer, D. EAST syndrome: Clinical, pathophysiological, and genetic aspects of mutations in KCNJ10. *Rare Dis.* **4**, e1195043 (2016).
188. Keiser, M. S., Monteys, A. M., Corbau, R., Gonzalez-Alegre, P. & Davidson, B. L. RNAi prevents and reverses phenotypes induced by mutant human ataxin-1. *Ann. Neurol.* **80**, 754–765 (2016).
189. Scoles, D. R. *et al.* Antisense oligonucleotide therapy for spinocerebellar ataxia type 2. *Nature* **544**, 362–366 (2017).
190. McLoughlin, H. S. *et al.* Oligonucleotide therapy mitigates disease in spinocerebellar ataxia type 3 mice. *Ann. Neurol.* **84**, 64–77 (2018).
191. Dell'Orco, J. M. *et al.* Neuronal Atrophy Early in Degenerative Ataxia Is a Compensatory Mechanism to Regulate Membrane Excitability. *J. Neurosci.* **35**, 11292–307 (2015).
192. Jahn, H. M., Scheller, A. & Kirchhoff, F. Genetic control of astrocyte function in neural circuits. *Frontiers in Cellular Neuroscience* **9**, (2015).
193. Ramani, B. *et al.* Comparison of spinocerebellar ataxia type 3 mouse models identifies early gain-of-function, cell-autonomous transcriptional changes in oligodendrocytes. *Hum. Mol. Genet.* **26**, 3362–3374 (2017).
194. Clark, H. B. *et al.* Purkinje cell expression of a mutant allele of SCA1 in transgenic mice leads to disparate effects on motor behaviors, followed by a progressive cerebellar dysfunction and histological alterations. *J. Neurosci.* **17**, 7385–7395 (1997).
195. Caston, J., Jones, N. & Stelz, T. Role of preoperative and postoperative sensorimotor training on restoration of the equilibrium behavior in adult mice following cerebellectomy. *Neurobiol. Learn. Mem.* **64**, 195–202 (1995).

196. Lalonde, R., Bensoula, A. N. & Filali, M. Rotorod sensorimotor learning in cerebellar mutant mice. *Neurosci. Res.* **22**, 423–426 (1995).
197. Wood, T. E. *et al.* Mutant huntingtin reduction in astrocytes slows disease progression in the BACHD conditional Huntington's disease mouse model. *Hum. Mol. Genet.* **28**, 487–500 (2019).
198. Wang, F. *et al.* Astrocytes Modulate Neural Network Activity by Ca2+-Dependent Uptake of Extracellular K+. *Sci. Signal.* **5**, ra26–ra26 (2012).
199. Djukic, B., Casper, K. B., Philpot, B. D., Chin, L.-S. & McCarthy, K. D. Conditional knock-out of Kir4.1 leads to glial membrane depolarization, inhibition of potassium and glutamate uptake, and enhanced short-term synaptic potentiation. *J. Neurosci.* **27**, 11354–65 (2007).
200. Power, E. M. & Empson, R. M. Functional contributions of glutamate transporters at the parallel fibre to Purkinje neuron synapse-relevance for the progression of cerebellar ataxia. *Cerebellum & ataxias* **1**, 3 (2014).
201. Buono, R. . *et al.* Association between variation in the human KCNJ10 potassium ion channel gene and seizure susceptibility. *Epilepsy Res.* **58**, 175–183 (2004).
202. Boni, J. L., Kahanovitch, U., Nwaobi, S. E., Floyd, C. L. & Olsen, M. L. DNA methylation: A mechanism for sustained alteration of KIR4.1 expression following central nervous system insult. *Glia* **68**, 1495–1512 (2020).
203. Ferro, A. *et al.* Inhibition of NF-κB signaling in IKKβF/F;LysM Cre mice causes motor deficits but does not alter pathogenesis of Spinocerebellar ataxia type 1. *PLoS One* **13**, (2018).
204. Zhao, X. F. *et al.* Targeting microglia using Cx3cr1-Cre lines: Revisiting the specificity. *eNeuro* **6**, 1–11 (2019).
205. Kaiser, T. & Feng, G. Tmem119-EGFP and Tmem119-creERT2 transgenic mice for labeling and manipulating microglia. *eNeuro* **6**, (2019).
206. Ferro, A., Sheeler, C. & Cvetanovic, M. Microglial Self-Recognition STINGs in A-T Neurodegeneration. *Trends in Neurosciences* **42**, 753–755 (2019).
207. Quek, H. *et al.* Rats with a missense mutation in Atm display neuroinflammation and neurodegeneration subsequent to accumulation of cytosolic DNA following unrepaired DNA damage. *J. Leukoc. Biol.* **101**, 927–947 (2017).
208. Asher, M. *et al.* Cerebellar contribution to the cognitive alterations in SCA1: Evidence from mouse models. *Hum. Mol. Genet.* **29**, 117–131 (2020).
209. Kersigo, J. *et al.* A RNAscope whole mount approach that can be combined with immunofluorescence to quantify differential distribution of mRNA. *Cell Tissue Res.* **374**, 251–262 (2018).
210. Wang, F. *et al.* RNAscope: A novel in situ RNA analysis platform for formalin-fixed, paraffin-embedded tissues. *J. Mol. Diagnostics* **14**, 22–29 (2012).

Appendix

A.1 Cell non-autonomous effect on cerebellar astrocytes

Even though we saw that there was no robust change in *Kcnj10* expression in the *ATXN1[82Q]* cerebellum (Fig. 10A), we did want to ensure that this was the case and therefore moved to slice electrophysiology experiments. In cell attached, as expected we saw a significant reduction in the intrinsic firing rate of Purkinje cells in the anterior lobules of *ATXN1[82Q]* mice controls (n_{cell} = 13, n_{mouse} = 3)($p > 0.05$, t = -0.970, df = 24) (Fig. Appendix 1B). Yet, when looking at Bergmann glia, the astrocytic subtype most likely to be affected in the *ATXN1[82Q]* mice due to their proximity and functional relationship with Purkinje cells, we found that Bergmann glial membrane properties remained intact (Fig. 15C-D). Furthermore, when we looked at Barium sensitive currents, we found that the variability in currents was too great (Fig. Appendix 1E-F). That being said, due to the lack of resting membrane potential and membrane resistance differences between *ATXN1[82Q]* and WT mice it is appropriate to conclude that there is not gross difference in Kir4.1 expression or conductance in the *ATXN1[82Q]* mice.

Due to the large distribution of Barium sensitive currents, we then correlated barium sensitive currents alongside near-neighbor Purkinje cell rate. Using Pearson product correlation in the WT mice, we found that there was no significant relationship between Barium sensitive conductance and Purkinje cell firing rate ($p>0.05$)(Fig. 16), whereas there was a significant correlation in the *ATXN1[82Q]* pairs ($r^2 = 0.56$; $p < 0.05$; slope = 1.23)(Fig. Appendix 2). This positive correlation between Purkinje cell firing rate and Bergmann glial Kir4.1 conductance is suggestive of a possible non-cell autonomous effect of Purkinje cell health on Bergmann glial function.

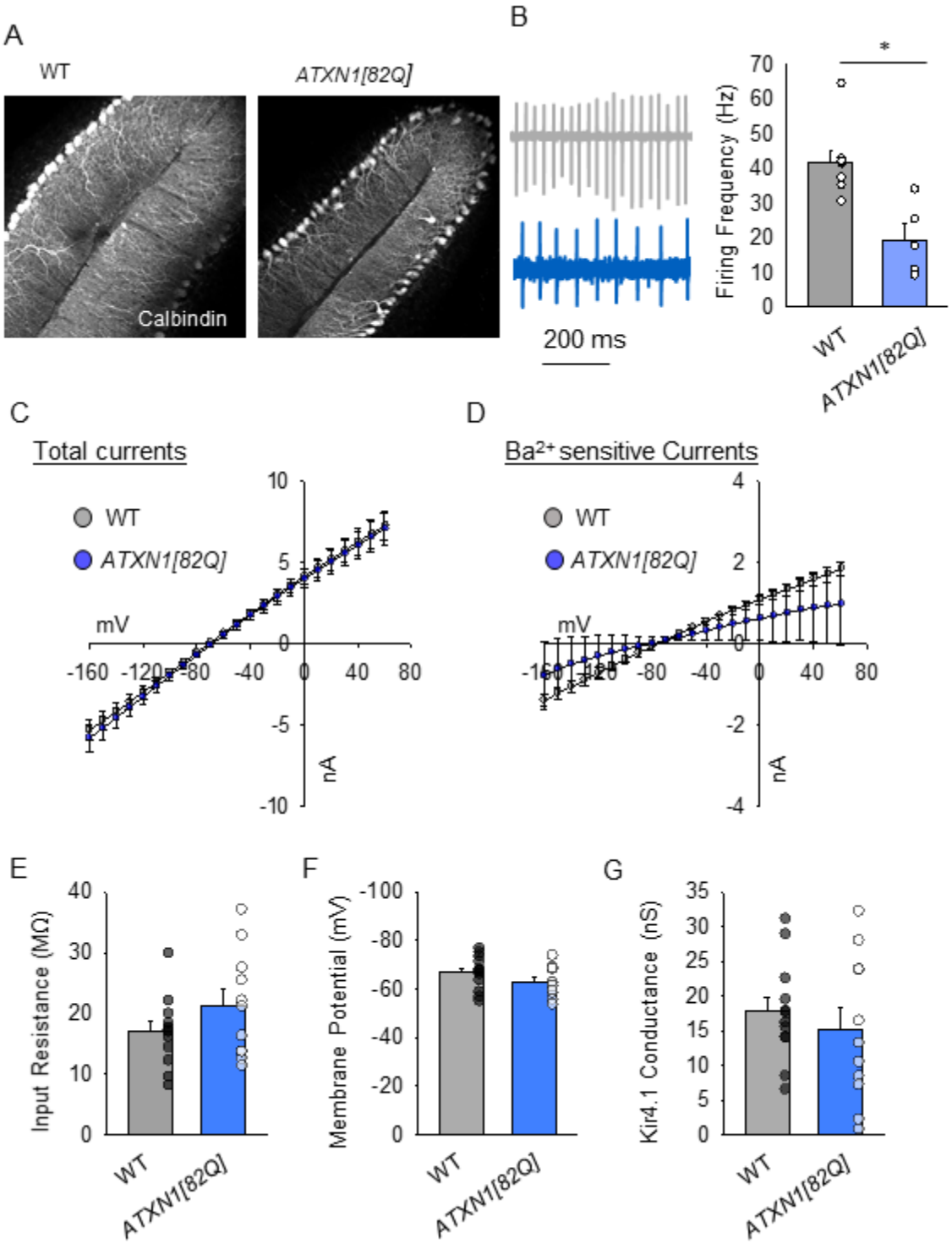

Appendix 1. The Purkinje cell specific *ATXN1[82Q]* transgenic model has Purkinje cell firing dysfunction in the absence of detectible Bergmann glial Kir4.1 dysfunction. (A) There is obvious Purkinje cell molecular layer thinning and loss at 15-20W. (B) Representative traces of Purkinje cell firing frequency where *ATXN1[82Q]* have decreased firing rate in cell attached mode ($p = 0.0176$, $t = 2.568$ $df = 22$). (C-D) Total and barium (Ba^{2+}) sensitive currents at 15-20W of both WT and *ATXN1[82Q]* Bergmann glia within anterior lobules. (E-G) Membrane properties and Kir4.1 conductance of WT and *ATXN1[82Q]* Bergmann glia are not significantly different ($p > 0.05$).

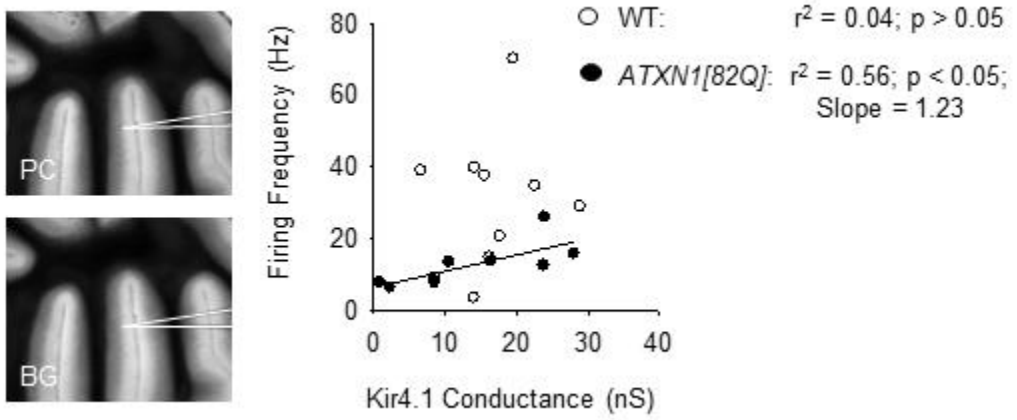

Appendix 2. Patching neighbor Purkinje cells and Bergmann glia reveals a deficit in Kir4.1 conductance only in *ATXN1[82Q]* mice. In WT mice, there is no significant correlation between Purkinje cell firing rate and Bergmann glial Kir4.1 conductance (n pairs = 10; p > 0.05) whereas there is a significant positive correlation in *ATXN1[82Q]* pairs (r^2 = 0.56; p < 0.05; Slope = 1.23).

Appendix Table 1. Tukey Post-hoc comparisons results of rotarod performance post Three-way ANOVA.

Comparisons for factor: Genotype

Comparison	Diff of Means	p	q	P	P<0.050
146Q - vs. 146Q +	69.738	2	25.635	<0.001	Yes

Comparisons for factor: Tx

Comparison	Diff of Means	p	q	P	P<0.050
TMX vs. Oil	0.211	2	0.0776	0.956	No

Comparisons for factor: Genotype within Day 1

Comparison	Diff of Means	p	q	P	P<0.050
146Q + vs. 146Q -	11.11	2	1.179	0.405	No

Comparisons for factor: Genotype within Day 2

Comparison	Diff of Means	p	q	P	P<0.050
146Q - vs. 146Q +	29.791	2	3.161	0.025	Yes

Comparisons for factor: Genotype within Day 3

Comparison	Diff of Means	p	q	P	P<0.050
146Q - vs. 146Q +	58.554	2	6.213	<0.001	Yes

Comparisons for factor: Genotype within Day 4

Comparison	Diff of Means	p	q	P	P<0.050
146Q - vs. 146Q +	64.936	2	6.891	<0.001	Yes

Comparisons for factor: Genotype within Day 5

Comparison	Diff of Means	p	q	P	P<0.050
146Q - vs. 146Q +	59.302	2	6.293	<0.001	Yes

Comparisons for factor: Genotype within Day 6

Comparison	Diff of Means	p	q	P	P<0.050
146Q - vs. 146Q +	57.615	2	6.114	<0.001	Yes

Comparisons for factor: Genotype within Day 7

Comparison	Diff of Means	p	q	P	P<0.050
146Q - vs. 146Q +	82.544	2	8.759	<0.001	Yes

Comparisons for factor: Genotype within Day 8

Comparison	Diff of Means	p	q	P	P<0.050
146Q - vs. 146Q +	87.183	2	9.251	<0.001	Yes

Comparisons for factor: Genotype within Day 9

Comparison	Diff of Means	p	q	P	P<0.050
146Q - vs. 146Q +	85.544	2	9.077	<0.001	Yes

Comparisons for factor: Genotype within Day 10

Comparison	Diff of Means	p	q	P	P<0.050
146Q - vs. 146Q +	92.879	2	9.856	<0.001	Yes

Comparisons for factor: Genotype within Day 11

Comparison	Diff of Means	p	q	P	P<0.050
146Q - vs. 146Q +	110.128	2	11.686	<0.001	Yes

Comparisons for factor: Genotype within Day 12

Comparison	Diff of Means	p	q	P	P<0.050
146Q - vs. 146Q +	119.498	2	12.68	<0.001	Yes

Appendix Table 3. Tukey Post-hoc comparisons results of rotarod performance of group by day.

Comparisons for factor: Group within Day 1

Comparison	Diff of Means	p	q	P
146o vs. 146t	51.877	4	4.031	0.023
146o vs. Wto	41.661	4	2.813	0.192
146o vs. Wtt	32.436	4	2.473	0.299
Wtt vs. 146t	19.441	4	1.672	0.638
Wtt vs. Wto	9.225	4	0.671	0.965
Wto vs. 146t	10.216	4	0.756	0.951

Comparisons for factor: Group within Day 2

Comparison	Diff of Means	p	q	P
Wtt vs. 146t	64.189	4	5.519	<0.001
Wtt vs. Wto	24.825	4	1.806	0.578
Wtt vs. 146o	20.218	4	1.541	0.696
146o vs. 146t	43.971	4	3.417	0.074
146o vs. Wto	4.607	4	0.311	0.996
Wto vs. 146t	39.364	4	2.914	0.166

Comparisons for factor: Group within Day 3

Comparison	Diff of Means	p	q	P
Wtt vs. 146t	84.911	4	7.301	<0.001

Wtt vs. 146o	52.505	4	4.003	0.024
Wtt vs. Wto	20.308	4	1.478	0.723
Wto vs. 146t	64.602	4	4.782	0.004
Wto vs. 146o	32.196	4	2.174	0.415
146o vs. 146t	32.406	4	2.518	0.283

Comparisons for factor: Group within Day 4

Comparison	Diff of Means	p	q	P
Wtt vs. 146t	94.752	4	8.147	<0.001
Wtt vs. 146o	56.061	4	4.274	0.013
Wtt vs. Wto	20.942	4	1.524	0.703
Wto vs. 146t	73.811	4	5.464	<0.001
Wto vs. 146o	35.119	4	2.372	0.336
146o vs. 146t	38.692	4	3.007	0.145

Comparisons for factor: Group within Day 5

Comparison	Diff of Means	p	q	P
Wtt vs. 146t	89.943	4	7.734	<0.001
Wtt vs. 146o	59.161	4	4.51	0.008
Wtt vs. Wto	30.5	4	2.219	0.396
Wto vs. 146t	59.443	4	4.4	0.01
Wto vs. 146o	28.661	4	1.935	0.519
146o vs. 146t	30.782	4	2.392	0.328

Comparisons for factor: Group within Day 6

Comparison	Diff of Means	p	q	P
Wtt vs. 146t	88.236	4	7.587	<0.001
Wtt vs. 146o	75.886	4	5.785	<0.001
Wtt vs. Wto	48.892	4	3.557	0.058
Wto vs. 146t	39.345	4	2.913	0.167
Wto vs. 146o	26.994	4	1.823	0.57

146o vs. 146t	12.351	4	0.96	0.905

Comparisons for factor: Group within Day 7

Comparison	Diff of Means	p	q	P
Wtt vs. 146t	101.975	4	8.768	<0.001
Wtt vs. 146o	99.546	4	7.589	<0.001
Wtt vs. Wto	36.433	4	2.651	0.239
Wto vs. 146t	65.542	4	4.852	0.003
Wto vs. 146o	63.113	4	4.262	0.014
146o vs. 146t	2.429	4	0.189	0.999

Comparisons for factor: Group within Day 8

Comparison	Diff of Means	p	q	P
Wtt vs. 146t	112.234	4	9.651	<0.001
Wtt vs. 146o	92.932	4	7.085	<0.001
Wtt vs. Wto	28.325	4	2.061	0.464
Wto vs. 146t	83.909	4	6.212	<0.001
Wto vs. 146o	64.607	4	4.363	0.011
146o vs. 146t	19.302	4	1.5	0.714

Comparisons for factor: Group within Day 9

Comparison	Diff of Means	p	q	P
Wtt vs. 146t	105.391	4	9.062	<0.001
Wtt vs. 146o	84.121	4	6.413	<0.001
Wtt vs. Wto	18.425	4	1.34	0.779
Wto vs. 146t	86.966	4	6.438	<0.001
Wto vs. 146o	65.696	4	4.436	0.009
146o vs. 146t	21.269	4	1.653	0.647

Comparisons for factor: Group within Day 10

Comparison	Diff of Means	p	q	P

Wtt vs. 146o	101.129	4	7.71	<0.001
Wtt vs. 146t	93.995	4	8.082	<0.001
Wtt vs. Wto	9.367	4	0.681	0.963
Wto vs. 146o	91.762	4	6.197	<0.001
Wto vs. 146t	84.629	4	6.265	<0.001
146t vs. 146o	7.133	4	0.554	0.98

Comparisons for factor: Group within Day 11

Comparison	Diff of Means	p	q	P
Wtt vs. 146t	122.952	4	10.572	<0.001
Wtt vs. 146o	111.404	4	8.493	<0.001
Wtt vs. Wto	14.1	4	1.026	0.887
Wto vs. 146t	108.852	4	8.058	<0.001
Wto vs. 146o	97.304	4	6.571	<0.001
146o vs. 146t	11.549	4	0.897	0.921

Comparisons for factor: Group within Day 12

Comparison	Diff of Means	p	q	P
Wtt vs. 146t	125.793	4	10.817	<0.001
Wtt vs. 146o	120.011	4	9.149	<0.001
Wtt vs. Wto	6.808	4	0.495	0.985
Wto vs. 146t	118.985	4	8.808	<0.001
Wto vs. 146o	113.202	4	7.645	<0.001
146o vs. 146t	5.782	4	0.449	0.989